

JORMUNGANDR WALHALLAENSIS:
A NEW MOSASAURINE (SQUAMATA:
MOSASAUROIDEA) FROM THE PIERRE SHALE
FORMATION (PEMBINA MEMBER: MIDDLE
CAMPANIAN) OF NORTH DAKOTA

AMELIA R. ZIETLOW

*Richard Gilder Graduate School and Division of Paleontology,
American Museum of Natural History, New York*

CLINT A. BOYD

North Dakota Geological Survey, Bismarck, ND

NATHAN E. VAN VRANKEN

*Biological Environmental Technology,
Eastern West Virginia Community and Technical College, Moorefield, WV*

BULLETIN OF THE AMERICAN MUSEUM OF NATURAL HISTORY

Number 464, 82 pp., 52 figures, 2 tables

Issued October 30, 2023

CONTENTS

Abstract.....	3
Introduction.....	3
Institutional Abbreviations.....	5
Systematic Paleontology, <i>Jormungandr walhallaensis</i> , gen. et sp. nov.....	6
Description.....	10
Skull.....	11
Palate.....	22
Mandible.....	28
Axial Skeleton.....	35
Phylogenetic Analysis.....	41
Discussion.....	47
Summary.....	59
Acknowledgments.....	60
References.....	60
Appendix 1. Character List Used in the Parsimony Analyses of Mosasauroid Phylogeny.....	65
Appendix 2. Data Matrix Used in the Parsimony Analyses of Mosasauroid Phylogeny.....	79

ABSTRACT

Mosasaurids are large, carnivorous aquatic lizards with a global distribution that lived during the Late Cretaceous. After 200 years of scientific study, new mosasaur species are still being discovered as new localities are explored and specimens collected long ago are reevaluated using modern standards of species delimitation. Even so, the phylogenetic positions of many key taxa are unresolved and therefore our understanding of mosasaur macroevolution is muddled. Here, we describe a new genus and species of mosasaurine mosasaur comprising a partial skull and skeleton from the Pembina Member of the Pierre Shale Formation in Cavalier County, North Dakota. The lower bound on the age of the specimen is 80.04 ± 0.11 Ma, provided by the underlying bentonite bed. Its skull and jaws are nearly complete, and the postcranial skeleton preserves seven cervical vertebrae with three hypapophyseal peduncles, 11 ribs, and five anterior dorsal vertebrae. The new specimen was scored into a modified version of an existing phylogenetic matrix of Mosasauridae and was recovered in a polytomy with *Clidastes*; however, given that its morphology is significantly different from that of *Clidastes*, we refer it to a new genus and species, *Jormungandr walhallaensis*. Notably, this new taxon shares a mosaic of features seen in both basal (e.g., *Clidastes*; high dental counts) and derived (e.g., *Mosasaurus*; subrectangular quadrate) mosasaurines, in addition to possessing its own unique suite of autapomorphies. Given that it possesses morphology intermediate between *Clidastes* and Plotosaurini, we suspect that future analyses of mosasaur phylogeny, following the addition of new characters and taxa, will recover *Jormungandr* as transitional between them. Its occurrence increases the known diversity of mosasaurids from the Pembina Member and is the earliest mosasaur to possess autapomorphies of Plotosaurini. Finally, we also analyzed the matrix using different outgroups to test their effect on tree topology and resolution, and found that including multiple nonmosasaurid anguimorphs increased resolution, but not support, of mosasaurid ingroup relationships.

INTRODUCTION

Mosasaurids are an extinct lineage of squamate reptiles that reigned as apex marine predators of oceans and waterways globally during the Late Cretaceous (98 to 66 mya; Polcyn et al., 2014). Although their exact position within Squamata has long been contested (e.g., Russell, 1967; Carroll and DeBraga, 1992; Lee, 1997; Rieppel and Zaher, 2001; Gauthier et al., 2012; Reeder et al., 2015; Simões et al., 2017) and will likely not be irrefutably settled for some time, they are generally recovered within Toxicodonta, and the most recent analyses using both morphological and molecular data have recovered Mosasauridae as sister to Varanoidea (Augusta et al., 2022; Polcyn et al., 2022). Within Mosasauridae, three major lineages of derived mosasaurids are recognized: Tylosaurinae, Plioplatecarpinae, and Mosasaurinae (Russell, 1967; Polcyn and Bell, 2005; Palci et al., 2013). Of these clades, the mosasaurines are arguably most morphologically diverse, with skulls and teeth adapted for a

wide range of dietary niches, from the robust jaws and serrated conical teeth of *Prognathodon* and kin conducive to tearing chunks of flesh or crunching the bones of other marine reptiles, to the gracile snout and slender teeth of the piscivorous *Plotosaurus* (Konishi et al., 2011; LeBlanc et al., 2013; Konishi et al., 2014; Longrich et al. 2022).

The relationships between Tylosaurinae, Plioplatecarpinae, and Mosasaurinae and the various basal mosasaurids, while critical to understanding the evolution of their aquatic adaptations, are ultimately unclear. For example, in most analyses of mosasaurid phylogeny, *Dallasaurus turneri*, which retains plesiomorphic (i.e., likely terrestrial) limb morphology, is recovered as the basalmost mosasaurine, suggesting that the limb-flipper transition occurred at least three times within Mosasauridae (Polcyn and Bell, 2005; Palci et al., 2013). However, other studies—e.g., Simões et al. (2017)—have found placement of *Dallasaurus* within Mosasaurinae unlikely, and



FIGURE 1. *Thor Slaying the Dragon*, painting by G.I. Gullickson (1918–1937) of a scene from Norse mythology in which the World Serpent, Jörmungandr, battles against the god Thor. Original painting on display in the North Dakota Heritage Center and State Museum (State Historical Society of North Dakota 07971).

favor a single evolution of flippers in Mosasauridae, with a reversal in Tethysaurinae. Given that addition of new taxa significantly improves accuracy of phylogenetic trees (Graybeal, 1998), discovery and description of new mosasaurs is critical to resolving ingroup relationships, furthering our understanding of morphological evolution within Mosasauriidea, and paving the way for future research comparing the path of their transition from

land to sea with that of other secondarily aquatic amniotes.

Here, we describe a new genus and species of mosasaurine mosasaur from the Pembina Member of the Pierre Shale Formation in North Dakota based on a single specimen (NDGS 10838) comprising a nearly complete skull, complete jaws, complete cervical series, and five anterior dorsal vertebrae, as well as several yet unprepared jackets containing additional postcranial material. The

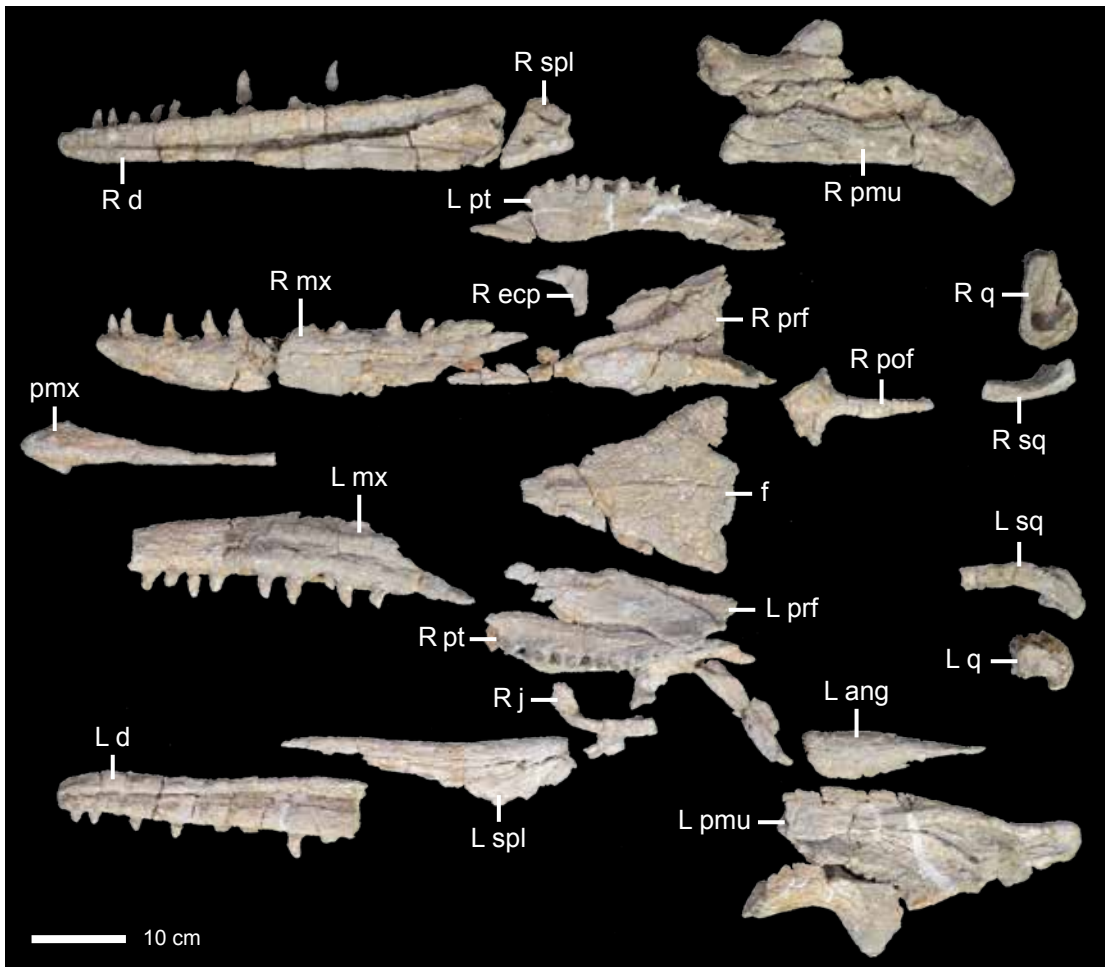


FIGURE 2. Skull and jaws of the holotype specimen, NDGS 10838. Abbreviations: **ang**, angular; **d**, dentary; **ecp**, ectopterygoid; **f**, frontal; **j**, jugal; **mx**, maxilla; **pmu**, posterior mandibular unit; **pmx**, premaxilla; **pof**, postorbitofrontal; **prf**, prefrontal; **pt**, pterygoid; **q**, quadrate; **spl**, splenial; **sq**, squamosal. Uppercase **L** and **R** indicate left and right bones, respectively, when applicable. Photograph by Mindy Householder.

Pembina Member of the Pierre Shale Formation is Middle Campanian in age (Bamburak et al., 2016) and preserves a variety of marine animals that inhabited the Western Interior Seaway of North America, including birds, squid, fishes, ammonites, and marine reptiles (Nicholls, 1988). Of the three major lineages of mosasaurids, plioplatacarpines are most common in the Pembina Member, representing approximately 85% of identified mosasaur remains, and mosasaurines are rarest, representing less than 1%; NDGS 10838 is the first

new genus, and only the second mosasaurine genus (after *Clidastes*) described from the Pembina Member (Nicholls, 1988). We test its position within Mosasauridae using traditional parsimony and implied weighting analyses.

INSTITUTIONAL ABBREVIATIONS

AMNH, American Museum of Natural History
 FHSM, Sternberg Museum of Natural History,
 Hays, KS

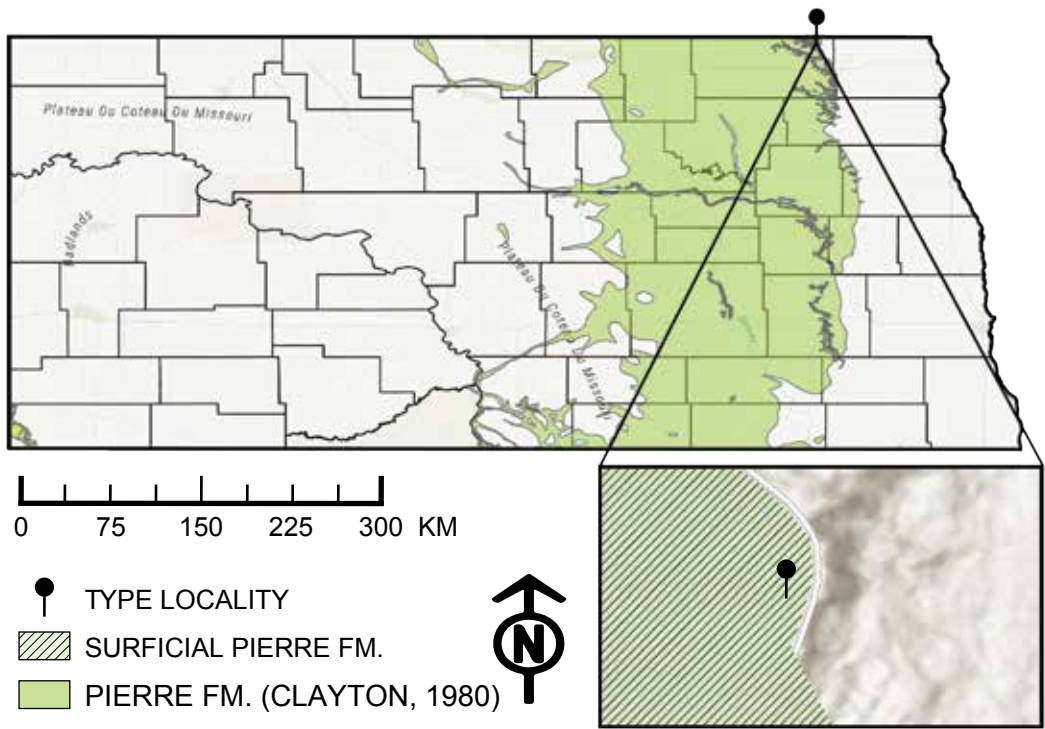


FIGURE 3. Map of holotype locality. Light green hatching represents the observed surficial exposure of the Pierre Formation, and solid green represents the undifferentiated Pierre Formation described by Clayton et al. (1980).

FMNH, Field Museum of Natural History, Chicago, IL
 IRScNB, Institut Royal des Sciences Naturelles de Belgique, Brussels, Belgium
 KUVF, University of Kansas Natural History Museum, Lawrence, KS
 MCZ, Harvard Museum of Comparative Zoology, Cambridge, MA
 MNHN, Muséum national d'Histoire naturelle, Paris, France
 NDGS, North Dakota State Fossil Collection, North Dakota Geological Survey, Bismarck, ND
 NJSM, New Jersey State Museum, Trenton, NJ
 TMP, Royal Tyrrell Museum of Palaeontology, Drumheller, Alberta, Canada
 YPM, Yale Peabody Museum, New Haven, CT

SYSTEMATIC PALEONTOLOGY

Squamata Oppel, 1811

Mososauridae Gervais, 1853

Mososaurinae Gervais, 1853

Jormungandr walhallaensis, gen. et sp. nov.

ETYMOLOGY: The specific epithet is named after Walhalla, North Dakota, near which the holotype and only specimen was found. In Norse mythology, the sea serpent Jormungandr (fig. 1), also referred to as the “World Serpent,” is the second child of god Loki and giantess Angrboða. The god Óðinn is said to have thrown Jormungandr into the ocean, where he

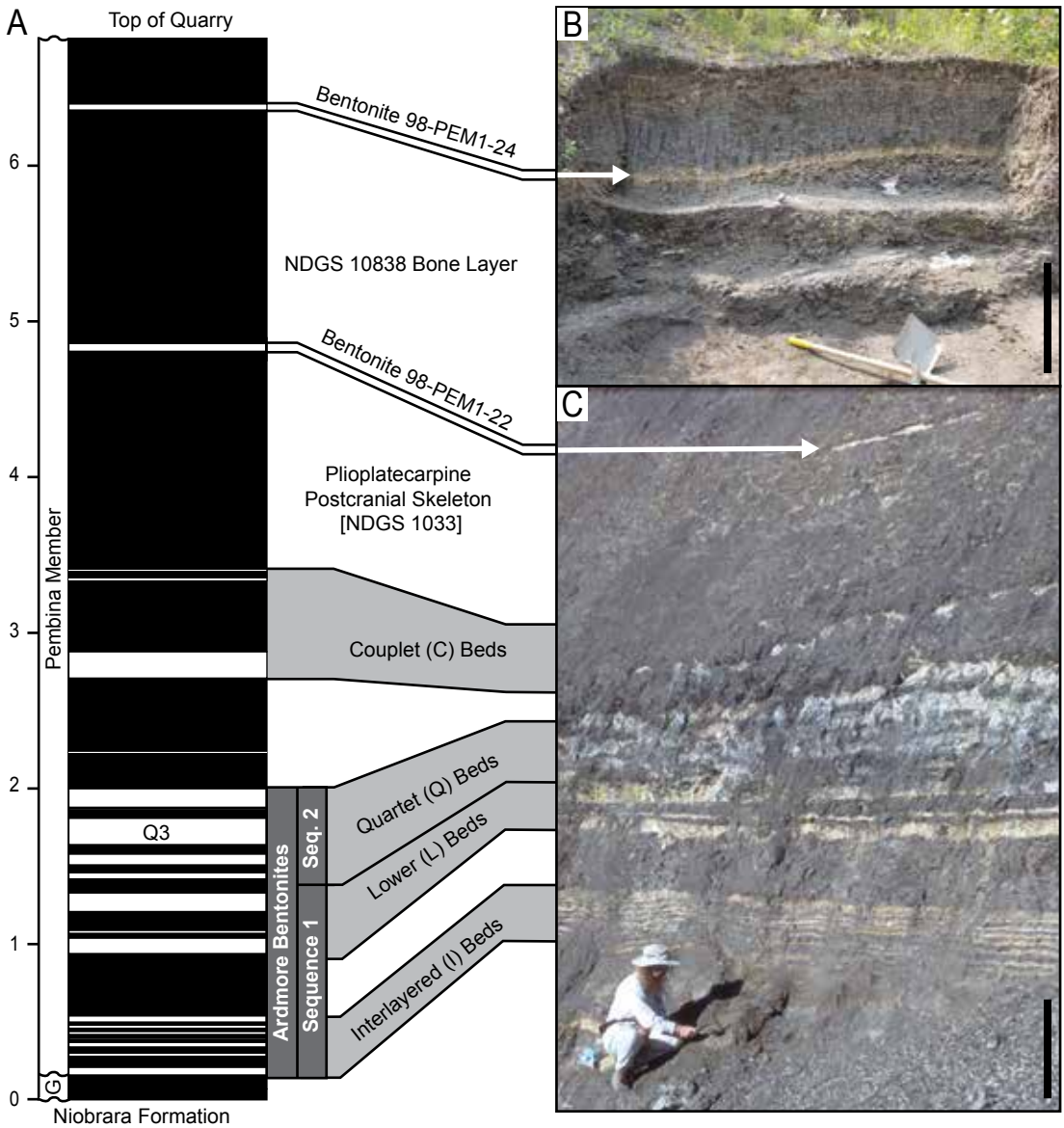


FIGURE 4. **A**, Stratigraphic column and **B**, **C**, photographs of the exposed rocks of the Pierre Formation at the study site. Measurements on the left side of the stratigraphic column are given in meters. Scale bars (**B**, **C**) = 1 m. Bentonite terminology adapted from Bertog et al. (2007) and Bamburak et al. (2013). Janet Bertog is shown in the lower left corner of **C** collecting samples and stratigraphic data that were used in future studies (e.g., Bertog et al., 2007; Bertog, 2010). Abbreviation: **G**, Gammon Member.

grew until he was large enough to encircle Earth by grasping his tail in his jaws. *Jormungandr* releasing his tail heralds the coming of *Ragnarøk*, the death of the gods followed by destruction and rebirth of the world as it is submerged in water. We chose *Jormungandr* as the generic name due to the origin of Walhalla from Norse Valhøll (Valhalla); Valhøll is the great hall of Óðinn occupied by warriors slain in combat who rise again to participate in the battles catalyzed by Ragnarøk.

HOLOTYPE: NDGS 10838, a nearly complete skull (missing only the nasals, braincase, parietal, septomaxilla, and scleral ossicles), complete mandibles, all seven cervical vertebrae, 11 disarticulated ribs, and five articulated anterior dorsal vertebrae (fig. 2). Several unprepared jackets, which were not found until after the submission of this manuscript, contain additional postcranial material including ribs, a scapula, and a coracoid.

TYPE LOCALITY: Pembina Member of the Pierre Shale Formation in Cavalier County, North Dakota (NDGS L47; fig. 3). The bone layer is situated between five and 5.5 meters above the contact with the underlying Niobrara Formation (fig. 4). The lower bound on the age of the specimen is 80.04 ± 0.11 Ma, calculated for the Q3 bentonite bed at the study area that is situated approximately 3.5 meters below the bone layer (Bamburak et al., 2016).

GEOLOGIC SETTING: The type locality is situated within the lower portion of the Pierre Shale Formation. Though there were recent attempts to extend the lithostratigraphic terminology of adjacent states to rocks of the Pierre Shale Formation in North Dakota (e.g., Martin et al., 2007; Bertog, 2010), we employ the lithostratigraphic terminology favored by the North Dakota Geological Survey, where the Pierre is kept at the Formation rank and is divided into five members (Murphy et al., 2009). Those members, from oldest to youngest, are as follows: Gammon; Pembina; Gregory; DeGrey; and Odanah. The geology of the exposed outcrop at this locality was previously described in detail (Bertog et al.,

2007; appendix 4), including a series of distinctive bentonites that are used to correlate these rocks with exposures of the Pierre Formation throughout the region (Bertog et al., 2007; Bertog, 2010; Bamburak et al., 2016). The series of bentonites within the lower 2.5 meters of the Pierre Shale Formation in the study area are collectively referred to as the Ardmore bentonite succession (Bertog, 2002; 2010). The base of the Ardmore bentonite succession marks the local contact between the underlying Gammon and overlying Pembina Members (Murphy et al., 2009). The type locality is situated well above the Ardmore bentonite succession, placing it within the Pembina Member (fig. 4).

The type locality is situated within rocks that are part of an active slump, and the in situ beds are often obscured by displaced talus accumulating on the surface. As a result, local stratigraphy is difficult to decipher without reviewing photographs of the hillside from the past 25 years that reveal short-term exposures of in situ ash layers and their shifting positions over time as the slide progresses. Combining that information with LiDAR data acquired via drone by the North Dakota Geological Survey at the study area over multiple years allowed the stratigraphic position of the type locality to be determined relative to previously documented bentonite beds (e.g., Bertog et al., 2007; Bertog, 2010), local lithostratigraphic contacts (e.g., Bamburak et al., 2016), and previously collected specimens (fig. 4).

The stratigraphic position of the type locality is within that portion of the Pembina Member that correlates with the upper portion of the Burning Brule Member (Sharon Springs Formation, Pierre Group) in central South Dakota (Martin et al., 2007; Bertog et al., 2007; Bertog, 2010). That correlation places the type locality within either the *Baculites obtusus* or *Baculites mclearni* ammonite range zones (e.g., Gill and Cobban, 1965; Martin et al., 2007; Bertog et al., 2007; Bertog, 2010), which are the two oldest range zones within the middle Campanian (Cobban et al., 2006). A sample taken from the Q3 bentonite (sensu Bamburak et al., 2013) at

TABLE 1

Skull and Jaw Measurements of the Holotype NDGS 10838

Measurements are rounded to the nearest whole millimeter. Em-dashes represent measurements that were unobtainable or inapplicable.

Element	Measurements (mm)	
Skull length	720	
Rostrum length	16	
Quadrate height, right	104	
Quadrate, ala thickness, right	9	
Quadrate, stapedial pit height, right	12	
Quadrate, stapedial pit width, right	7	
Frontal, length	287	
Frontal, posterior width	180	
Jaw length, right	808	
	Toothrow, total	Toothrow, tooth 1–6
Maxilla, right	389	127
Pterygoid, left	210	86
Pterygoid, right	209	90
Dentary, left	—	118
Dentary, right	466	118

the study area was dated at 80.04 ± 0.11 Ma (U-Pb zircon age: Bamburak et al., 2016), which is consistent with dates obtained elsewhere from bentonites within the Ardmore bentonite succession (e.g., Obradovich, 1993; Hicks et al., 1999) and provides a lower bound on the age of the type locality.

DIAGNOSIS: Mosasaurine mosasaur possessing the following suite of characters: edentulous premaxillary rostrum of intermediate length (e.g., longer than one tooth position but shorter than two tooth positions) and blunt in lateral view but pointed in dorsoventral views; premaxilla internarial bar T-shaped in cross section along its entire length; presence of premaxilla dorsal keel; 15 maxillary teeth; frontal of intermediate width (i.e., between 1.5 and 2 times longer than wide) and possesses a low

but distinct dorsal keel; presence of postorbitofrontal transverse ridge; jugal angle slightly obtuse; quadrate stapedial pit a narrow (1.8× taller than wide) oval; quadrate posteroventral ascending rim a high, triangular crest; groove present in anterolateral portion of the quadrate alar rim; quadrate mandibular condyle distinctly convex in all views; 16 pterygoid teeth; 16 dentary teeth; dentary anterior projection longer than one tooth position; splenial-angular articular surfaces grooved; zygospheles and zygantra present on cervical vertebrae; hypapophyses present on second through seventh cervicals; and hypapophyseal peduncle lacking on cervical seven. It is also distinguished from all other known mosasaurids by: a quadrate stapedial pit set within a sulcus that is bounded ventrally by a ridge; both maxillae and dentaries

TABLE 2

Vertebral Measurements of the Holotype NDGS 10838

Measurements are rounded to the nearest whole millimeter. Em-dashes represent measurements that were unobtainable or inapplicable. Abbreviations: **H**, height; **W**, width.

Vertebra	Measurements (mm)					
	Intercentrum W	Centrum (H, W)	Cotyle (H, W)	Condyle (H, W)	Synapophysis (H, W)	Hypapophyseal Facet Length
Atlas	56	—	—	—	13, 7	—
Axis	40	51, 96	—	37, 45	20, 53	33
Cervical III	—	43, 94	39, 46	44, 51	20, 41	29
Cervical IV	—	50, 100	40, 54	47, 49	25, 50	26
Cervical V	—	48, 93	42, 50	44, 50	39, 47	26
Cervical VI	—	47, 90	40, 53	44, 45	41, 36	23
Cervical VII	—	40, 82	37, 50	41, 47	49, 34	—
Dorsal I	—	37, 74	44, 51	42, 50	49, 36	—
Dorsal II	—	36, 73	41, 54	42, 51	46, 37	—
Dorsal III	—	31, 73	45, 54	44, 50	40, 28	—
Dorsal IV	—	40, 82	45, 55	39, 50	34, 25	—

that are twice as wide as the tooth bases (as opposed to only slightly wider in other taxa); and prefrontal-postorbitofrontal contact that is prevented by a thin ridge of the frontal.

DESCRIPTION

NDGS 10838 includes a nearly complete skull, missing the parietal, braincase, nasals, scleral ossicles, and septomaxillae. The specimen also includes nearly complete mandibles, the first 12 vertebrae (including three disarticulated hypapophyseal peduncles), and 11 ribs (fig. 2). Although surface preservation is poor, most bones are minimally distorted, and NDGS 10838 preserves several bones that are rarely found, recognized, or observable in mosasaur fossils (e.g., vomer, palatine, a tentative lacrimal, ectopterygoid, and epipterygoid). The skull and most of the left mandible (i.e., everything except for the articular-prearticular and surangular) are

completely disarticulated, but some bones are in contact with one another, obscuring some details. The posterior and anterior mandibular units of the right mandible are each preserved articulated but are separate from one another. All seven cervical vertebrae are disarticulated, and the five dorsal vertebrae are articulated. Most ribs and hypapophyseal peduncles were found near, but not in direct articulation with, their associated vertebrae. Here, we describe NDGS 10838 with an emphasis on comparisons with other mosasaurines. Key measurements of the skull and jaws are given in table 1, and vertebral measurements are given in table 2.

The holotype was surface scanned using a Shining 3D EinScan-SP; smaller bones were scanned with the automated turn table, while larger scans utilized multiple fixed scans that were automatically stitched together in ExScan S v. 3.1.2.0. All scans were uploaded to MorphoSource (<https://www.morphosource.org/proj->

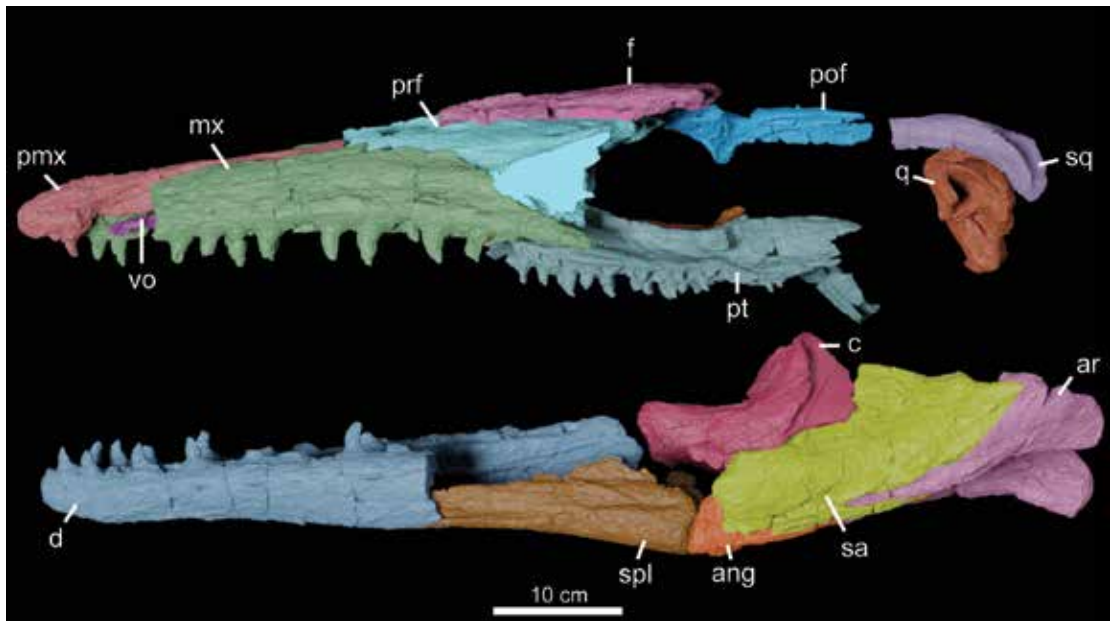


FIGURE 5. Rearticulated skull and jaw of NDGS 10838 in left lateral view, with left bones labeled. Matte surfaces of the left prefrontal and frontal represent the surfaces of the bone that, as preserved, are obscured by the right pterygoid and left postorbitofrontal, respectively. Abbreviations: **ang**, angular; **ar**, articular; **c**, coronoid; **d**, dentary; **f**, frontal; **mx**, maxilla; **pmx**, premaxilla; **pof**, postorbitofrontal; **prf**, prefrontal; **pt**, pterygoid; **q**, quadrate; **sa**, surangular; **spl**, splenial; **sq**, squamosal; **vo**, vomer.

ects/000566333); a list of the scans with direct links to each may be found in the online supplement (<https://doi.org/10.5531/sd.sp.60>). When NDGS 10838 is rearticulated, its skull is gracile in lateral view (figs. 5–7), with a long, slender muzzle. In dorsal and ventral views, the skull is narrow and tapered anteriorly (figs. 8–11). The bony nares begin above the sixth maxillary tooth and terminate above the 13th tooth (figs. 8, 9). The right maxilla preserves 15 tooth positions, and the right and left pterygoids preserve at least 15 and 16 tooth positions, respectively (fig. 10). Marginal teeth are bladelike and labiolingually compressed.

The anterior mandibular unit (dentary, splenial) is slender and just over half (60%) of the total jaw length. The posterior mandibular unit (coronoid, angular, surangular, prearticular-articular) is robust, with a shallow lateral surangular fossa (figs. 5–7, 12). The coronoid posterodorsal process is tall as is characteristic of

mosasaurines, forming nearly a right angle with the anterior ramus of the bone and the dentary tooththrow. The surangular is excluded from the ventral margin of the posterior mandibular unit in lateral view by the angular and prearticular-articular. The right dentary preserves 16 tooth positions, and morphology of preserved teeth matches that of the maxillary teeth.

SKULL

PREMAXILLA: The premaxilla (fig. 13) possesses a rostrum that is arcuate in lateral view, similar to *Tylosaurus* and *Plesiotylosaurus crassidens* (Lindgren, 2009), but broadly pointed in dorsal view, as is typical of mosasaurines (Russell, 1967: 16; A.R.Z., personal obs.); this shape is also present in *Plotosaurus* (LeBlanc et al., 2013). It bears a total of four tooth positions, as is typical for mosasaurids (Russell, 1967: 14), and the anterior pair of alveoli is slightly smaller than

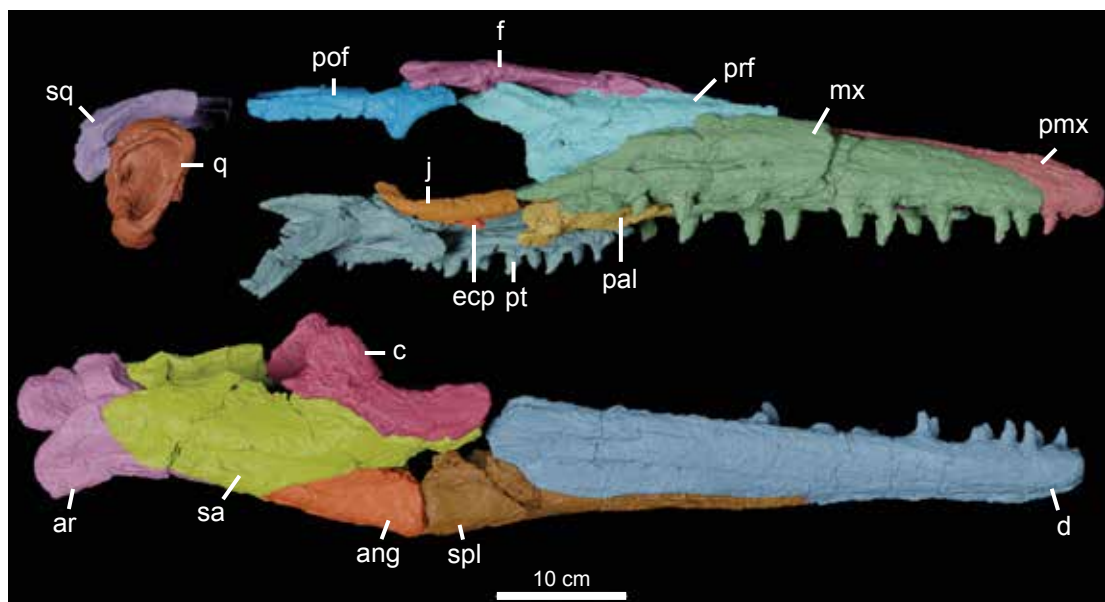


FIGURE 6. Rearticulated skull and jaw of NDGS 10838 in right lateral view, with right bones labeled. Abbreviations: **ang**, angular; **ar**, articular; **c**, coronoid; **d**, dentary; **ecp**, ectopterygoid; **f**, frontal; **j**, jugal; **mx**, maxilla; **pal**, palatine; **pmx**, premaxilla; **pof**, postorbitofrontal; **prf**, prefrontal; **pt**, pterygoid; **q**, quadrate; **sa**, surangular; **spl**, splenial; **sq**, squamosal.

the posterior pair. The teeth are not procumbent, as they are in some taxa (e.g., *Selmasaurus johnsoni* FHSM VP-13910, *Prognathodon solvayi* IRScNB R 33), and are separated from one another ventrally by a grooved median ridge sensu Russell (1967), as is typical of mosasauids (e.g., *Tylosaurus proriger* MCZ 4374, *Clidastes propython* AMNH FARB 1507). The incisive processes (a pair of posteroventral projections of the premaxilla) are broken and missing. The dorsal midline of the premaxilla has a subtle crest, like *Mosasaurus hoffmannii* (e.g., NJSM 11053). Neurovascular foramina are concentrated on the anterior surface of the rostrum and are otherwise distributed randomly and not in distinct rows as seen in some plioplatecarpines (e.g., *Platecarpus tympaniticus* AMNH FARB 1820/1821, *Plesio-platecarpus planifrons* FHSM VP-2116).

In lateral view, the anterior suture with the maxilla is straight and nearly vertical before sloping gently dorsally toward the external naris, as in *Mosasaurus hoffmannii*. It terminates posteriorly above the midline of the sixth maxillary tooth

position, as in *Clidastes propython* (e.g., FMNH P12856; Russell, 1967: 130). In dorsal view, the base of the posterior process is nearly as wide as the rostrum anteriorly before tapering gradually to about one fifth the width of the rostrum between the nares and is T-shaped in cross section. The dorsal surface of the posterior process is broad, and the ventral surface has a thin, deep, ventrally projecting blade that nearly reaches the level of the tooth alveoli. Posteriorly, the blade is bounded laterally on both sides by shallow, oblong facets, similar to those present in *Mosasaurus hoffmannii*, possibly for articulation with the nasals (Russell, 1967).

MAXILLA: The right maxilla is complete and, because the posterior terminus of the premaxilla-maxilla suture does not vary bilaterally in mosasaurs (e.g., *Tylosaurus proriger* FHSM VP-3, *Platecarpus tympaniticus* AMNH FARB 1820/1821, *Clidastes liodontus* AMNH FARB 192) and it occurs above the midline of the sixth tooth in the right maxilla, we infer that the left maxilla is missing only the first three tooth posi-

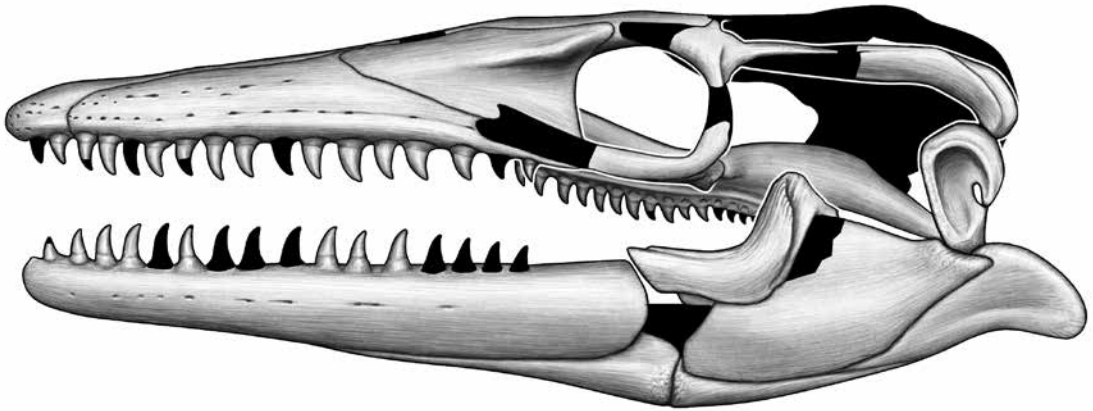


FIGURE 7. Idealized drawing of the skull and jaws of *Jormungandr walhallaensis*, gen. et sp. nov., in left lateral view. Note: the overall shape of the bones as drawn here are an estimate of what they may have looked like before distortion, and not an exact line drawing of NDGS 10838. Illustration by Henry Sharpe.

tions (fig. 14). Tooth attachment is thecodont (i.e., teeth are set within sockets; Bertin et al., 2018; LeBlanc et al., 2020), as is typical of mosasaurids. The right maxilla bears 15 tooth positions, like *Clidastes liodontus* (e.g., AMNH FARB 192), *Mosasaurus lemonnieri* (e.g., IRScNB R 299) and *Moanasaurus mangahouangae* (Wiffen, 1990) and unlike most large-bodied taxa (e.g., 13 in *Tylosaurus proriger* FHSM VP-3 and *Mosasaurus hoffmannii* NJSM 11053). The first tooth and last three teeth are the smallest (i.e., crown about 75% the height of the other teeth), and the rest are approximately equal in size. Carinae are present on both mesial and distal edges, but the tooth surfaces are too eroded to confidently assess the presence or absence of serrations and other fine textural details. Unlike the premaxillary teeth, which have circular cross sections at their bases, the cross sections of the maxillary teeth are mediolaterally compressed, as in *Clidastes* (e.g., AMNH FARB 192), *Mosasaurus conodon* (e.g., AMNH FARB 1380), and *Mosasaurus lemonnieri* (Lingham-Soliar, 2000; IRScNB R 299).

In lateral view, the maxillae of NDGS 10838 are very similar in overall shape to those of *Mosasaurus hoffmannii*. A row of neurovascular foramina for terminal branches of the maxillary

nerve are present dorsal and parallel to the toothrow, increasing in size posteriorly. The dorsal margin of the maxilla is gently convex until the terminus of the premaxilla-maxilla suture, posterior to which the margin is slightly concave in lateral view and, in dorsal view, the medial margin is distinctly bowed laterally; these concavities mark the lateral and anterior margins, respectively, of the external bony naris. The posteriormost extent of the contribution of the maxilla to the lateral margins of external nares occurs dorsal to the tenth tooth position. Posterior to the external nares, the dorsal margin of the maxilla appears to slope gently ventrally, as in *Mosasaurus*, although it is unclear whether the absence of a long posterodorsal process, which excludes the prefrontals from the nares in *Tylosaurus*, *Plotosaurus*, and *Ectenosaurus* (Russell, 1967), is taphonomic.

The maxilla is robust in ventral view, approximately twice as wide as the toothrow, in contrast to only slightly wider than the toothrow in most other mosasaurids (fig. 15). It begins to widen at the sixth tooth position, is widest between the seventh and tenth tooth positions, and then tapers somewhat abruptly at the 14th tooth position. In dorsal view, the supraddental

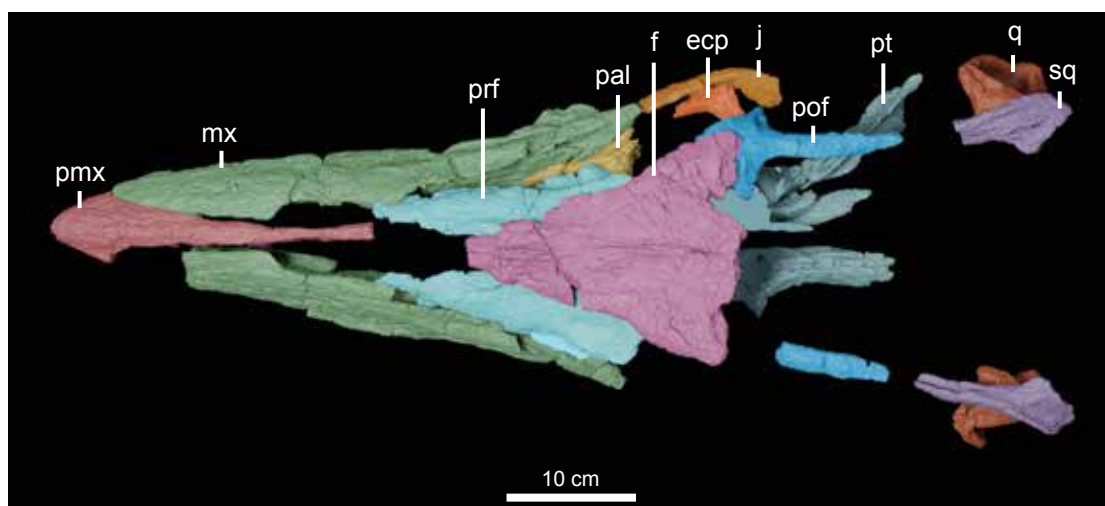


FIGURE 8. Rearticulated skull of NDGS 10838 in dorsal view. Matte surfaces of the right pterygoid and left prefrontal represent the surfaces of those bones that, as preserved, are obscured by one another. Abbreviations: **ecp**, ectopterygoid; **f**, frontal; **j**, jugal; **mx**, maxilla; **pal**, palatine; **pmx**, premaxilla; **pof**, postorbitofrontal; **prf**, prefrontal; **pt**, pterygoid; **q**, quadrate; **sq**, squamosal.

shelf is large and broad. Anteriorly, the medial surfaces of both maxillae are perforated by a large foramen dorsal to the fourth tooth position, and appears connected to a second, smaller foramen dorsal to the fifth tooth position by a shallow groove. Another groove runs along most of the ventral margin of the bone, parallel to the toothrow. On the right maxilla, the anterolateral margin of the vomeronasal fenestra is present as a shallow embayment just anteromedial to the third tooth position, and the facet for the vomer is present medial to the first tooth position.

LACRIMAL: Mosasauroid lacrimals are rarely well preserved and poorly understood (Russell, 1967: 21). NDGS 10838 preserves a disarticulated bone that strongly resembles a right lacrimal (fig. 16), and is particularly similar in overall shape to the lacrimal of the dolichosaur *Coniasaurus gracilodens* (Polcyn et al., 2022); however, because it is much larger relative to the muzzle than other known mosasauroid lacrimals, and because we could not determine whether our failure to confidently articulate it with the prefrontal and maxilla is due to crushing of those bones or because this element is

not truly a lacrimal, we consider our identification of this bone tentative. In lateral view, the bone is triangular, rather than quadrilateral, as the lacrimal in *Clidastes* (Russell, 1967), or lenticular, as in *Tylosaurus* (Osborn 1899; Russell, 1967). The dorsal surface curves gently inward posteriorly, potentially demarcating the lateral margin of the lacrimal foramen. A facet that may be for the maxilla is present anterodorsally, and another facet, potentially for the prefrontal, is present dorsally, suggesting that, if this element is truly the lacrimal, it was located laterally on the skull of NDGS 10838 and not enclosed within the orbit as it is in *Plotosaurus* (Russell, 1967).

PREFRONTAL: Both prefrontals are preserved, though the right bone is crushed and is stuck to the right palatine, and the left bone is preserved in contact with the right pterygoid, obscuring its lateral surface (figs. 17, 18). Its outline is triangular in lateral and dorsal views. Its anterior process is long and narrow and underlies the maxilla. Along its anterolateral margin, there is a shallow groove that may have articulated with a posterodorsal process of the maxilla, but it lacks the sharp, pronounced ridges present in *Tylosaurus*

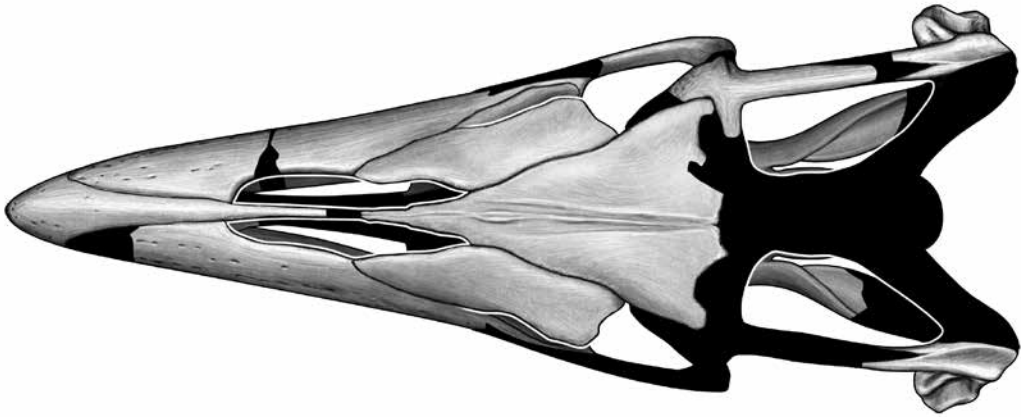


FIGURE 9. Idealized drawing of the skull of *Jormungandr walhallaensis* in dorsal view. The overall shape of the bones as drawn here are an estimate of what they may have looked like before distortion, and not an exact line drawing of NDGS 10838. Illustration by Henry Sharpe.

(e.g., *Tylosaurus proriger* AMNH FARB 1555). Its anteromedial margin forms the posterolateral margin of the external naris. Posteriorly along the midline, its articulation with the frontal is an elongate, triangular facet. It possesses a laterally projecting supraorbital ridge. A descending lamina forms the anterior margin of the orbit, and its medial surface bears a large, triangular fossa that borders the nasal capsule. The lacrimal facet is a slot in the ventral portion of the orbital margin; posterior to it, the palatine facet is present as a subcircular rugosity.

FRONTAL: The frontal approximates an arrow-head in dorsal view (fig. 19). Its lateral margins are slightly sinusoidal above the orbits, like in *Clidastes liodontus* (e.g., YPM VP 24914), *Mosasaurosaurus* (e.g., *Mosasaurosaurus hoffmannii* NJSM 11052), and *Platecarpus* (e.g., *Platecarpus tympaniticus* AMNH FARB 1820/1821). The posterolateral alae are long and acute with rounded termini, and the posteromedial margin of the frontal is similar to that of *Gnathomortis stadmani* (Lively, 2020) and *Globidens dakotensis* (e.g., FMNH PR846) in that it invades the parietal as a rectangular ala that is embraced laterally by notches for anterior extensions of the parietal postorbital processes. Along its posterior mid-

line, the frontal-parietal suture is complex and interdigitating. Although the parietal is missing, there is neither notch nor other indication of the parietal foramen touching, much less invading, the frontal-parietal suture. Finally, it lacks the large posterior prongs that embrace the parietal foramen in *Mosasaurosaurus hoffmannii*, though it is possible that small prongs, as in *Clidastes*, were present but have broken off.

Its anterior process is long and narrow, contributing to the posteriormost part of the internarial bar. The anterior tip is pointed and its ventrolateral surfaces are slightly concave and continuous with what we interpret as the nasal facets on the premaxilla (figs. 18, 20). At the posterior end of the anterior process, its lateral margins are slightly embayed—but not invaded—by the nares. The dorsal crest does not reach the posterior margin of the bone. A groove is present along the midline of the anterior half of the frontal; this feature was interpreted by Street and Caldwell (2017) as separate dorsal and ventral grooves that articulate with the premaxilla. Because the anterior process of NDGS 10838 is broken, and the grooves are dorsoventrally continuous, we posit that this structure may also represent incomplete fusion of separate left and

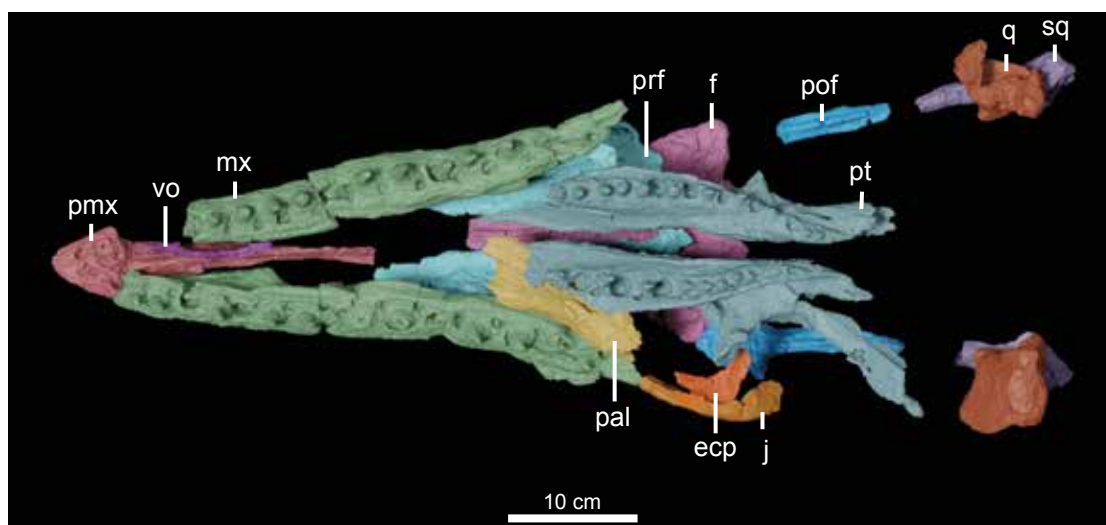


FIGURE 10. Rearticulated skull of NDGS 10838 in ventral view. Matte surface of the right jugal represents the surface of the bone that, as preserved, is obscured by an unidentified fragment. Abbreviations: **ecp**, ectopterygoid; **f**, frontal; **j**, jugal; **mx**, maxilla; **pal**, palatine; **pmx**, premaxilla; **pof**, postorbitofrontal; **prf**, prefrontal; **pt**, pterygoid; **q**, quadrate; **sq**, squamosal; **vo**, vomer.

right frontals. Separate left and right frontals are typical of most squamates and were noted by Lingham-Soliar (2000) in some specimens of *Mosasaaurus lemonnieri*, though the extent of the “suture” is much longer in that taxon than in NDGS 10838. A condition more similar to what is seen in NDGS 10838 was observed in *Ectenosaurus clidastoides* (e.g., FHSM VP-401) and *Mosasaaurus hoffmannii* (e.g., NJSM 11052), but not *Tylosaurus proriger* (e.g., AMNH FARB 4909), *Clidastes liodontus* (e.g., YPM VP 24914), nor *Platecarpus tympaniticus* (e.g., AMNH FARB 1820/1821). Holmes (1996) also attributed a similar structure in *Plioplatecarpus primaevus* CMN 11835 to represent incomplete fusion of the frontals due to immaturity of the specimen; however, we note that in CMN 11835, the suture is only open dorsally, unlike dorsally and ventrally as in NDGS 10838.

In ventral view, the prefrontal facet is an elongate triangle located dorsal to the orbit and lateral to the olfactory canal (figs. 19, 20). It is separated from the subrectangular postorbitofrontal facet by a low, narrow ridge that prevented contact between the two bones. Like

Clidastes (Russell, 1967), the postorbitofrontal facet is about half as long as the prefrontal facet. Posteriorly, semicircular facets bounded anteriorly by a groove receive anterior extensions of the parietal (fig. 19B, D).

The sulci for the anterior process of the planum supraseptale (sensu Bahl, 1937; Oelrich, 1956; and Polcyn et al., 2022) are deep and sickle shaped, like in most mosasaurids (e.g., *Tylosaurus proriger* AMNH FARB 1585, *Platecarpus tympaniticus* AMNH FARB 1820/1821) (figs. 19, 20). They lie lateral to a narrow, subrectangular fossa that covers part of the forebrain and are medial to the cristae cranii. Of note, Konishi and Caldwell (2009: 420) interpret these structures as the “roofs of the cerebral hemispheres,” citing Russell (1967); however, Russell (1967: 21) describes the outlines of the cerebral hemispheres on the frontal ventral surface as “not clearly defined,” whereas these structures are very clearly defined, and match the shape of the sulci for the anterior process of the planum supraseptale figured by Oelrich (1956: 30) and Polcyn et al. (2022: 132) perfectly. Konishi and Caldwell (2011) label these structures in *Lato-*

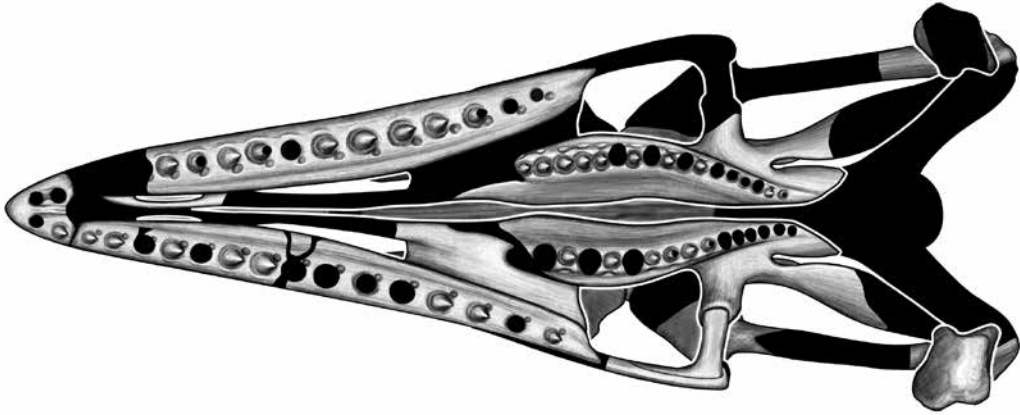


FIGURE 11. Idealized drawing of the skull of *Jormungandr walhallaensis* in ventral view. The overall shape of the bones as drawn here are an estimate of what they may have looked like before distortion, and not an exact line drawing of NDGS 10838. Illustration by Henry Sharpe.

platecarpus willistoni as the “orbitosphenoid articulation grooves,” which connect the orbitosphenoid to the ventral surface of the frontal via the “pila preoptica,” another name for the structures (in addition to planum suprasetale) given by Bahl (1937). Given that the sulci would have received the cartilaginous structures (the planum suprasetale) rather than the orbitosphenoid bones themselves, we elect to use the terminology of Oelrich (1956) and Polcyn et al. (2022).

The *cristae cranii* (*descensi processi frontalis sensu* Konishi and Caldwell, 2009) begin as descending processes posterior to the internarial bar, flaring abruptly laterally before curving back medially, terminating just anterior to the sulci for the anterior process of the planum suprasetale and level to the posterior margin of the prefrontal facets. They lie lateral to a pair of deep fossae (parolfactory bulb recesses, *sensu* Konishi and Caldwell, 2009) that form the roof of the olfactory bulbs (Bahl, 1937; Bellairs, 1949). Posteriorly, the *cristae cranii* broaden and flatten, particularly lateral to the sulci for the planum suprasetale. The olfactory canal is never enclosed by descending flanges of the *cristae cranii*.

POSTORBITOFRONTAL: The right postorbitofrontal is preserved but incomplete (fig. 21). It

resembles an arrow in dorsal view, with articular surfaces for the parietal, frontal, jugal, and squamosal. The posterior squamosal process is long and slender, with a deep ventral keel that fits into a slot on the dorsal surface of the squamosal. It receives the dorsal ramus of the jugal in a slot along the posterior surface of the jugal process. The facet for the frontal is rugose and, posterior to it, a transverse ridge perpendicular to the squamosal process is present, as in *Clidastes* and *Globidens* (Russell, 1967), and the parietal facet is deep.

JUGAL: The right jugal is preserved but incomplete (fig. 22). It is slender and simple, as it is in *Clidastes* (e.g., *Clidastes liodontus* AMNH FARB 192) and, like *Clidastes*, lacks the posteroventral process present in most other mosasaurids (e.g., *Tylosaurus proriger* FHSM VP-3, *Mosasaurus hoffmannii* MNHN AC 9648; Street and Caldwell, 2017), interpreted by Russell (1967: 24) as the attachment point for the quadratomaxillary ligament. The medial surface is concave, and, while broken anteriorly, bears a deep sulcus that would have received the lateral process of the ectopterygoid. The horizontal ramus is reniform in cross section, and the angle between the horizontal and vertical rami is slightly obtuse (approximately 110°), which is similar to what is typically

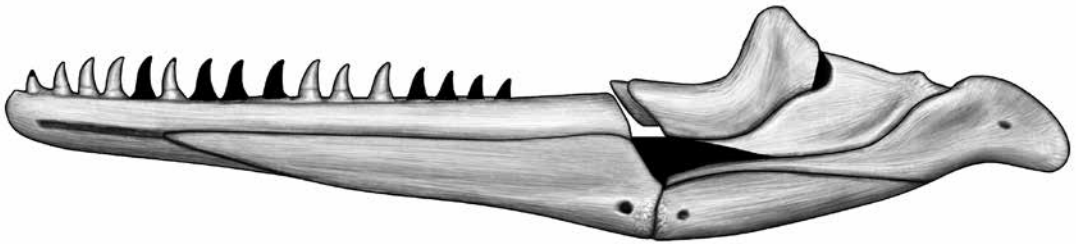


FIGURE 12. Idealized drawing of the jaw of *Jormungandr walhallaensis* in right medial view. The overall shape of the bones as drawn here are an estimate of what they may have looked like before distortion, and not an exact line drawing of NDGS 10838. Illustration by Henry Sharpe.

seen in *Platecarpus* (e.g., *Platecarpus tympaniticus* FHSM VP-322), but less than in *Clidastes* (e.g., approximately 125° in *Clidastes propython* KUVV 1000) and greater than in derived mosasaurines and *Tylosaurus* (e.g., approximately 90° in *Mosasaurus hoffmannii* MNHN AC 9648 and *Tylosaurus proriger* FHSM VP-3).

SQUAMOSAL: Both squamosals are preserved but incomplete (fig. 23). In dorsal and ventral views, they approximate a curved arrow, with a triangular body and long, slightly curved anterior ramus; overall, the squamosal is more slender in NDGS 10838 than in *Mosasaurus hoffmannii* (Street and Caldwell, 2017). The ventral margin is recurved and medially inset posteriorly, producing a pointed, anteriorly oriented process that marks the beginning of the quadrate facet, which is narrow and triangular in ventral view. The anterior ramus bears a deep groove to receive the ventral keel of the postorbitofrontal. Its medial margin curves laterally, forming a tall crest that borders an oblique, grooved, subtriangular fossa for the suspensorial ramus of the parietal. In dorsal view, its posterior margin is broadly pointed, rather than sharply acuminate as it is in most other mosasaurids.

QUADRATE: The right quadrate is complete and largely undistorted, while only the top third

of the left is preserved but crushed (figs. 24, 25). It is most similar to *Mosasaurus* in overall shape; in lateral view, it is taller than wide, and its anterior margin is straight and not distinctly curved as it is in *Mosasaurus missouriensis* (Konishi et al., 2014). The tympanic ala rim has a distinct anterodorsal corner but lacks the anteroventral corner diagnostic of *Mosasaurus hoffmannii* (Street and Caldwell, 2017). The suprastapedial process is of moderate length, ending near the midpoint of the main shaft and enclosing an almond-shaped stapedial notch sensu Russell (1967). It is not fused to the “infrastapedial process,” which comprises a posterolateral bulge and posteromedial process sensu Palci et al. (2021). Like *Clidastes propython*, the posterolateral bulge and posteromedial process are level with one another and connected posteriorly by a subtle ridge, unlike in *Mosasaurus*, in which the posterolateral bulge (process) is ventral to the posteromedial process (Palci et al., 2021).

The tympanic ala rim is grooved and the alar conch is deep, as in *Mosasaurus* (Konishi et al., 2014; Palci et al., 2021), though not quite as deep as in plioplatecarpines (Russell, 1967). The posteroventral margin of the alar rim curves steeply dorsally, forming a crest that is continuous with the posterolateral bulge. This is some-

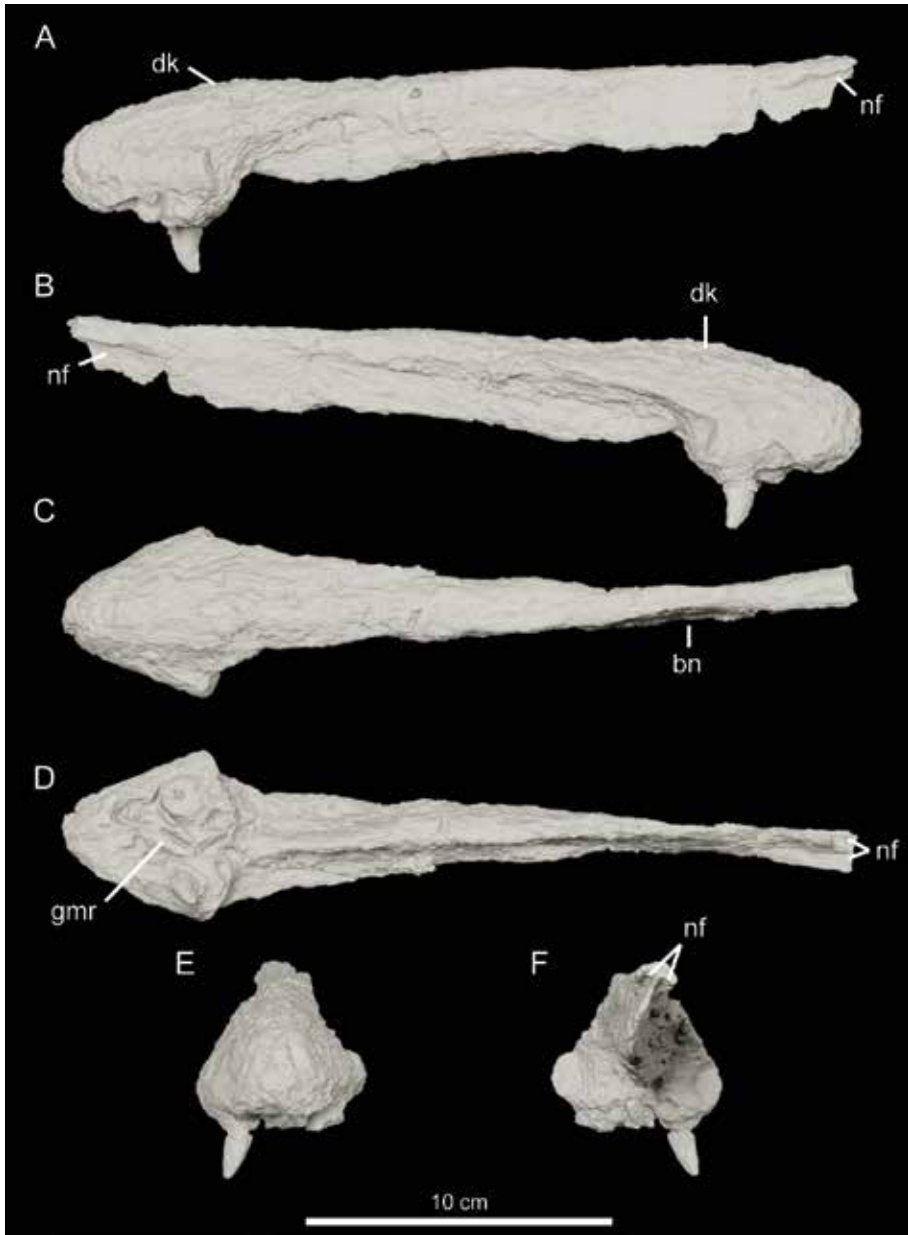


FIGURE 13. Premaxilla of NDGS 10838 in **A**, left lateral; **B**, right lateral; **C**, dorsal; **D**, ventral; **E**, anterior; and **F**, posterior views. Abbreviations: **bn**, bony naris; **dk**, dorsal keel; **gmr**, grooved median ridge; **nf**, nasal facet.

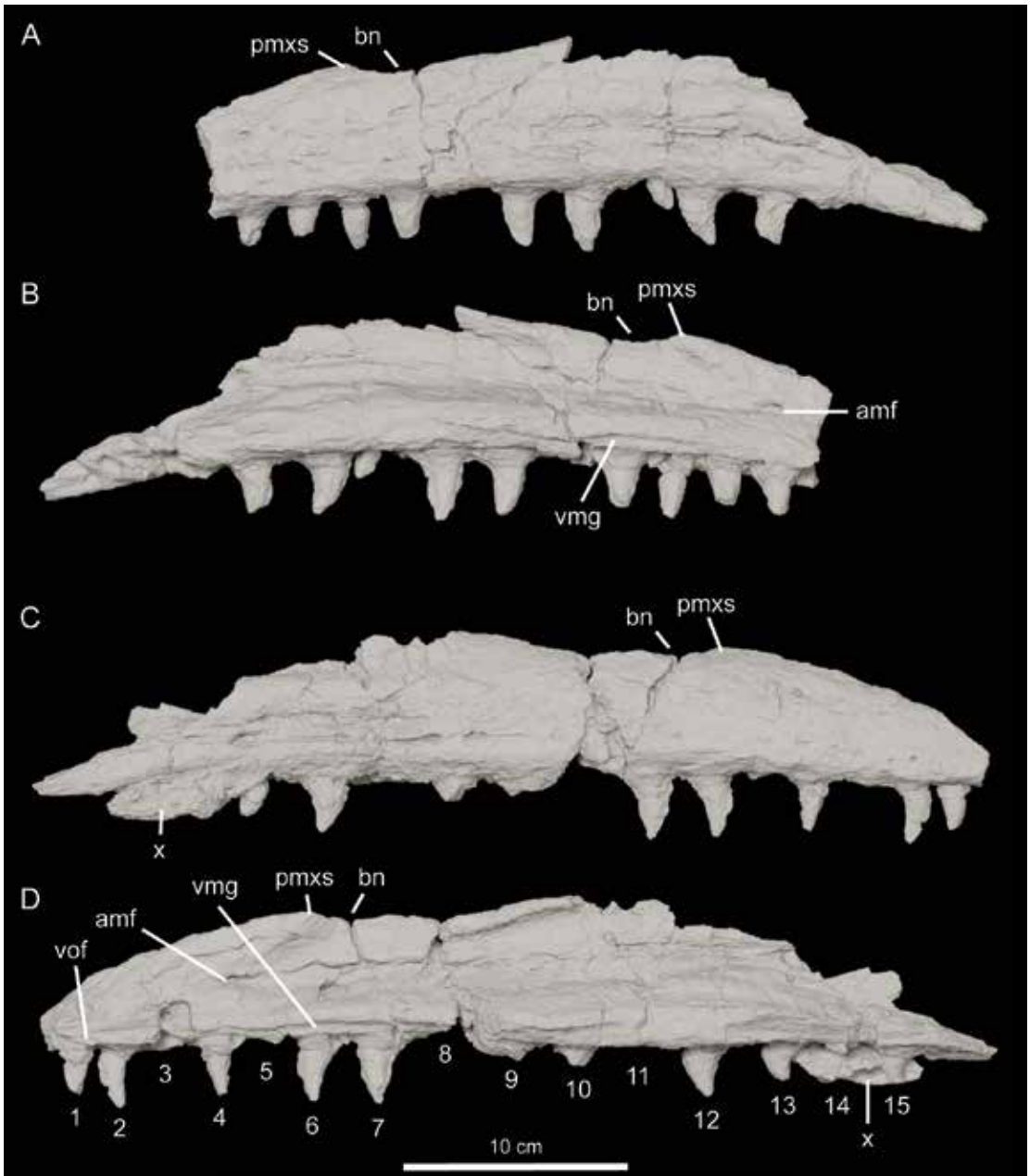


FIGURE 14. **A, B**, Left and **C, D**, right maxillae of NDGS 10838 in **A, C**, lateral and **B, D**, medial views. In **D**, tooth positions are numbered. Abbreviations: **amf**, anterior medial foramen; **bn**, bony naris; **pmxs**, posterior terminus of the suture with the premaxilla; **vmg**, ventromedial groove; **vof**, vomer facet; **x**, unidentified fragment.

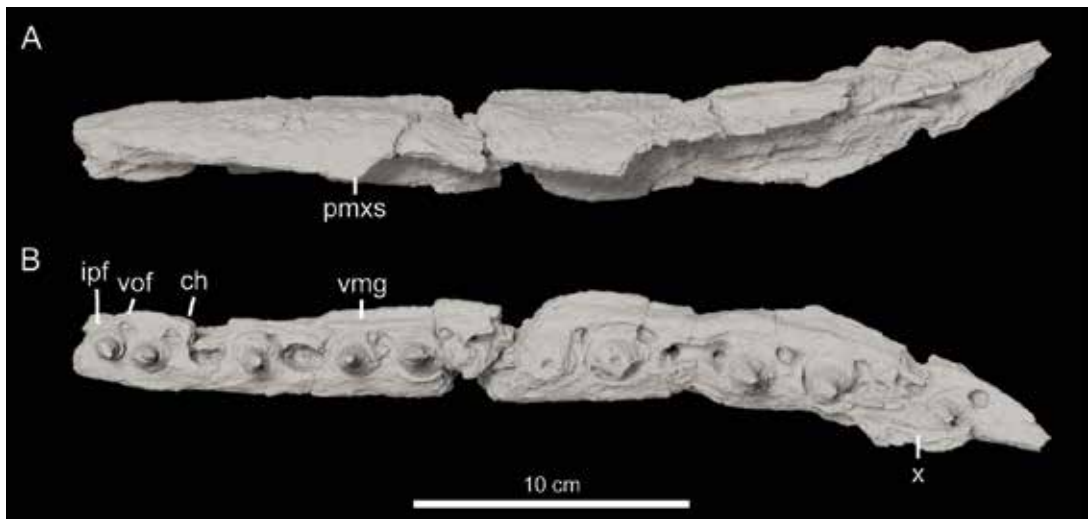


FIGURE 15. Right maxilla of NDGS 10838 in **A**, dorsal and **B**, ventral views. Abbreviations: **ch**, lateral margin of the choana; **ipf**, facet for the incisive process of the premaxilla; **pmxs**, posterior terminus of the suture with the premaxilla; **vmg**, ventromedial groove; **vof**, vomer facet; **x**, unidentified fragment.

what similar to what is seen in *Clidastes* and *Tylosaurus peminensis*, but in NDGS 10838, the crest is sharper and longer, forming a much more acute angle with the shaft and approaching the condition of the posterolateral process seen in *Mosasaurus hoffmannii* (Palci et al., 2021). As is typical in mosasauroids, the quadrate is triradiate in dorsal view, giving rise to the suprastapedial process, alar rim, and cephalic condyle.

In anterior view, the outline of the quadrate is rectangular, like in *Mosasaurus*, except that the lateral margin is slightly convex, as in *Clidastes*. Its anterior surface is flat except for a dorsal, subrectangular depression, interpreted by Russell (1967) and Street and Caldwell (2017) as the origin of the *M. adductor mandibulae externus profundus* in *Mosasaurus hoffmannii*. At the midpoint of the ventral margin, there is a slight dorsal extension of the mandibular condyle. The mandibular condyle is mediolaterally elongate, and its ventral surface is straight to slightly convex, rather than distinctly convex as in *Mosasaurus* (e.g., *Mosasaurus hoffmannii* NJSM 11052), *Gnathomortis* (Lively, 2020), and *Platecarpus* (e.g., *Platecarpus*

tympaniticus KUVV 27816) or concave and saddlelike as in *Clidastes* (e.g., *Clidastes propython* AMNH FARB 1575) and *Tylosaurus* (e.g., *Tylosaurus proriger* AMNH FARB 1555).

In posterior view, the suprastapedial process is slightly medially deflected, like in mosasaurines and *Tylosaurus proriger* (Russell, 1967), and mediolaterally constricted, like in *Clidastes* (e.g., *Clidastes liodontus* YPM VP 1335), *Tylosaurus proriger* (e.g., AMNH FARB 1555), *Gnathomortis* (Lively, 2020), and *Prognathodon overtoni* (e.g., KUVV 950). Its tip is broad, does not taper, and has a gently concave distal margin. The suprastapedial process also bears a distinct, rectangular depression for attachment of the *M. depressor mandibulae*; the attachment site is larger than that of *Clidastes*, but smaller than that of *Mosasaurus hoffmannii* (e.g., MNHN AC 9648).

The stapedial pit is a narrow oval (i.e., 1.8× taller than wide) like that of *Clidastes liodontus* (e.g., AMNH FARB 192), rather than either a broad oval, as in *Mosasaurus* (e.g., 1.5× taller than wide in *Mosasaurus hoffmannii* NJSM 11052), or nearly circular, as in *Prognathodon overtoni* (e.g., 1.1× wider than tall in KUVV 950). Like *Mosasaurus* (e.g., *Mosasaurus hoffmannii*

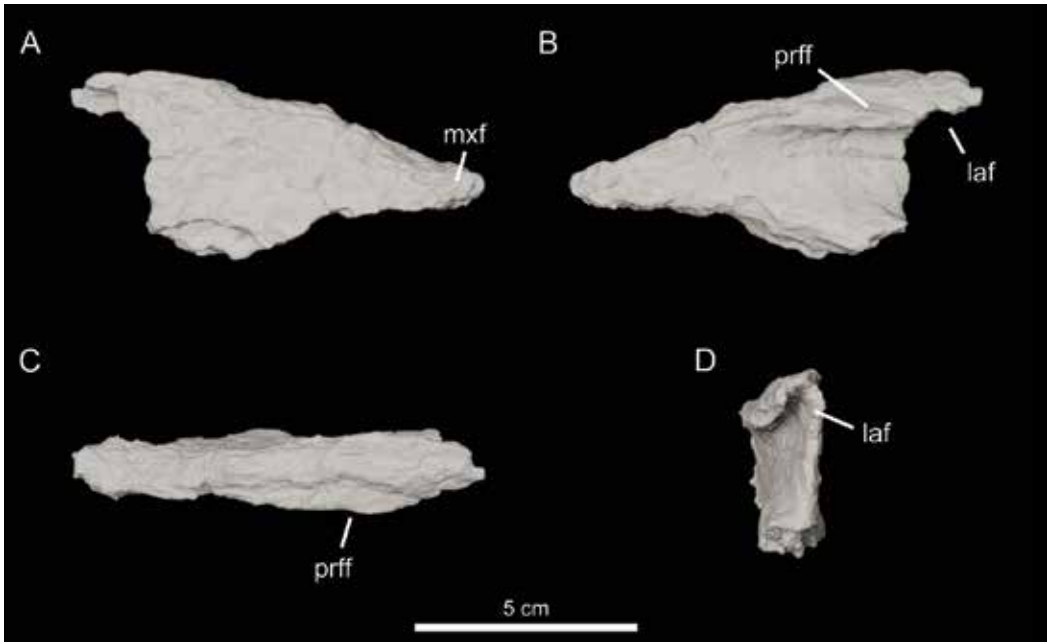


FIGURE 16. Bone tentatively identified as the right lacrimal of NDGS 10838 in **A**, lateral; **B**, medial; **C**, dorsal; and **D**, posterior views. Abbreviations: **laf**, lacrimal foramen; **mxf**, maxilla facet; **prff**, prefrontal facet.

MNHN AC 9648), the stapedia pit is set within a sulcus on the medial face of the bone. However, unlike any other known mosasaurid, the ventral terminus of the sulcus is lipped, rather than flush with the surface of the bone, and its anterior margin is distinctly taller than its posterior margin in both quadrates. In medial view, the anterior margin of the bone is straight and possesses an anterodorsal corner.

PALATE

VOMER: The anterior portion of the left vomer is preserved and disarticulated (fig. 26), providing the first opportunity to describe this bone in a mosasaurine in three dimensions. Anterolaterally, an oblong, gently concave facet cups the maxilla. In dorsal and ventral views, the posterior margin of the maxilla facet is notched, demarcating the anterior margin of the vomeronasal fenestra. The main body of the bone is mediolaterally compressed and possesses grooves medially and ventrally.

PALATINE: The incomplete and crushed right palatine is preserved stuck to the right prefrontal (figs. 17, 27). The vomer process is incomplete and forms the medial margin of the choana. In ventral view, the articular surface for the pterygoid is a shallow, subtriangular fossa bounded medially by a low crest. The maxilla facet is a deep, slotlike groove on the lateral margin of the bone; posterior to it, a foramen (possibly for the palatine branch of the maxillary artery) is present (Polcyn et al., 2022: suppl.).

PTERYGOID: Both pterygoids are preserved and nearly complete, the right bone more so than the left (figs. 18, 28). The left bone preserves at least 16 tooth positions, and the right preserves at least 15 tooth positions, which is most like *Clidastes*, *Plotosaurus*, and basal mosasauroids (e.g., *Tethysaurus*; Bardet et al., 2003); such a high tooth count for a large (>5 m body length) mosasaur individual is unusual, given that other large-bodied taxa (e.g., *Mosasaurus*, *Tylosaurus*, *Prognathodon*) typically only have between eight and 10 tooth positions

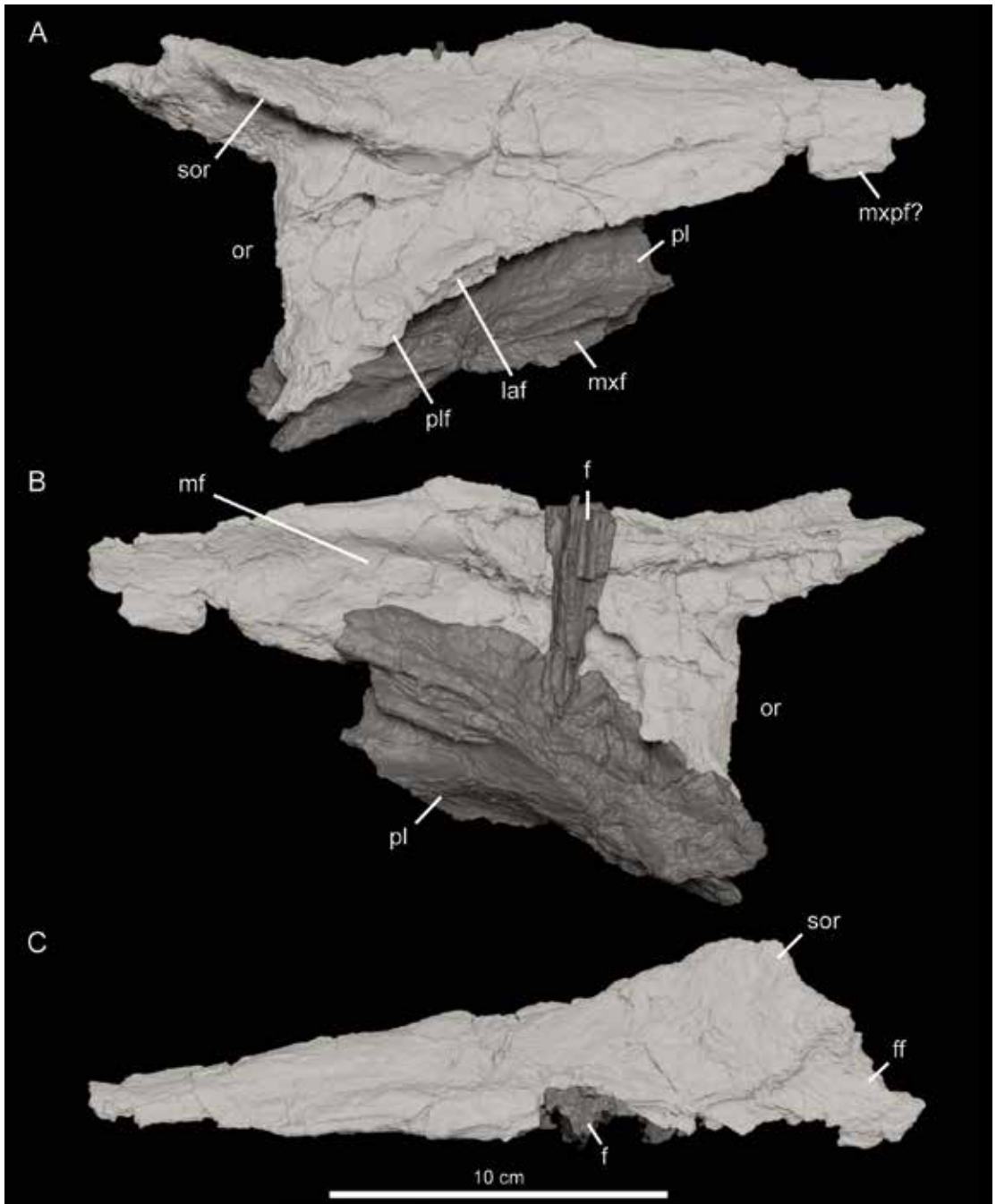


FIGURE 17. Right prefrontal (light) and right palatine of NDGS 10838, with focus on the prefrontal in **A**, lateral; **B**, medial; and **C**, dorsal views. Abbreviations: **f**, frontal; **ff**, frontal facet of the prefrontal; **laf**, lacrimal facet of the prefrontal; **mf**, medial fossa of the prefrontal; **mxf**, maxilla facet of the palatine; **mxpf?**, possible maxilla posterodorsal process facet of the prefrontal; **or**, orbit; **pl**, palatine; **plf**, palatine facet of the prefrontal; **sor**, supraorbital ridge of the prefrontal.

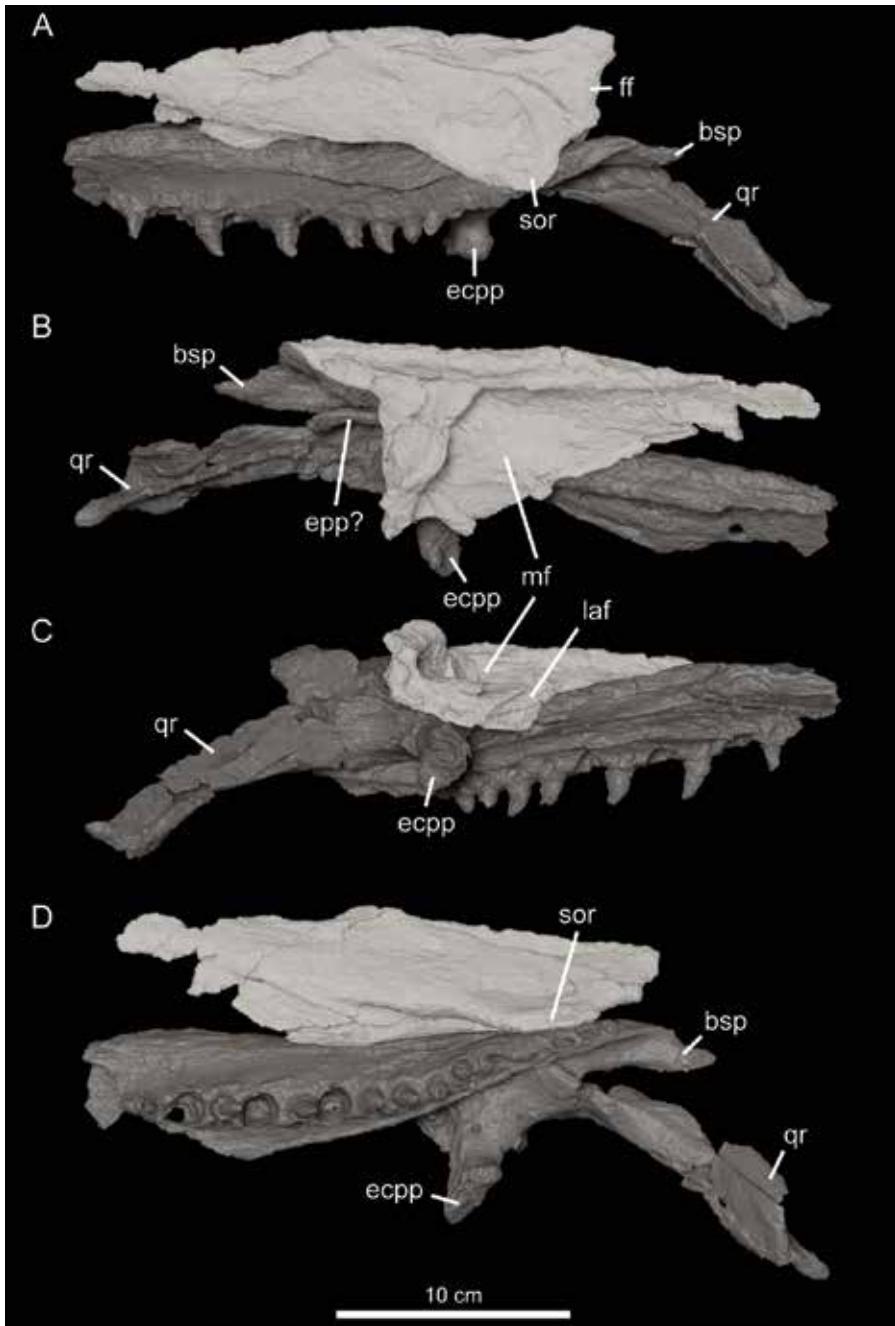


FIGURE 18. Left prefrontal (light) and right pterygoid (dark) of NDGS 10838. **A**, prefrontal in dorsal view; **B**, prefrontal in medial view; **C**, pterygoid in lateral view; and **D**, pterygoid in ventral view. Abbreviations: **bsp**, basisphenoid process of the pterygoid; **ecpp**, ectopterygoid process of the pterygoid; **epp?**, possible epipterygoid; **ff**, frontal facet of the prefrontal; **laf**, lacrimal facet of the prefrontal; **mf**, medial fossa of the prefrontal; **qr**, quadratic ramus of the pterygoid; **sor**, supraorbital ridge of the prefrontal.

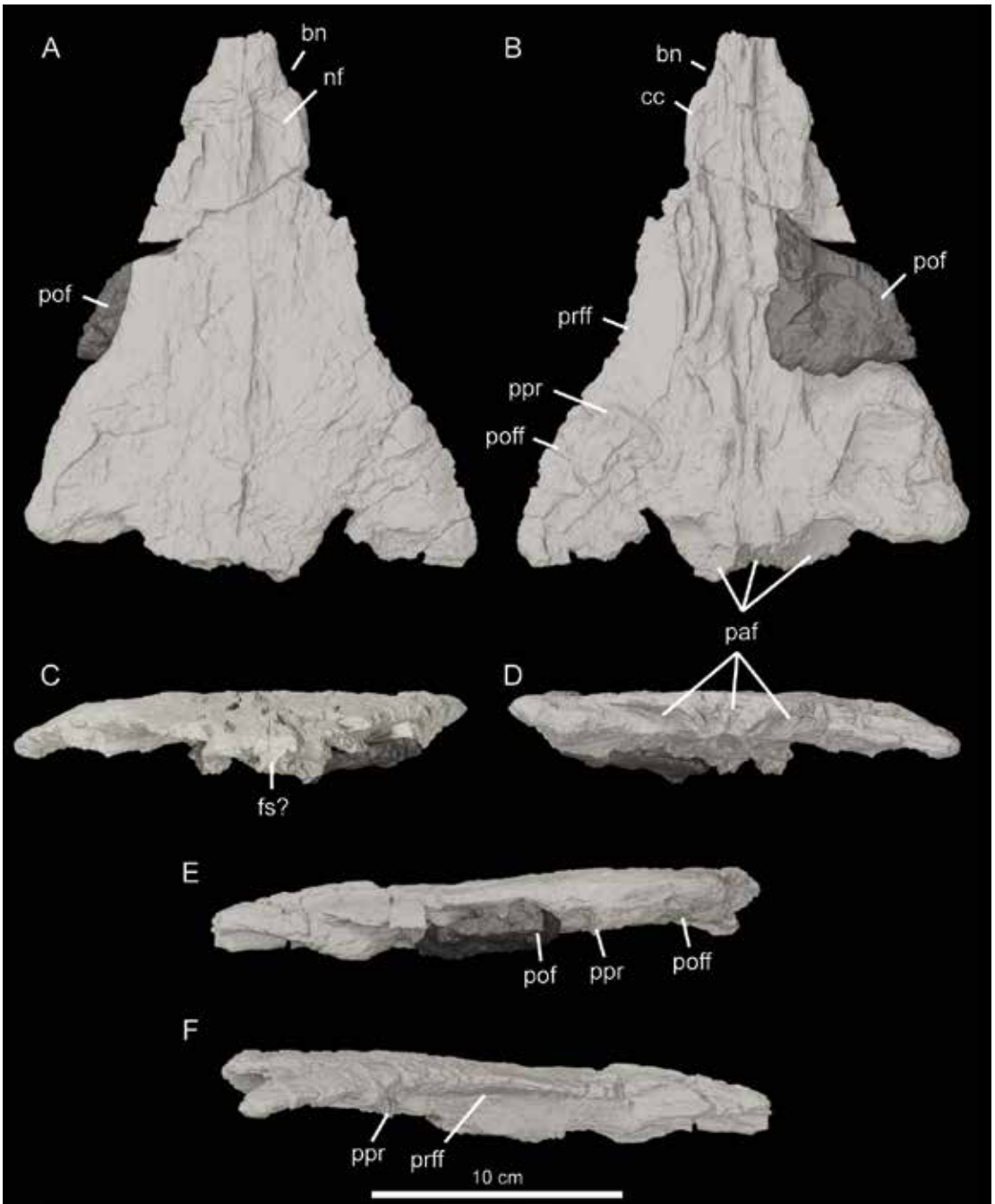


FIGURE 19. Frontal of NDGS 10838 in **A**, dorsal, **B**, ventral, **C**, anterior, **D**, posterior, **E**, left lateral, and **F**, right lateral views. Abbreviations: **bn**, bony naris; **cc**, crista cranium; **fs?**, possible suture between frontals; **nf**, narial fossa; **paf**, parietal facet; **pof**, postorbital foramen; **poff**, postorbital foramen facet; **ppr**, ridge separating prefrontal and postorbital foramen; **prff**, prefrontal facet.

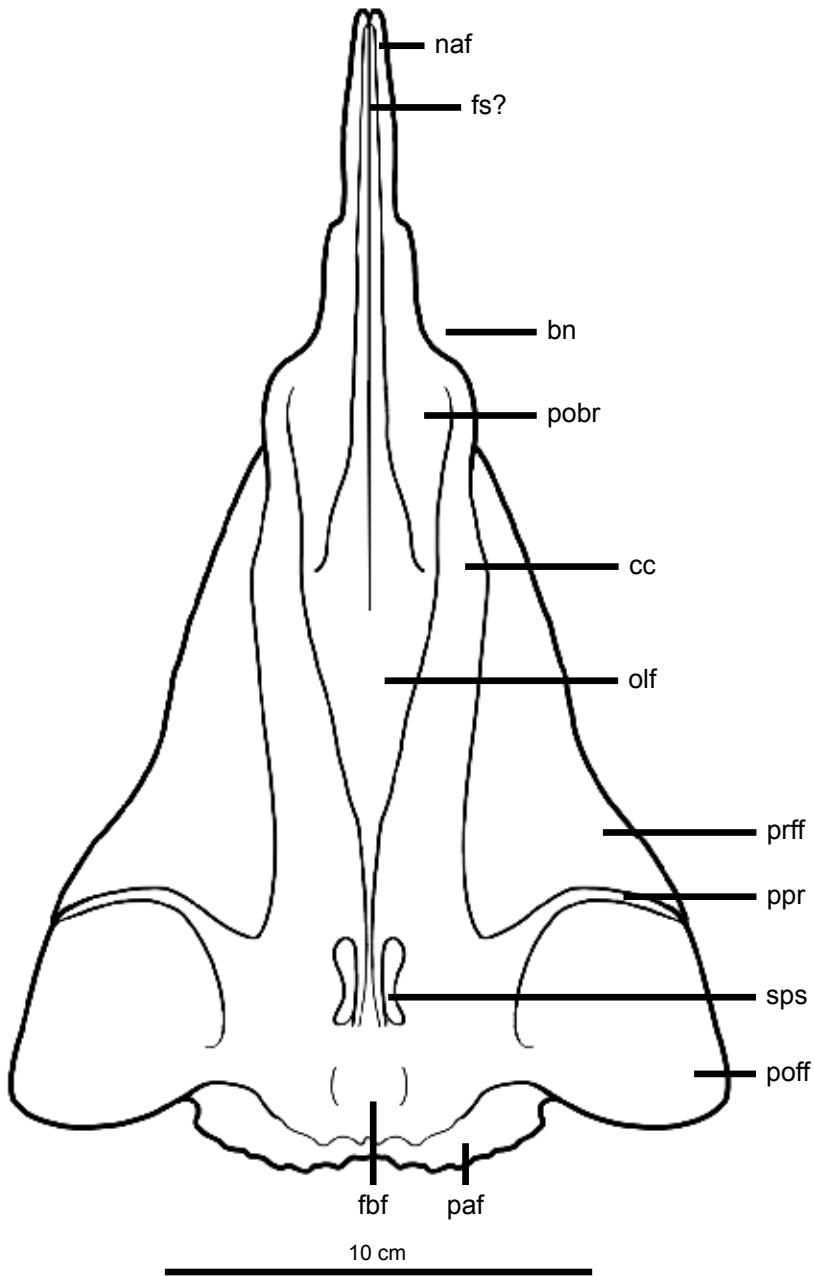


FIGURE 20. Idealized drawing of the frontal of *Jormungandr walhallaensis* in ventral view. Notes: the anterior process is preserved stuck to the right prefrontal, and has been rearticulated here; the overall shape of the bone as drawn here is an estimate of what it may have looked like before distortion, and *not* an exact line drawing of NDGS 10838. Abbreviations: **bn**, bony naris; **cc**, crista cranium; **fbf**, forebrain fossa; **fs?**, possible suture between unfused frontals; **naf**, nasal facet; **olf**, olfactory canal; **paf**, parietal facet; **pobr**, parolfactory bulb recess; **poff**, postorbitofrontal facet; **ppr**, ridge separating prefrontal and postorbitofrontal facets; **prff**, prefrontal facet; **sps**, sulcus for the planum suprasetale.

in each pterygoid (Russell, 1967; Lingham-Soliar, 1995; Konishi et al., 2011; Zietlow, 2020; but see Konishi and Caldwell [2007: 71] for the high pterygoid tooth count variation in *Plesio-platecarpus planifrons*). The pterygoid teeth are distinctly smaller than the marginal teeth; they are largest in the middle of the toothrow and become progressively smaller posteriorly. The basal cross sections of the pterygoid teeth are circular, rather than mediolaterally compressed like the marginal teeth. Like *Mosasaurus* (Street and Caldwell, 2017), the toothrow projects ventrally from the main shaft of the bone on a descending flange. In ventral view, the path of the toothrow along the bone is slightly curved; while it is not nearly sigmoidal as it is in *Tylosaurus* (e.g., *Tylosaurus proriger* AMNH FARB 4909) and *Platecarpus* (e.g., *Platecarpus tympaniticus* AMNH FARB 1820/1821), it is not perfectly straight, as it is in *Clidastes* (e.g., *Clidastes liodontus* AMNH FARB 192). Like *Clidastes*, the toothrow extends nearly the entire ventral length of the bone.

The basisphenoid process is short and pointed, and the ectopterygoid process projects at a slightly acute angle from the main shaft of the bone. Its articular surface for the ectopterygoid is ovate and rugose, its base continuous with the elongate quadratic ramus. The posterior margin of the quadratic ramus is spatulate in ventral view, its dorsal surface possesses a tall keel, and its medial surface is deeply excavated by a fossa (fig. 18). Like *Clidastes* (Russell, 1967: 44), a deep groove is present lateral to the dorsal keel, possibly for insertion of the *M. protractor pterygoideus*. In dorsal view the anterolateral surface of the main shaft is covered by a large, broad, obliquely oriented fossa. A thin, rodlike bone is preserved dorsal to the right pterygoid, between it and the overlying left prefrontal; given its position and general shape, this may be an epipterygoid, but it could not be examined in detail without damaging the specimen.

ECTOPTERYGOID: The delicate right ectopterygoid is preserved, though incomplete, and slightly dorsoventrally flattened (fig. 29). It is very similar

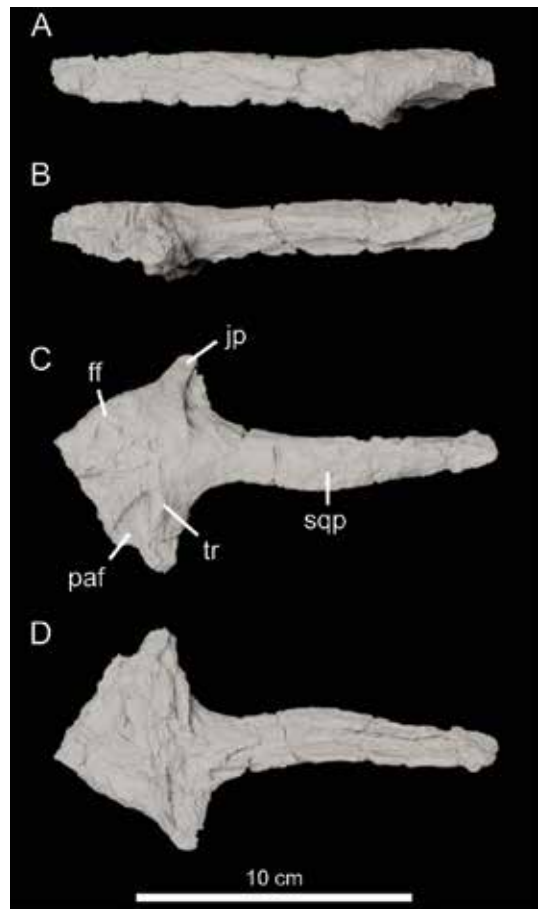


FIGURE 21. Right postorbitofrontal of NDGS 10838 in **A**, lateral; **B**, medial; **C**, dorsal; and **D**, ventral views. Abbreviations: **ff**, frontal facet; **jp**, jugal process; **paf**, parietal facet; **sqp**, squamosal process; **tr**, transverse ridge.

in shape to that of *Mosasaurus hoffmannii* (Street and Caldwell, 2017), which was previously misidentified as a lacrimal (Lingham-Soliar, 1995); in dorsal and ventral views, the preserved portion approximates a boomerang. Its ventral surface is gently convex and its posterior margin is slightly ventrally deflected. Both dorsal and ventral surfaces are smooth, like in *Mosasaurus* (Lingham-Soliar, 1995; Street and Caldwell, 2017). The pterygoid ramus is shorter and more robust than the anteriorly incomplete jugal ramus, which bears a shallow anterolateral notch at its base. The



FIGURE 22. Right jugal of NDGS 10838 in **A**, lateral and **B**, medial views. Abbreviations: **ecpf**, ectopterygoid facet; **x**, unidentified fragments.

rami converge posterolaterally at nearly a right angle, and the curvature along the anteromedial margin is arcuate.

MANDIBLE

DENTARY: Both dentaries are preserved; the right is complete and the left is incomplete beyond the 12th tooth position (figs. 30, 31). The right dentary bears 16 tooth positions, like *Cleidastes liodontus* (e.g., AMNH FARB 192) and *Mosasaurus lemonnieri* (e.g., IRScNB R 299), and similar to *Mosasaurus conodon* (AMNH FARB 1380; at least 15) but more than is typical in *Mosasaurus hoffmannii* (14 in NJSM 11053, MNHN AC 9648, IRScNB R 26, and IRSNB R 27) and other large-bodied mosasaurs (e.g., 13 in *Tylosaurus proriger* FHSM VP-3 and *Progathodon solvayi* IRScNB R 33; 14 in *Progathodon overtoni* TMP 2007.034.0001), as well as plioplatecarpines (e.g., 12 in *Platecarpus tympaniticus* FHSM VP-322 and AMNH FARB

1820/1821). Like the maxilla, the dentary is mediolaterally robust (approximately twice as wide as the tooth bases), particularly in its middle. Tooth morphology is identical to that of the maxilla, including the laterally compressed crown base.

In lateral view, the dentary is elongate and approximately rectangular, deepening posteriorly; at its maximum height, it is approximately five times as long as tall. Its anterior margin is only slightly convex. A row of neurovascular foramina is present parallel to the toothrow, as is typical of mosasauroids and other nonophidian squamates, and they are not set within a sulcus. An edentulous anterior projection is present and long (i.e., at least one tooth position long) and it lacks the distinct dorsal ridge present in *Tylosaurus proriger* (e.g., AMNH FARB 1555) and *Plesiotylosaurus crassidens* (Lindgren, 2009).

The Meckelian canal is a deep, slotlike groove that begins at a point about level with the anterior margin of the first tooth position and expands dorsoventrally into the mandibular channel posteriorly. Anteriorly, the mandibular symphysis is present as indistinct dorsal and ventral rugosities just posterior to the anterior margin. The lateral and medial dentary walls are level, as in all mosasauroids except *Plioplatecarpus marshi* and *Gavialimimus almaghribensis*, in which the medial wall is taller (Konishi and Caldwell, 2011: appendix 3; Strong et al., 2020).

SPLENIAL: Both splenials are preserved, the right in articulation with the dentary (figs. 30, 32). They are approximately half as long as the dentary, and are exposed ventral to the dentary in lateral view. The dorsal half of the lateral surface possesses a shallow facet, bounded anteroventrally by a groove, for articulation with the dentary.

A deep dorsal slot receives the prearticular process of the fused prearticular-articular posteriorly and is bounded laterally and medially by thin ascending alae. The dorsolateral ala is low and broadly convex, as is typical of mosasauroids. The dorsomedial ala is tall and roughly

triangular like in some *Platecarpus* (e.g., *Platecarpus tympaniticus* KUVV 1001), *Mosasaurus conodon* (e.g., AMNH FARB 1380), *Gnathomortis stadtmani* (Lively, 2020), and some *Mosasaurus hoffmannii* (e.g., AMNH FARB 14815), unlike the low, broadly arcuate ala present in *Tylosaurus* (e.g., *Tylosaurus nepaeolicus* AMNH FARB 134), some *Clidastes* (e.g., *Clidastes propython* KUVV 1000), and other *Platecarpus* (e.g., *Platecarpus* sp. AMNH FARB 2155). Due to breakage, it is unclear whether it once possessed a recurved dorsal process, as seen in some *Mosasaurus* (e.g., *Mosasaurus hoffmannii* IRScNB R 302; Street and Caldwell, 2017). Its anterodorsal margin lacks the deep notch diagnostic of *Tethysaurus nopcsai* (Bardet et al., 2003).

On its medial surface, the anterior mylohyoid foramen is just anterior to the angular facet. It is roughly subcircular, neither elongate, like in *Mosasaurus* (Street and Caldwell, 2017) and *Gnathomortis* (Lively, 2020), nor circular as is typically seen in *Clidastes* (e.g., *Clidastes propython* AMNH FARB 1593), *Tylosaurus* (e.g., *Tylosaurus proriger* AMNH FARB 14799), and *Platecarpus* (e.g., *Platecarpus tympaniticus* KUVV 1001). The angular facet is ovoid with a flat, vertical medial margin, similar to that of *Mosasaurus hoffmannii* (Street and Caldwell, 2017). Its center is mostly concave, bounded by three low flanges (one dorsally and two ventrally).

ANGULAR: Both angulars are preserved, the left disarticulated (fig. 33) and the right in articulation with the rest of the posterior mandibular unit (fig. 34). They are approximately half as long as the splenials. The splenial facet is convex and mirrors the angular facet on the splenial. With respect to overall shape, the angulars of NDGS 10838 are very similar to those of *Clidastes* (e.g., *Clidastes liodontus* AMNH FARB 192, *Clidastes propython* KUVV 1000), where both dorsomedial and dorsolateral alae are low and broadly convex. The dorsolateral ala is taller than the dorsomedial ala, and they bound a deep, V-shaped slot that

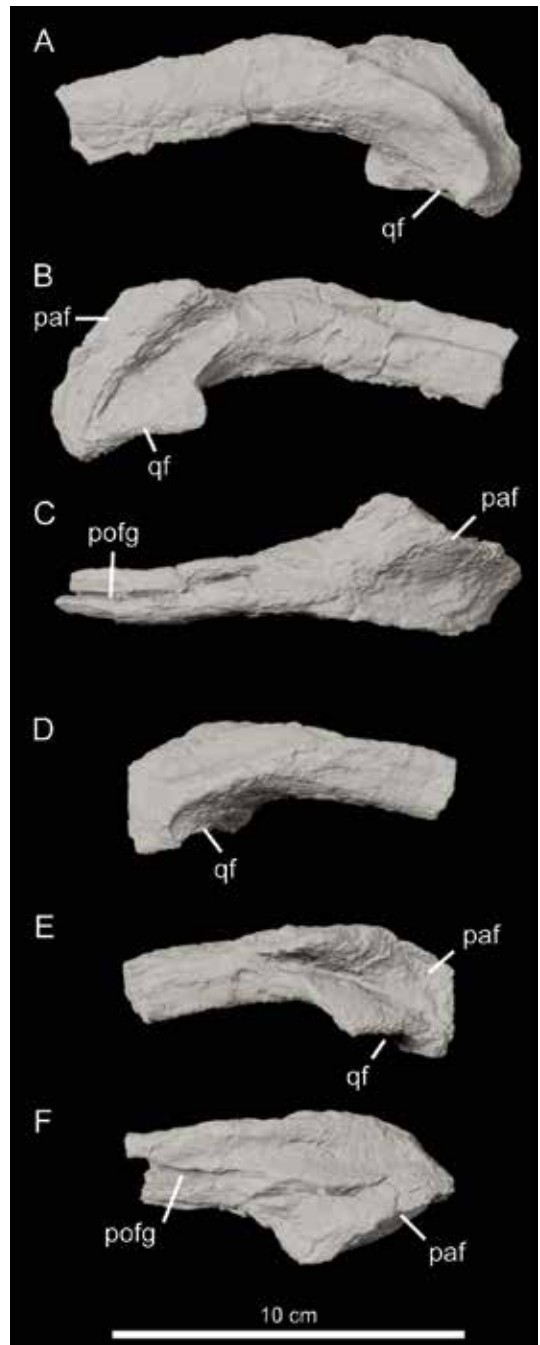


FIGURE 23. A–C, Left and D–F, right squamosals of NDGS 1838 in A, D, lateral, B, E, medial, and C, F, dorsal views. Abbreviations: **paf**, parietal facet; **pofg**, groove for the posterior process of the postorbitofrontal; **qf**, facet for the cephalic condyle of the quadrate.

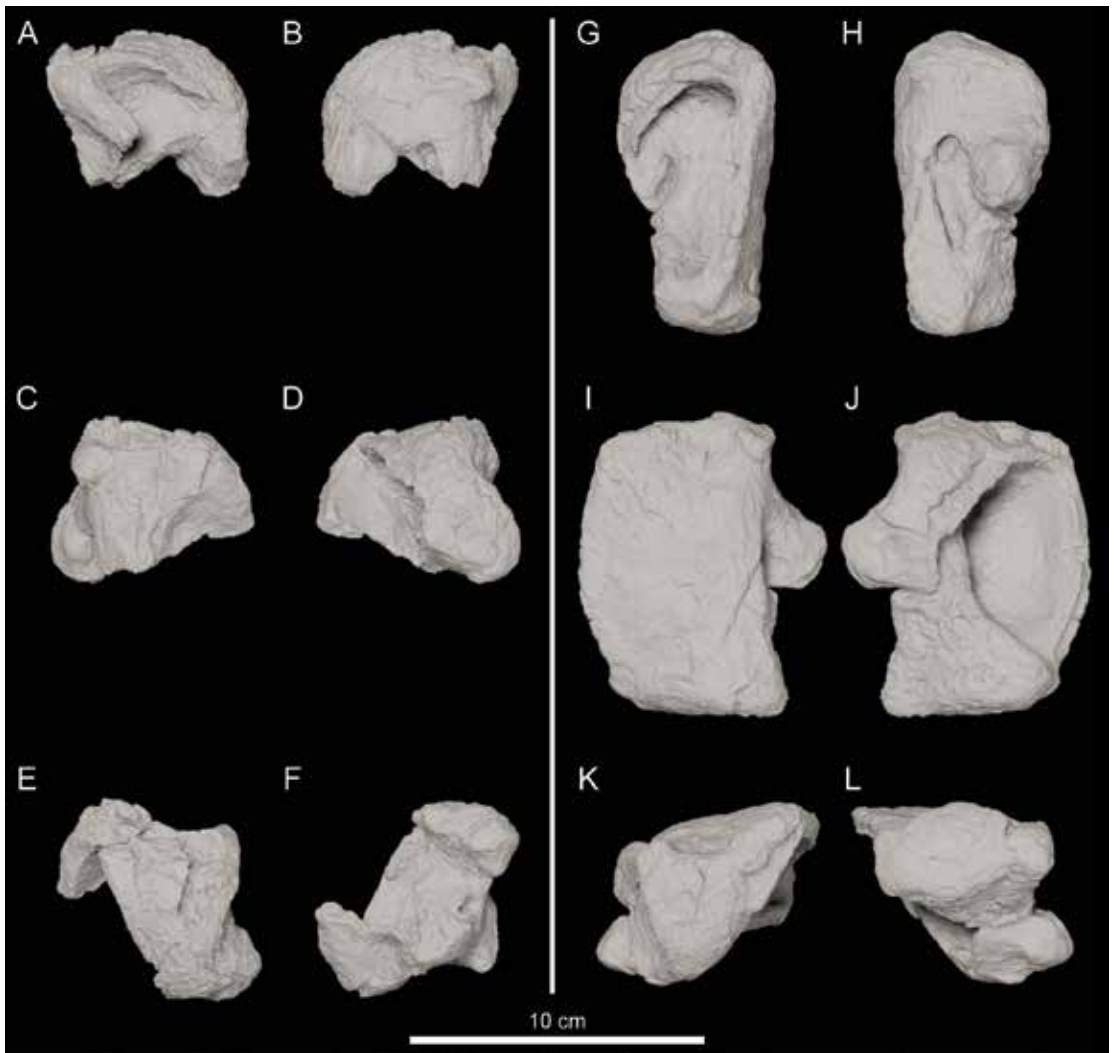


FIGURE 24. Left, A–F, and right, G–L, quadrates of NDGS 10838 in A, G, lateral; B, H, medial; C, I, anterior; D, J, posterior; E, K, dorsal; and F, L, ventral views.

articulates with the surangular laterally and prearticular process medially. It is unclear whether the dorsomedial ala articulated with the medial descending wing of the coronoid, as is typical of mosasaurines (Russell, 1967). Its dorsolateral surface has a shallow fossa that underlies part of the surangular. The posterior mylohyoid foramen is small and oblong.

CORONOID: Both coronoids are preserved, the left disarticulated (fig. 35) and the right in articu-

lation with the rest of the posterior mandibular unit (fig. 30). As is typical of mosasaurids, the bone is saddlelike, with lateral and medial descending wings that sheathe the surangular dorsally. Like *Mosasaurus* (e.g., *Mosasaurus conodon* AMNH FARB 1380) and *Prognathodon* (e.g., *Prognathodon overtoni* KUVVP 950), both descending wings are well developed and extend farther ventrally than in *Clidastes* (e.g., *Clidastes liodontus* AMNH FARB 192), *Tylosaurus* (e.g., *Tylosaurus*

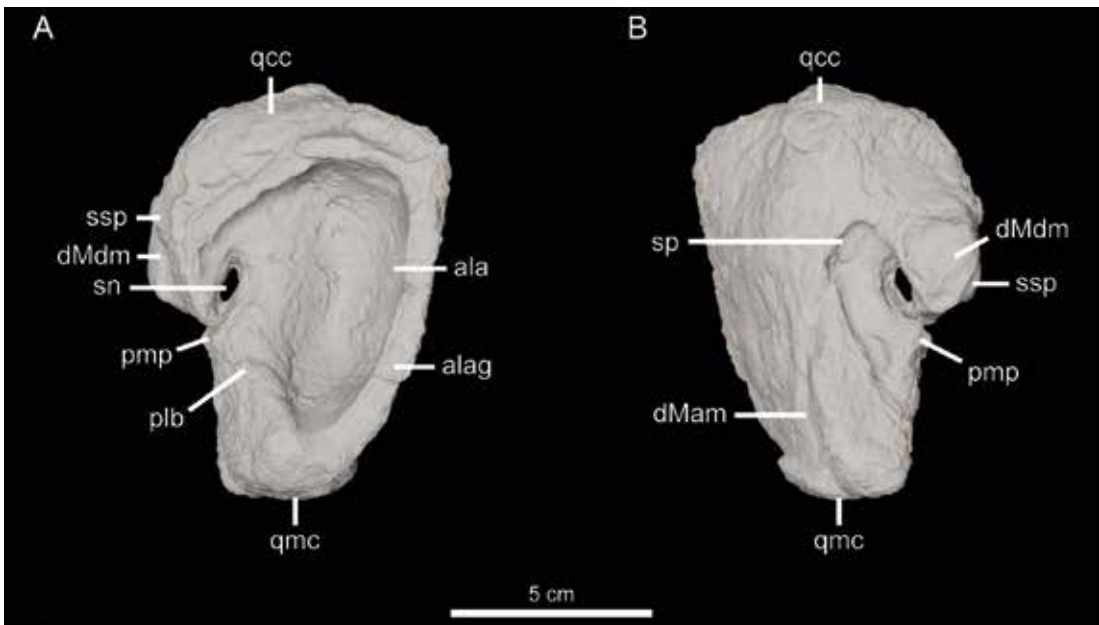


FIGURE 25. Right quadrate of NDGS 108383 in **A**, lateral, and **B**, medial, views, with key anatomical details labeled. Abbreviations: **ala**, tympanic ala; **alag**, alar groove; **dMam**, depression for the origin of the adductor mandibulae externus profundus; **dMdm**, depression for the attachment of the depressor mandibulae; **plb**, posterolateral bulge; **pmp**, posteromedial process; **qcc**, cephalic condyle; **qmc**, mandibular condyle; **sn**, stapedial notch; **sp**, stapedial pit; **ssp**, suprastapedial process.

nepaeolicus AMNH FARB 1565), and *Platecarpus* (e.g., *Platecarpus tympaniticus* KUVV 1007). The medial descending wing is not excavated by a medial crescentic pit, as exemplified by *Mosasaurus hoffmannii* (e.g., NJSM 11053). Like most mosasaurines (e.g., *Mosasaurus conodon* AMNH FARB 1380, *Prognathodon overtoni* KUVV 950, *Clidastes propython* KUVV 1000), the dorsal margin is strongly concave; the posterior wing forms an angle of approximately 110° with dorsal margin of the anterior ramus, which is slightly steeper than that of *Clidastes liodontus* (e.g., AMNH FARB 192; 120°). Like *Clidastes* (e.g., *Clidastes liodontus* AMNH FARB 192), *Prognathodon overtoni* (Konishi et al., 2011), and *Mosasaurus* (e.g., *Mosasaurus conodon* AMNH FARB 1380), the lateral surface of the posterior wing is excavated by a sulcus that is continuous with the lateral surangular adductor fossa. The ventrolateral margin of the bone is broadly U-shaped and only gently emarginated anteriorly, rather than possessing

a deep, C-shaped notch as in *Mosasaurus hoffmannii* (e.g., NJSM 11052).

SURANGULAR: The left surangular is preserved in articulation with the prearticular-articular (fig. 34), and the right is preserved in articulation with the rest of the posterior mandibular unit (fig. 30). Both bones are mostly complete, roughly trapezoidal in overall shape, and deeper (about $2.4\times$ as long as it is tall) than those of *Clidastes* (e.g., *Clidastes liodontus* AMNH FARB 192; about $3.4\times$ longer than tall), similar to some specimens of *Mosasaurus hoffmannii* (e.g., IRScNB R 24; Street and Caldwell, 2017) but not quite as deep as other specimens (e.g., IRScNB R 302, $2.2\times$ longer than tall; Street and Caldwell, 2017). The coronoid buttress is bladelike, as is typical of mosasaurines, and, as in *Mosasaurus*, its apex is pointed (Konishi et al., 2014; Street and Caldwell, 2017). The lateral surangular adductor fossa is shallow and indistinct, as it is in tylosaurines

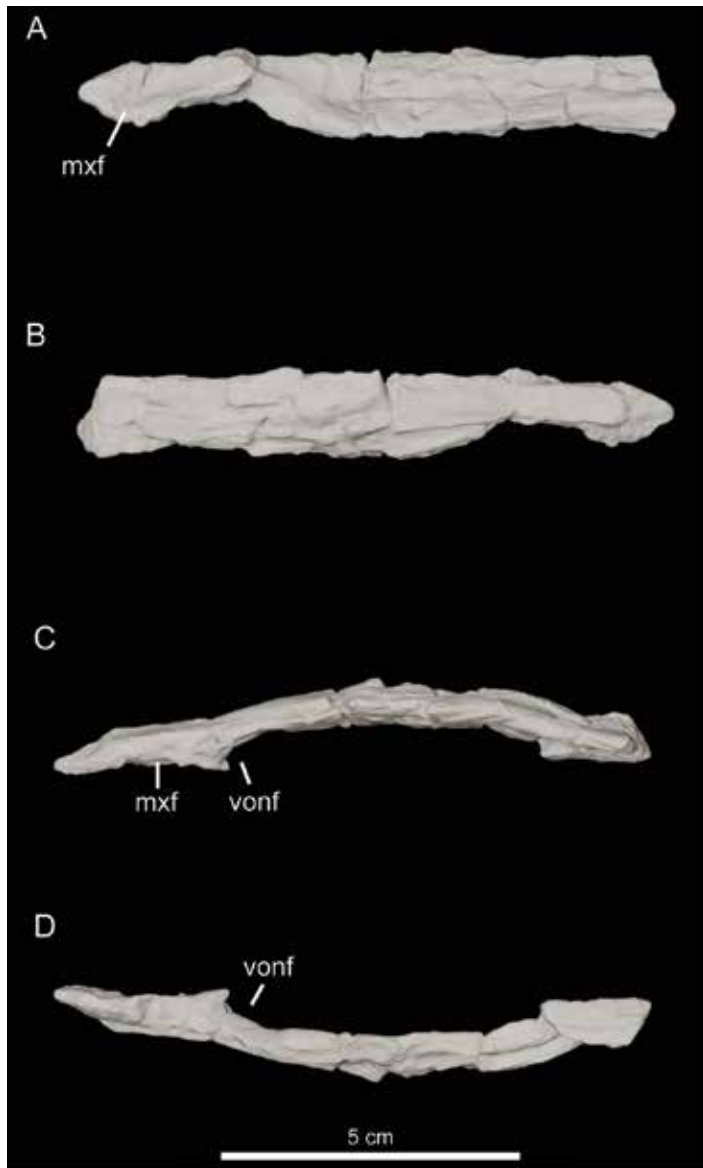


FIGURE 26. Left vomer in **A**, lateral, **B**, medial, **C**, dorsal, and **D**, ventral, views. Abbreviations: **mx**, maxilla facet; **vnf**, vomeronasal fenestra.

(e.g., *Tylosaurus nepaeolicus* AMNH FARB 1565, *Tylosaurus proriger* AMNH FARB 4909), *Mosasaurus hoffmannii* (Street and Caldwell, 2017), and plioplatecarpines (e.g., *Platecarpus tympaniticus* FHSM VP-322, *Plesioplatecarpus planifrons* FHSM VP-2116). This differs from the deep, distinct fossa bounded posteroven-

trally by a crest, as seen in *Gnathomortis stadmani* (Lively, 2020), *Clidastes liodontus* (e.g., AMNH FARB 192), and *Prognathodon overtoni* (Konishi et al., 2011).

On its lateral surface, the posterior surangular foramen is present just anterior to the glenoid fossa, and another foramen is present within the

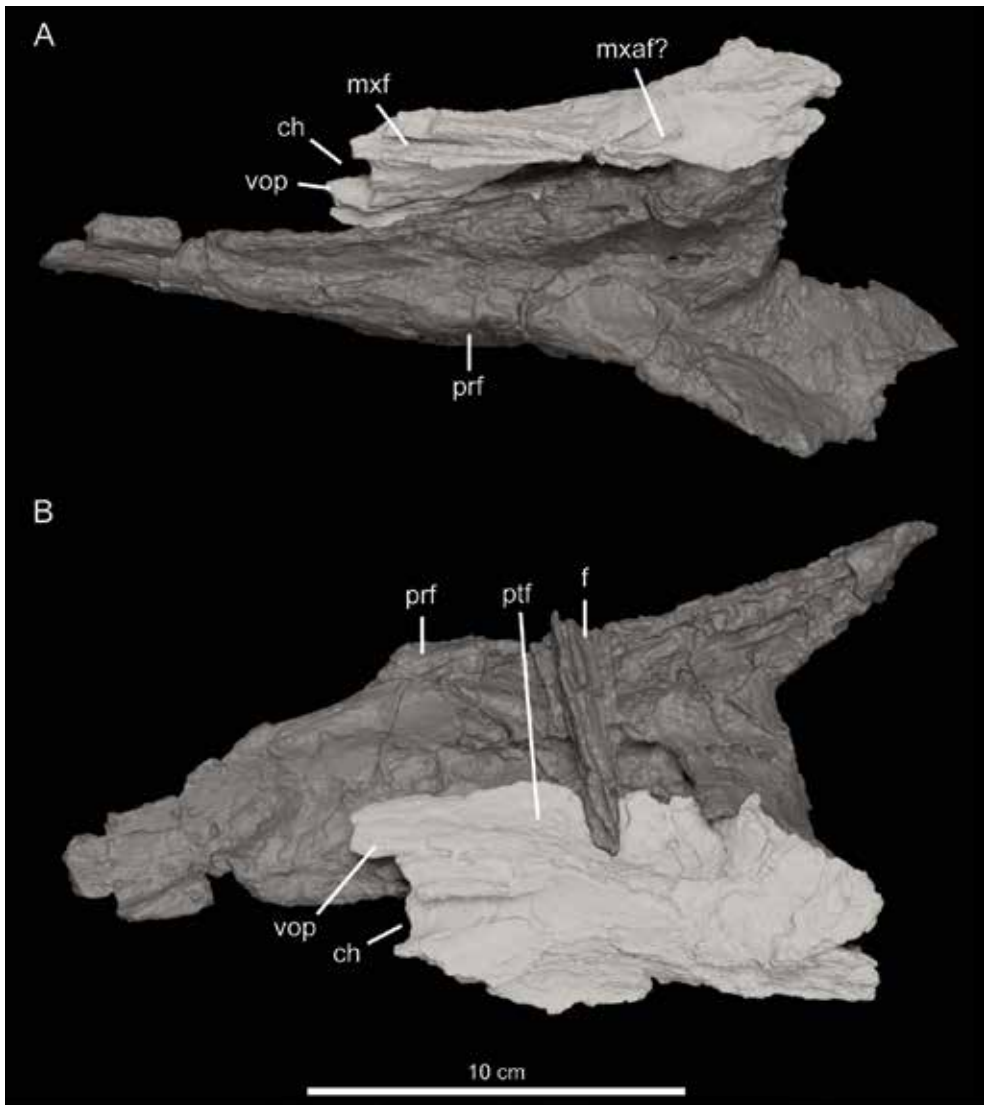


FIGURE 27. Right prefrontal and right palatine of NDGS 1838, with focus on the palatine in **A**, lateral and **B**, ventral views. Abbreviations: **ch**, internal choana; **f**, frontal; **mxaf?**, possibly the foramen for the palatine branch of the maxillary artery; **mxf**, maxilla facet of the palatine; **prf**, prefrontal; **ptf**, pterygoid facet of the palatine; **vop**, vomere process of the palatine.

glenoid fossa, directly posterior to the coronoid buttress. The surangular-articular suture is posterior to the glenoid fossa in lateral view, and descends anteriorly at a gentle angle, similar to *Tylosaurus*, in contrast to the vertical, zigzag suture present in *Mosasaurus* (Konishi et al., 2014; Street and Caldwell, 2017). Posterodorsally, the

surangular contributes to the anterior and lateral margins of the glenoid fossa. As is typical of mosasaurids, the anteromedial border of the glenoid fossa is continuous with a sharp ridge that bounds the medial surangular adductor fossa ventrally and articulates with the dorsal surface of the prearticular process.

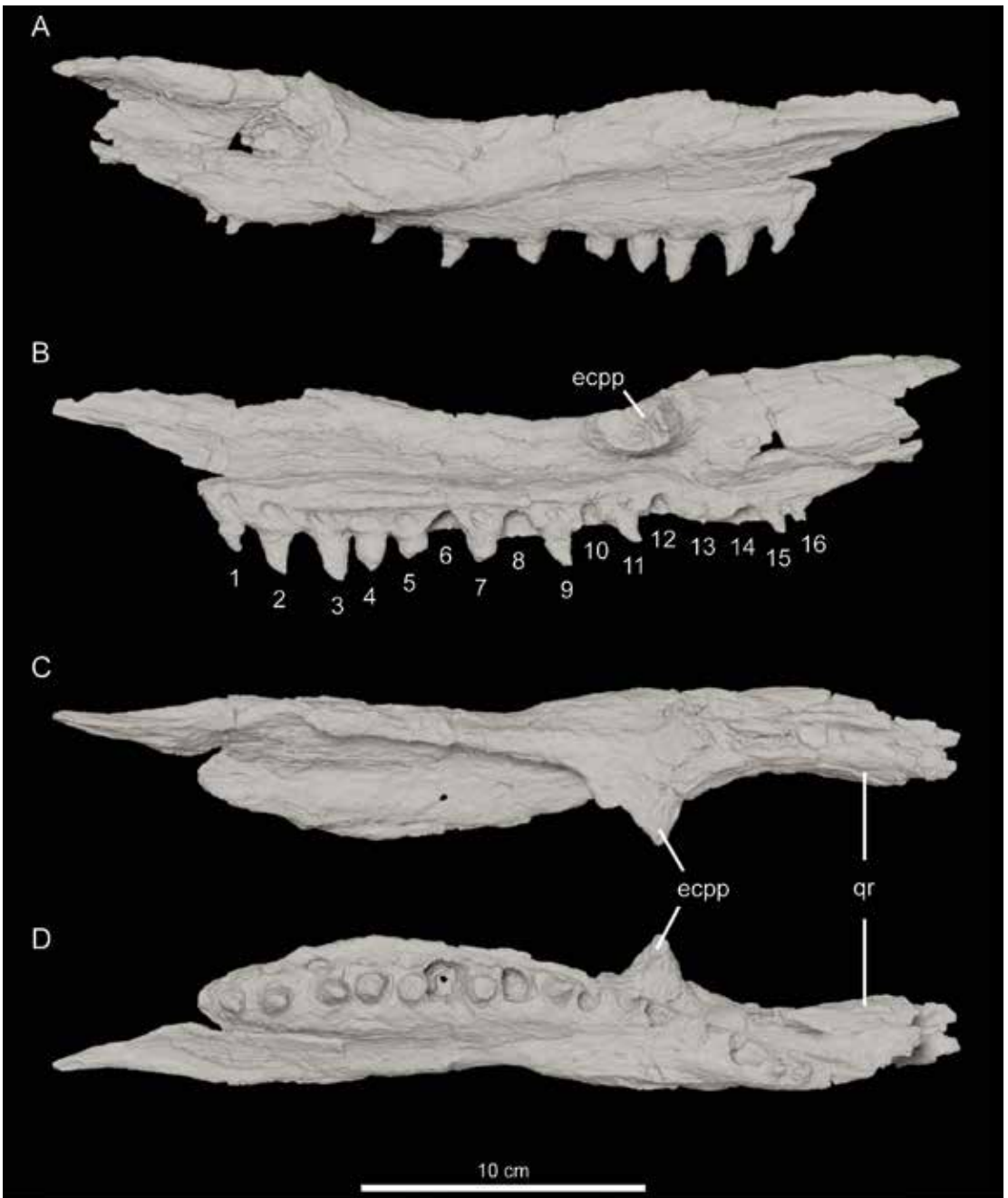


FIGURE 28. Left pterygoid of NDGS 10838 in **A**, medial, **B**, lateral, **C**, dorsal, and **D**, ventral, views. In **B**, tooth positions are numbered. Abbreviations: **ecpp**, ectopterygoid process; **qr**, quadratic ramus.

PREARTICULAR-ARTICULAR: Both left and right prearticular-articulars are preserved in articulation with their corresponding surangulars, and both are nearly complete (figs. 30, 34). Like all mosasaurs and other squamates, the prearticular is fused to the articular as an anteriorly projecting process (Oelrich, 1965; Russell, 1967). It is a dorsoventrally deep blade of bone that lies ventral to the medial surangular adductor fossa. Anteriorly, a triangular facet on its medial surface articulates with the angular; it is approximately half the length of the entire prearticular-articular, and its ventral margin is gently convex.

The retroarticular process is dorsoventrally shallow and fan shaped, as in *Clidastes* (e.g., *Clidastes liodontus* AMNH FARB 192), and it is not strongly medially inflected as it is in *Mosasaurus* (Street and Caldwell, 2017). There are no foramina on the lateral surface of the retroarticular process as there are in plioplacarpines (e.g., *Platycarpus tympaniticus* AMNH FARB 1820/1821). The foramen for the chorda tympani is located on the medial surface at approximately the center of the retroarticular process. A thick, medial ridge forms the posterior and ventral surfaces of the glenoid fossa.

AXIAL SKELETON

ATLAS: The atlas is complete and disarticulated, except for the atlas centrum preserved in articulation with the axis (figs. 36, 37). The anterior margin of the atlantal arch is notched, as is typical of mosasaurines (Russell, 1967), and projects anteriorly from the body of the bone at a more acute angle than is seen in all other taxa (e.g., *Tylosaurus proriger* AMNH FARB 1555, *Mosasaurus conodon* AMNH FARB 1380, *Clidastes propython* AMNH FARB 1513) except *Phosphorosaurus ponpetelegans* (Konishi et al., 2015). A shallow posterolateral fossa separates the atlantal arch from the synapophysis, which is long and extends far beyond the ventral margin of the atlantal arch; both traits are typical of

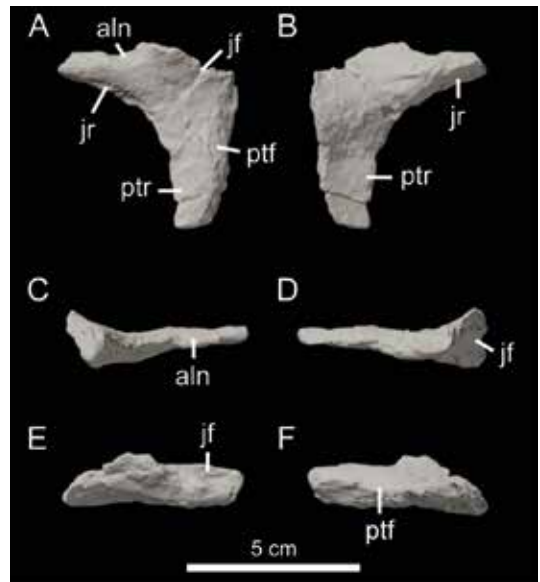


FIGURE 29. Right ectopterygoid of NDGS 10838 in **A**, dorsal, **B**, ventral, **C**, anterior, **D**, posterior, **E**, lateral, and **F**, medial, views. Abbreviations: **aln**, anterolateral notch; **jf**, jugal facet; **jr**, jugal ramus; **ptf**, pterygoid facet; **ptr**, pterygoid ramus.

Mosasaurus. The anterior facet for the occipital condyle is reniform, and the medial articular surface for the atlas centrum is subtriangular.

In anterior and posterior views, the intercentrum is reniform in overall shape; its dorsal margin is M-shaped and its ventral margin is gently convex, its contour only broken by a low tubercle on the midline demarcating an attachment point for the *M. longus colli* (Russell, 1967). The occipital condyle facet is gently concave, vertically inclined, and bounded ventrally by a ridge, and the facet for the centrum is flat. The centrum is attached, but not completely fused, to the axis, as is typical for mosasaurids (Russell, 1967). Its morphology is also typical of mosasaurids; it is subrectangular in anterior view, triangular in lateral view, and its dorsal surface is gently concave.

AXIS: The axis is complete and, overall, typical in shape for a mosasaurid (fig. 37). Its robust neural spine is hatchet shaped in lateral view, with a gently convex dorsal margin and concave

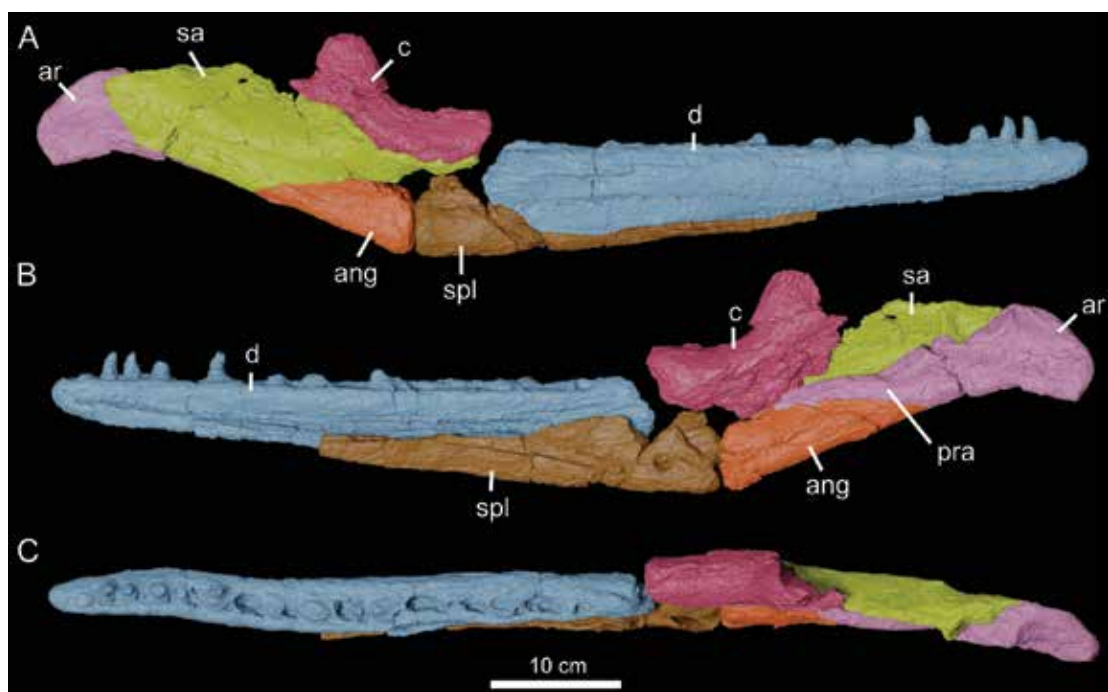


FIGURE 30. Right jaw of NDGS 10838 in **A**, lateral; **B**, medial and **C**, dorsal views. Abbreviations: **ang**, angular; **ar**, articular; **c**, coronoid; **d**, dentary; **pra**, prearticular; **sa**, surangular; **spl**, splenial.

anterior and posterior margins. The synapophyses are thick, subrectangular, and horizontally oriented in lateral view. Zygantra are present as pits on the medial surfaces of the postzygapophyses, like in other mosasaurines (e.g., *M. hoffmannii* NJSM 11053). The articular condyle of the centrum is subcircular in posterior view, and the anterior articular cotyle is obscured by the atlas centrum. Anteroventrally, the axis intercentrum is fused to the centrum; its anterior face is subtriangular, and the tubercle for the *M. longus colli* (Russell, 1967) is particularly well developed, bladelike, and posteriorly hooked. The hypapophysis is robust and extends posteroventrally, bearing a teardrop shaped facet distally to articulate with the peduncle.

CERVICAL VERTEBRAE THREE THROUGH SEVEN: Cervical vertebrae three through seven are preserved disarticulated (figs. 38, 39). The neural spines of cervicals three through six are triangular in profile, with convex anterior mar-

gins, concave posterior margins, and pointed apices. The neural spine of cervical seven, however, is more similar in morphology to those of the anterior dorsals and is rectangular in lateral view with a broadly convex dorsal margin. Zygosphenes and zygantra are present on cervicals three through seven and well developed. The interarticular surfaces of the centra are smooth and procoelous, as is typical of squamates (Romer, 1956), and oriented vertically, as is typical of mosasaurids (Russell, 1967). Like other mosasaurines except for *Moanasaurus* (Wiffen, 1990), the interarticular surfaces are nearly circular (Russell, 1967), and the dorsal notch is subtle, rather than well defined as it is in *Mosasaurus conodon* (e.g., AMNH FARB 1380). All cervical centra, excluding the atlas, are similar in length (i.e., less than 2 cm difference between longest and shortest vertebrae; table 2). The synapophysis of the third cervical is, like that of the axis, oriented horizontally;

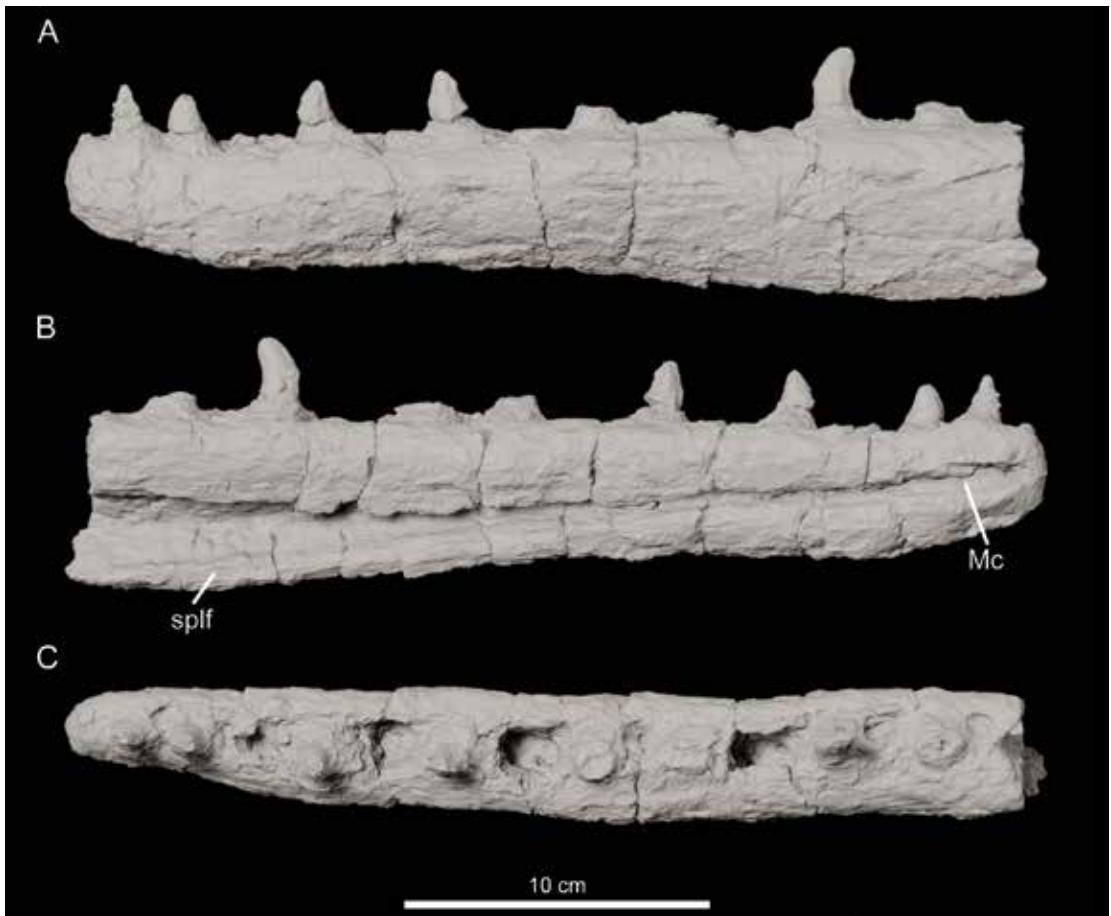


FIGURE 31. Left dentary of NDGS 10838 in **A**, lateral; **B**, medial; and **C**, dorsal views. Abbreviations: **Mc**, Meckelian canal; **splf**, splenial facet.

posteriorly, the synapophyses gradually shift to a more vertical orientation. The synapophyses are reniform and never extend ventral to the centra, as they do in some basal mosasaurs (e.g., *Tethysaurus*, Bardet et al., 2003; *Halisaurus*, Holmes and Sues, 2000). A broad ridge connects the synapophyses to the prezygapophyses, forming a 45° angle with the centra.

Hypapophyseal peduncles three through five are preserved disarticulated and loose, and the sixth peduncle is stuck to the left lateral side of the sixth cervical (figs. 39, 40). The anteriormost hypapophyseal peduncles are subtriangular in lateral view, and the posterior hypapophyses are more rectangular. They decrease in size

posteriorly and terminate on the sixth cervical vertebra, as in *Clidastes* (e.g., *Clidastes liodontus* YPM VPPU 17249). Unlike *Clidastes*, the seventh cervical vertebra possesses a hypapophysis lacking a ventral peduncle; this is also observed in *Mosasaurus conodon* (Ikejiri and Lucas, 2014). Hypapophyseal facets on cervical vertebrae three through six are teardrop shaped in ventral view and dimpled in the center; the dimples correspond to a small tubercle in the center of the dorsal articular facets of the disarticulated peduncles.

DORSAL VERTEBRAE: The first four dorsal vertebrae are preserved complete and in articulation, and the fifth is present but incomplete

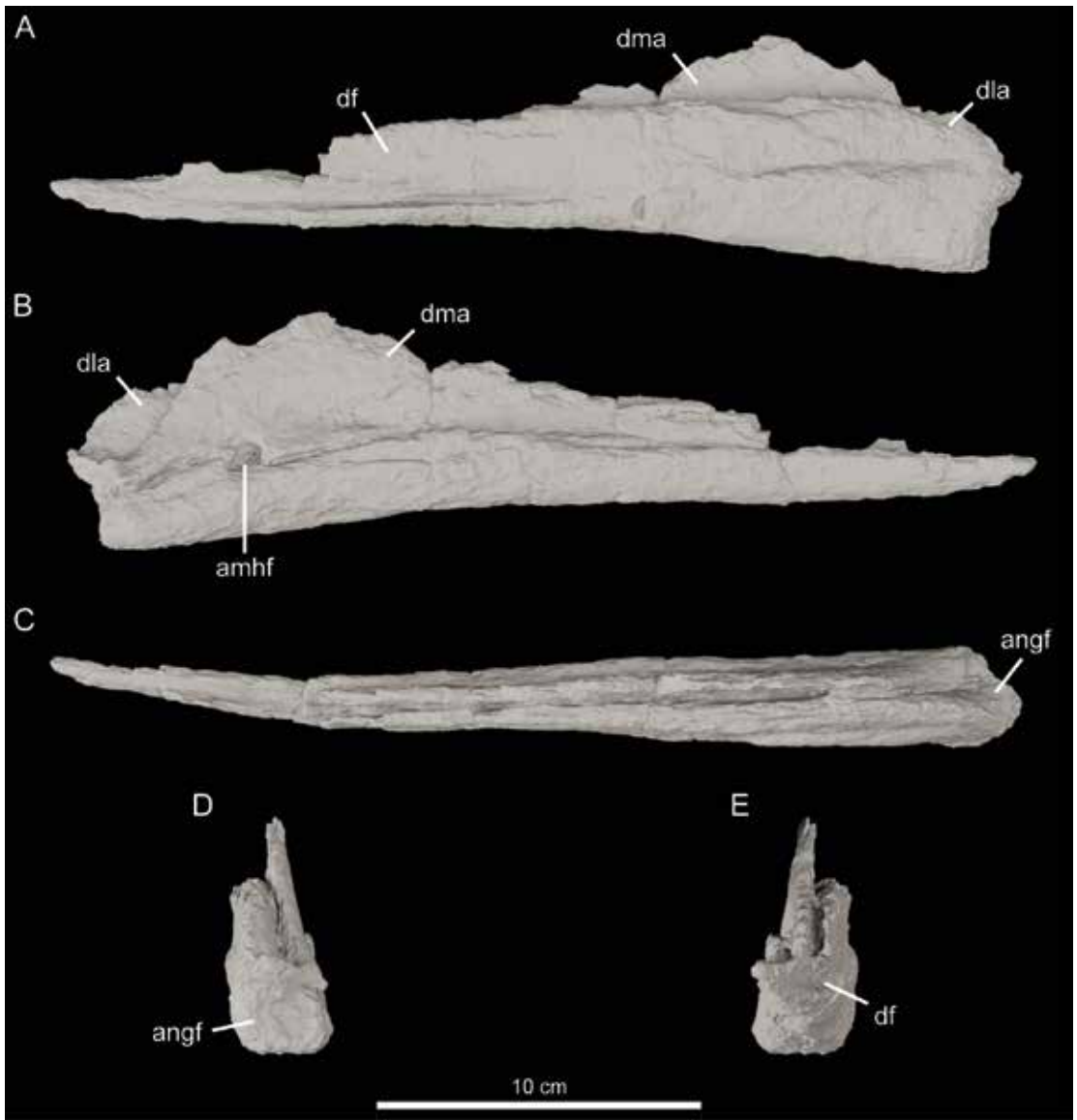


FIGURE 32. Left splenial of NDGS 10838 in **A**, lateral; **B**, medial; **C**, dorsal; **D**, posterior; and **E**, anterior views. Abbreviations: **amhf**, anterior mylohyoid foramen; **angf**, angular facet; **df**, dentary facet; **dla**, dorso-lateral ala; **dma**, dorsomedial ala.

(fig. 41). The neural spines are rectangular in lateral view. Zygosphenes and zyantra are absent from the dorsal vertebrae, as in *Mosasauros* and *Plotosaurus* but unlike *Clidastes* (Russell, 1967). The synapophyses are vertically oriented and reniform, becoming gradually shorter and wider on the posterior vertebrae.

The centra, like those of the cervicals, are circular in cross section. The first dorsal possesses a subtle bump on its ventral surface, which may represent a second rudimentary hypapophysis. Dorsal four possesses damage that we interpret as bite marks on the dorsolateral, ventrolateral, and ventral surfaces (see Discussion).

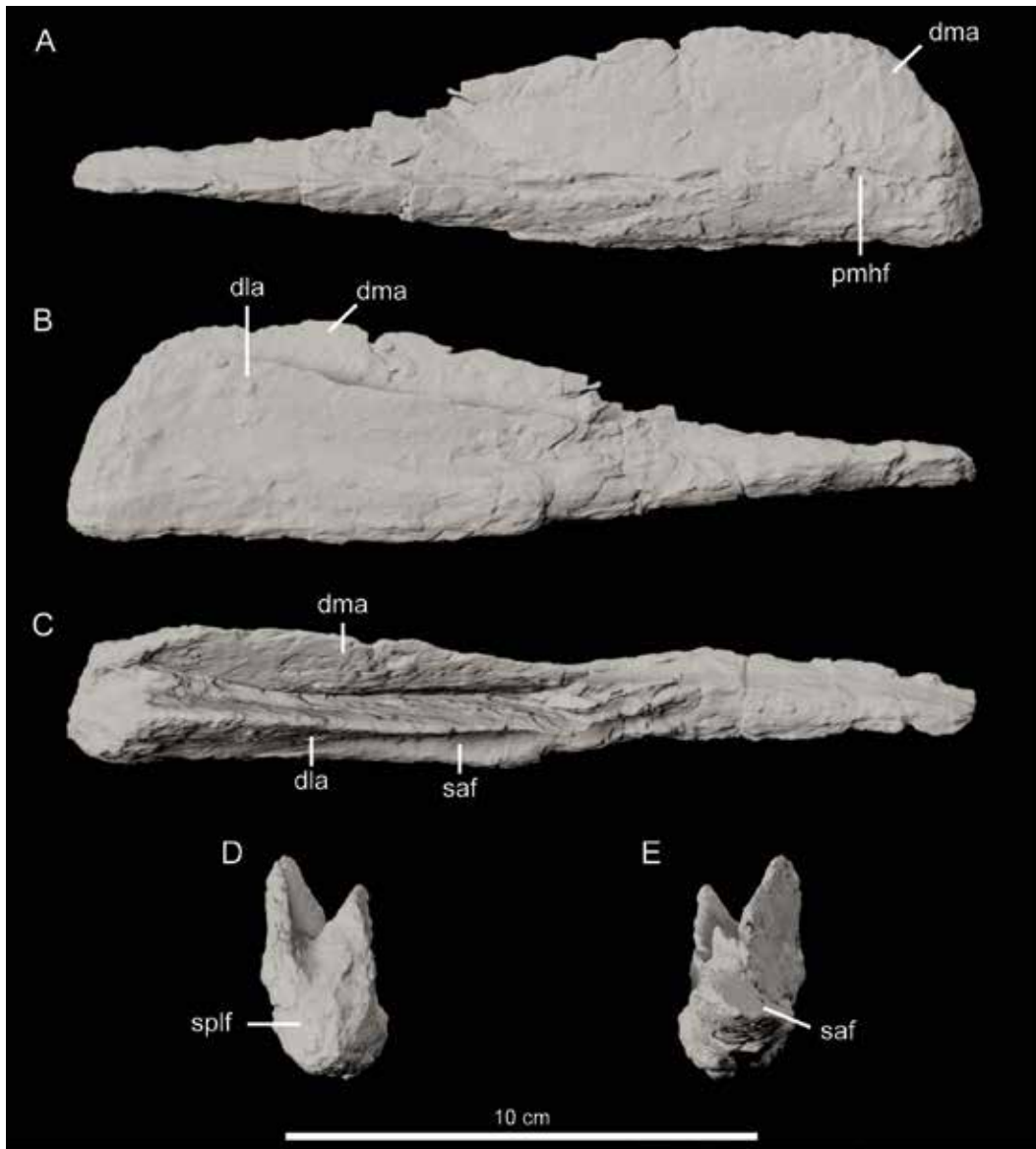


FIGURE 33. Left angular of NDGS 10838 in **A**, medial; **B**, lateral; **C**, dorsal; **D**, anterior; and **E**, posterior views. Abbreviations: **dla**, dorsolateral ala; **dma**, dorsomedial ala; **pmhf**, posterior mylohyoid foramen; **saf**, surangular facet; **splf**, splenial facet.

RIBS: Eleven ribs (five cervical, five dorsal, one unidentified) are preserved in varying degrees of completeness (figs. 42, 43), increasing in size posteriorly along the axial column. Overall, the rib morphology of NDGS 10838 is typical of mosasaurids. The ribs are unicapitate

and anteroposteriorly flattened with articular facets that are oval in proximal view. Their posterior surfaces possess a vascular groove and, proximally, their anterior surfaces possess a shallow, subtriangular fossa. Distally, the ribs are gently curved.

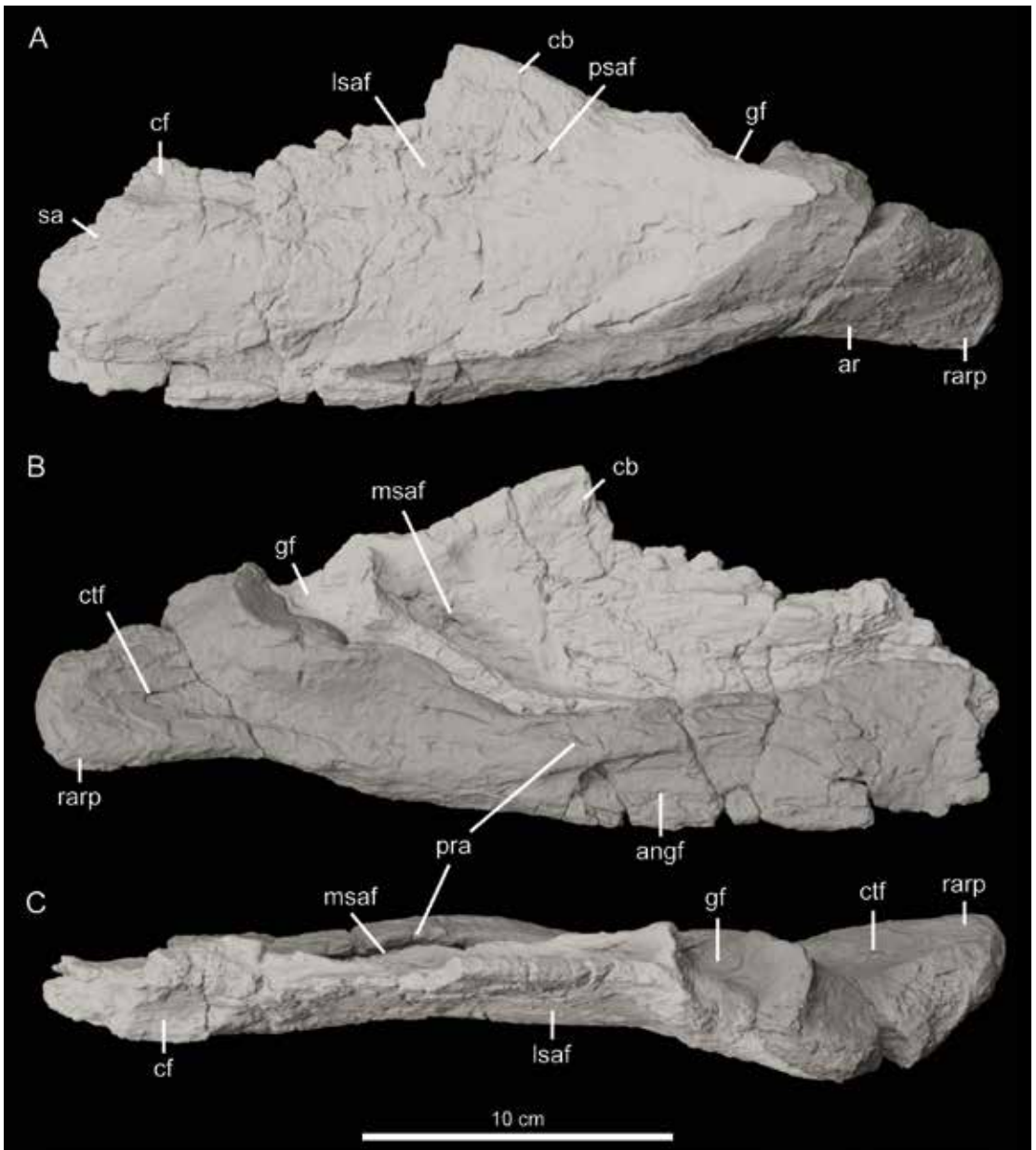


FIGURE 34. Left posterior mandibular unit of NDGS 10838 in **A**, lateral; **B**, medial; and **C**, dorsal views. Abbreviations: **angf**, angular facet; **ar**, articular; **cb**, coronoid buttress of the surangular; **cf**, coronoid facet; **ctf**, foramen for the chorda tympani; **gf**, glenoid fossa; **lsaf**, lateral surangular fossa; **msaf**, medial surangular fossa; **pra**, prearticular; **psaf**, posterior surangular foramen; **rarp**, retroarticular process; **sa**, surangular.

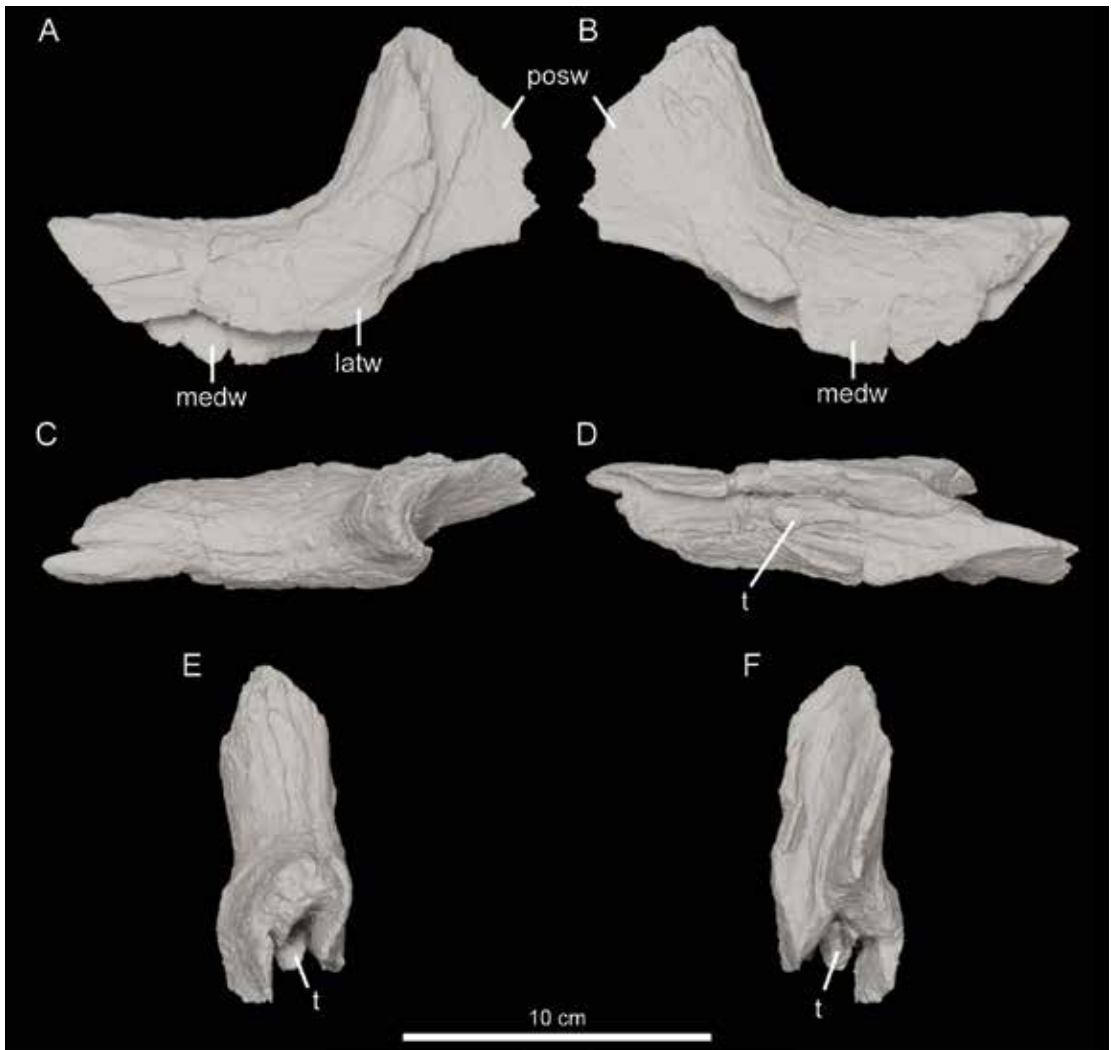


FIGURE 35. Left coronoid of NDGS 10838 in **A**, lateral; **B**, medial; **C**, dorsal; **D**, ventral; **E**, anterior; and **F**, posterior views. Abbreviations: **latw**, lateral descending wing; **medw**, medial descending wing; **posw**, posterior wing; **t**, tooth.

PHYLOGENETIC ANALYSIS

To place NDGS 10838 within Mosasauoidea, it was scored using a character list (appendix 1) modified from that of Strong et al. (2020), which was the most recent version of the original comprehensive mosasaur matrix by Bell (1997). To better represent the range of variation present in observed specimens, the states of 11 existing characters were amended and scores for 22 taxa were

revised based on firsthand and literature observations. Five taxa (*Globidens schurmanni*, *Gnathomortis stadtmani*, *Latoplatecarpus nichollsae*, *Pluridens serpentis*, *Tylosaurus peminensis*) were added to include recently described species and better represent the Pembina Member fauna, and one taxon (*Tylosaurus bernardii*) was removed from the matrix following safe taxonomic deletion (i.e., its scores were identical to, but less complete than, those for *Tylosaurus proriger*).

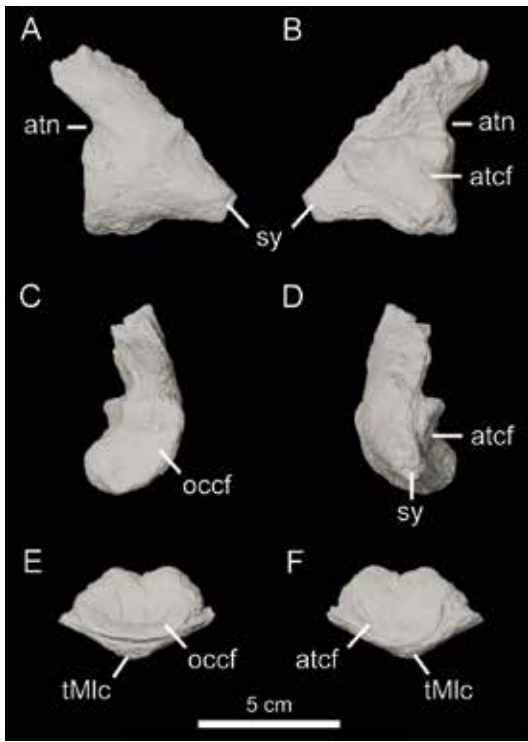


FIGURE 36. Left atlantal arch and atlas intercentrum of NDGS 10838. **A–D**, atlantal arch in **A**, lateral; **B**, medial; **C**, anterior; and **D**, posterior views. **E–F**, atlas intercentrum in **E**, anterior and **F**, posterior views. Abbreviations: **atcf**, facet for the atlas centrum; **atn**, atlantal arch notch; **occf**, facet for the occipital condyle; **sy**, synapophysis; **tMlc**, tubercle for the *M. longus colli*.

Simões et al. (2017) were the first to use dolichosaurs, rather than extant anguimorphs, as the outgroup taxon in an analysis derived from the matrix of Bell (1997). They argue that previous use of an artificial (i.e., not based on a single taxon nor single specimen), composite anguimorph outgroup was flawed because it (1) introduced “unnecessary polymorphism” (Simões et al., 2017: 3) and (2) may not be reflective of the position of mosasauroids within Squamata. While we do agree that the use of an artificial composite outgroup is flawed, we do not think that the total exclusion of anguimorph outgroups as done by Simões et al. (2017) and nearly all other analyses of mosasaur phylogeny since is

warranted because the character states were originally conceived and polarized using Anguimorpha as the point of reference (Bell, 1997). Furthermore, in contrast to the second point made by Simões et al. (2017), use of anguimorph lizards as the outgroup to Mosasauroida is justified given the recent placement of mosasauroids as sister to varanoids based on morphological and molecular datasets (Augusta et al., 2022; Polcyn et al., 2022).

Therefore, we added six nonmosasauroid anguimorph taxa (*Shinisaurus crocodilurus*, *Heloderma horridum*, *Lanthanotus borneensis*, *Varanus komodoensis*, *Estesia mongoliensis*, *Ovo gurvel*) to the matrix, bringing the total number of operational taxonomic units to 58. *Shinisaurus crocodilurus* was used as the outgroup taxon in accordance with recent molecular studies placing it as the most stemward anguimorph among these taxa (Burbrink et al., 2020). To test the effects of outgroup choice, we also analyzed the matrix using each nonmosasauroid anguimorph as the outgroup individually (i.e., completely excluding the other five), as well as one analysis in which *Adriosaurus suessi* is the outgroup and all six nonmosasauroid anguimorph taxa are excluded.

The matrix (appendix 2; see also online supplement: <https://doi.org/10.5531/sd.sp.60>) was compiled in Mesquite v. 3.70 and trees were recovered using parsimony analysis in TNT v. 1.5 (Goloboff et al., 2008; Goloboff and Catalano, 2016); following Napoli et al. (2021), new technology searches were replicated until the shortest length was hit 20 times, and TBR branch swapping was applied to these best trees. All characters were treated as unweighted and unordered, and zero-length branches were collapsed. Tree statistics and character state changes of the resultant strict consensus tree were described using PAUP v. 4.0a.

The unweighted analysis of the full dataset recovered 86 most parsimonious trees, each with a length of 577, consistency index (CI) of 0.286, retention index (RI) of 0.686, and rescaled consistency index (RCI) of 0.196. Both the strict

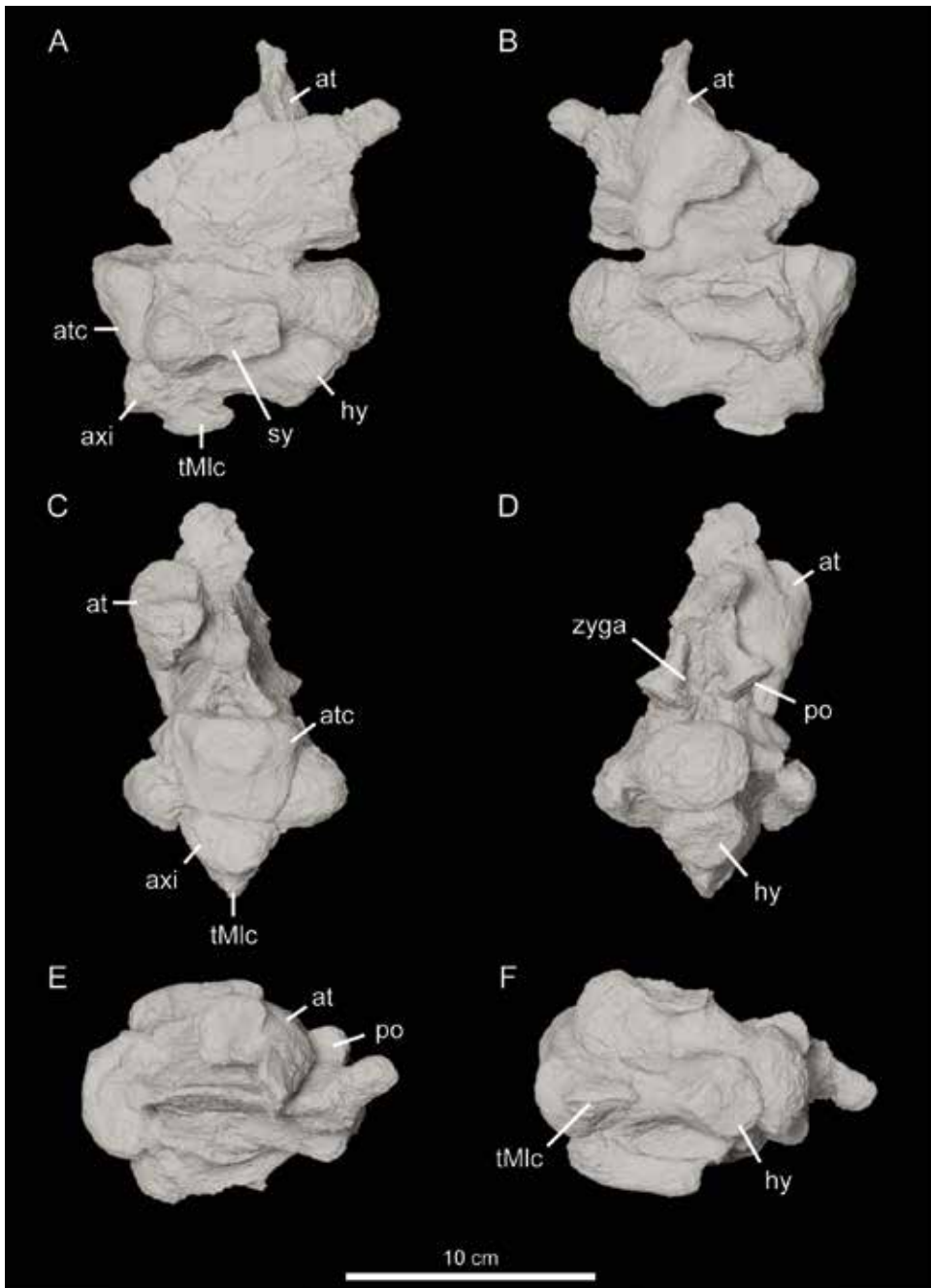


FIGURE 37. Axis of NDGS 10838 in **A**, left lateral; **B**, right lateral; **C**, anterior; **D**, posterior; **E**, dorsal, and **F**, ventral views. Abbreviations: **at**, right atlantal arch; **atc**, atlas centrum; **axi**, axis intercentrum; **hy**, hypapophysis; **po**, postzygapophysis; **sy**, synapophysis; **tMlc**, tubercle for the *M. longus colli*; **zyga**, zygantra.

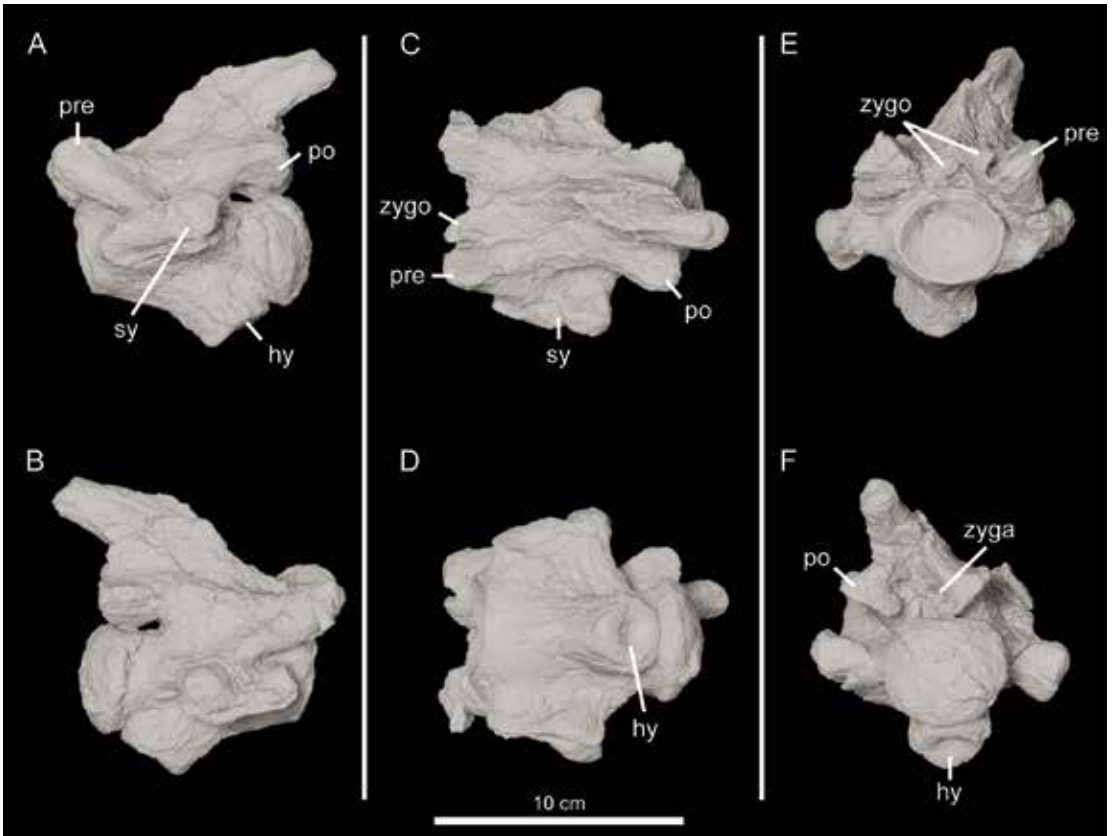


FIGURE 38. Third cervical vertebra in **A**, left lateral; **B**, right lateral; **C**, dorsal; **D**, ventral; **E**, anterior; and **F**, posterior views. Abbreviations: **hy**, hypopophysis; **pre**, prezygapophysis; **po**, postzygapophysis; **sy**, synapophysis; **zyga**, zygantra; **zygo**, zygosphenes.

consensus (fig. 44) and the Adams consensus, (fig. 45) were generated. NDGS 10838 is recovered within Mosasaurinae, in a polytomy with *Clidastes* and one node above *Dallasaurus turneri*, which is recovered as the basalmost mosasaurine. The position of NDGS 10838 is supported by the following character states: premaxilla rostrum distinctly protruding; frontal that is long and narrow; 15–16 maxillary teeth; maxilla-premaxilla suture terminates between the fourth and ninth maxillary teeth; 15–16 dentary teeth; and tooth facets present. The following character states are recovered as local autapomorphies of NDGS 10838: premaxilla rostrum very large; premaxilla internarial bar T-shaped in cross section; premaxilla dorsal keel

present; frontal that is of intermediate dimensions (i.e., between 1.5 and 2× longer than wide); frontal midline dorsal keel that is present and low; postorbitofrontal transverse dorsal ridge present; jugal posteroventral angle that is slightly obtuse; quadrate stapedial pit that is a narrow oval; quadrate posteroventral ascending tympanic rim that is a high triangular crest; groove present in anterolateral edge of quadrate tympanic ala; quadrate mandibular condyle gently domed; dentary anterior projection long; splenial-angular articular surfaces with distinct horizontal tongues and grooves; and zygosphenes and zygantra present on cervical vertebrae.

TESTING THE EFFECT OF OUTGROUP CHOICE AND NEW DATA: To test the effect of outgroup

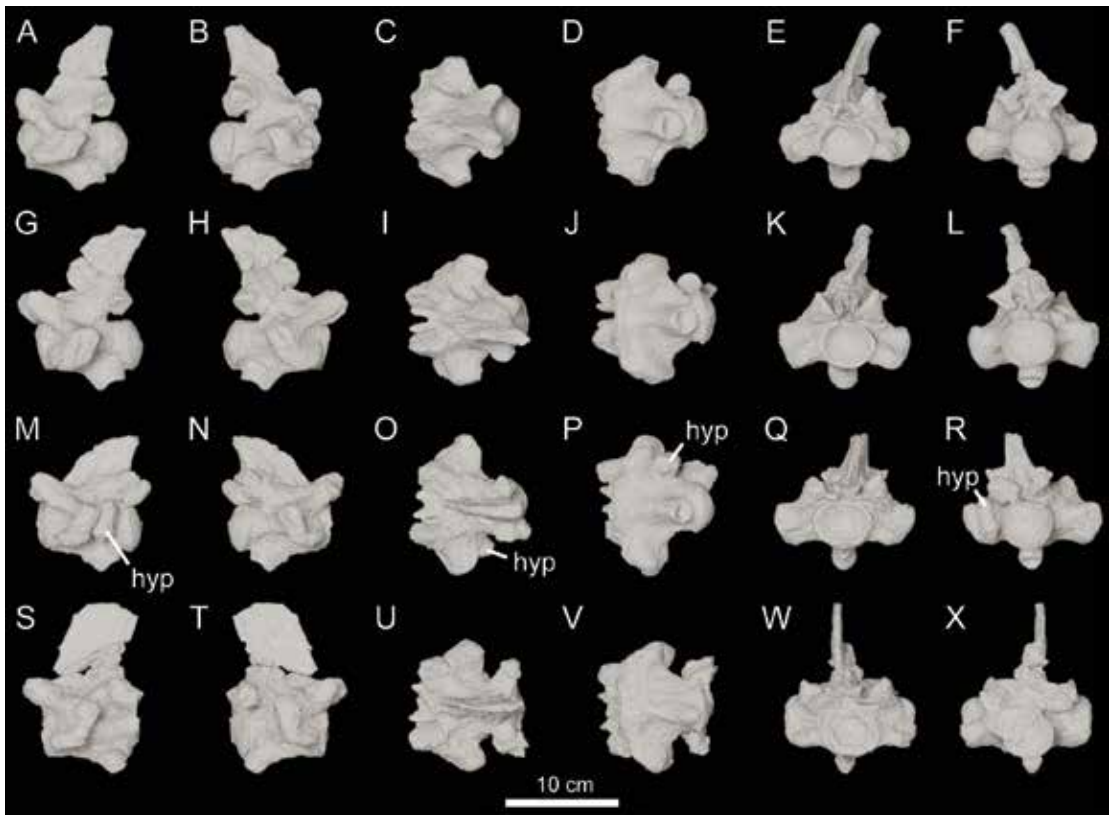


FIGURE 39. Cervical vertebrae A–F, four, G–L, five, M–R, six, and S–X, seven, in A, G, M, S, left lateral; B, H, N, T, right lateral; C, I, O, U, dorsal; D, J, P, V, ventral; E, K, Q, W, anterior; and F, L, R, X, posterior views. Abbreviation: **hyp**, sixth hypapophyseal peduncle.

choice on tree topology, we also analyzed the matrix using each nonmosasauroid anguimorph individually, as well as once using only dolichosaurs as the outgroup (figs. 46–49). The original multistate matrix from Strong et al. (2020) was also analyzed using our TNT parameters to test the effect of including the revised character states, new taxa, and revised scores, as well as the inclusion of nonmosasauroid anguimorph outgroups on tree topology (fig. 46). In our analysis of the full dataset, we found greater resolution of basal mosasauroids, Mosasauridae, and within Mosasaurinae compared to the strict tree recovered by analysis of the unaltered Strong et al. (2020) matrix using our TNT parameters. However, we found that, without nonmosasauroid anguimorph outgroups, while

the addition of new taxa, new outgroups, and revised scores significantly improved resolution among mosasaurines, resolution of all other clades except Tethysaurinae and Tylosaurinae was lost and overall Bremer support values decreased (fig. 46).

When each of the nonanguimorph taxa were used as individual outgroups, we find better resolution using the extant outgroups (*Shinisaurus crocodilurus*, *Heloderma horridum*, *Lanthanotus borneensis*, *Varanus komodoensis*; figs. 47, 48) than the extinct ones (*Ovoogurvel*, *Estesia mongoliensis*; fig. 49), which we interpret as a consequence of missing data in the extinct taxa. Tethysaurinae and Tylosaurinae are the only clades consistently recovered in all six analyses. All analyses except the one in which *Ovoogurvel*

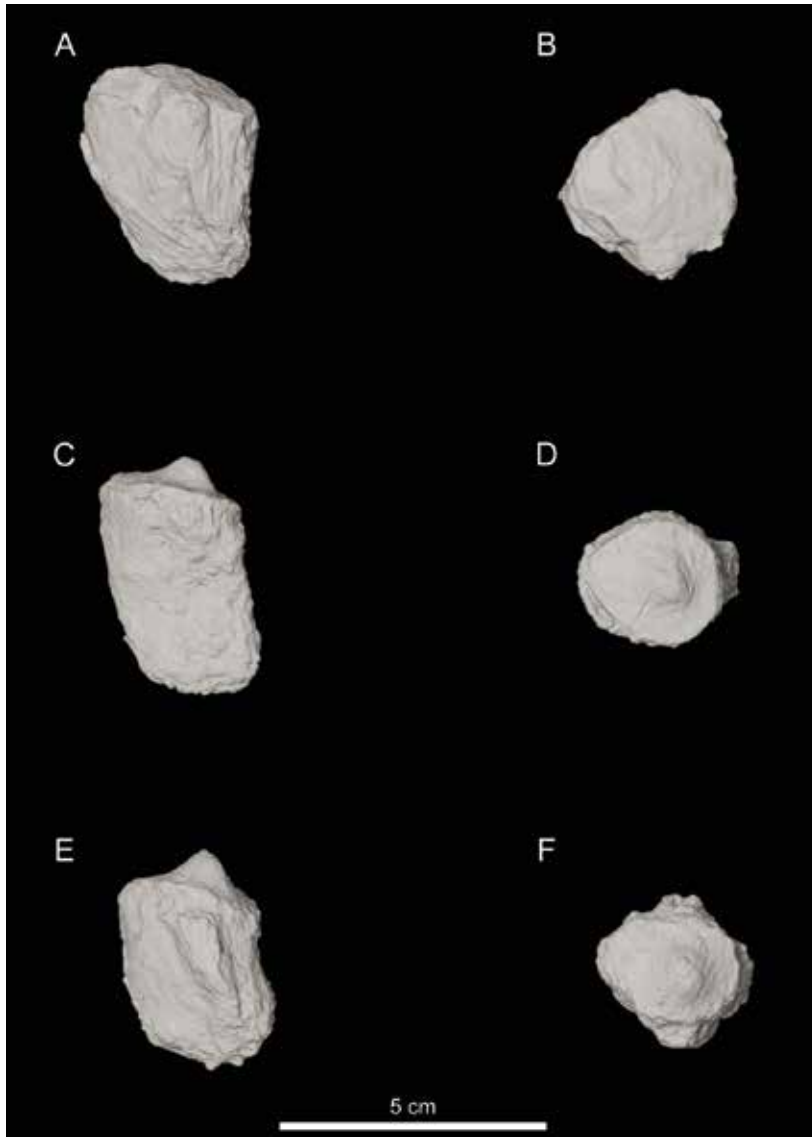


FIGURE 40. Hypapophyseal peduncles A–B, three; C–D, four; and E–F, five in A, C, E, left lateral and B, D, F, dorsal views.

gurvel is the outgroup also recover Dolichosauridae, Yaguarasaurinae, and Plioplatecarpinae, and all analyses using extant outgroups also recover Mosasaurinae. The analyses including *Heloderma horridum*, *Lanthanotus borneensis*, and *Varanus komodoensis* each recovered higher Bremer support values than when all six taxa were included.

IMPLIED WEIGHTING: Implied weighting is hypothesized to reduce the impact of homoplasy on tree topology and thus provide more accurate results from analyses of incomplete datasets, such as those comprised of primarily fossil taxa (Goloboff, 2014; Goloboff et al., 2018). Therefore, we also analyzed the full dataset using an implied weighting function of $k =$

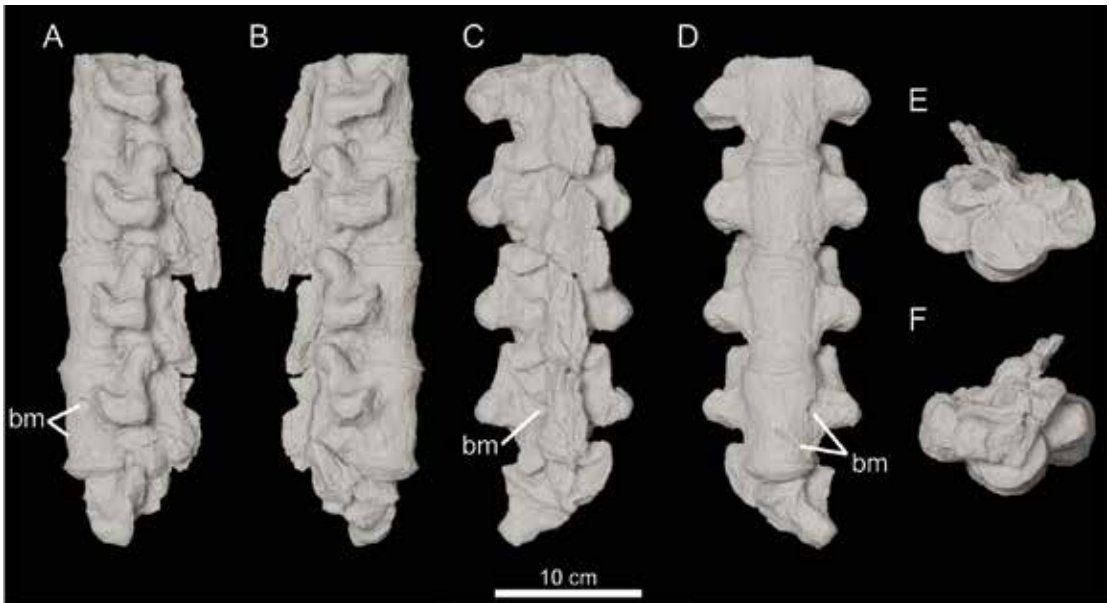


FIGURE 41. Dorsal vertebrae one through five in **A**, left lateral; **B**, right lateral; **C**, dorsal; **D**, ventral; **E**, anterior; and **F**, posterior views. Abbreviation: **bm**, bite mark.

12, following Goloboff et al. (2018). The weighted analysis recovered five trees, each with a fit value of 24.346, length of 588, CI of 0.281, RI of 0.678, and RCI of 0.190; from these five trees, strict consensus and jackknife trees were generated (fig. 50). Overall, the topology of the weighted tree is similar to that of the unweighted tree except that: nonmosasauroid taxa are recovered as a basal polytomy; *Halisaurus* is recovered outside of Russellosaurinae, sister to Mosasaurinae; Tethysaurinae is recovered outside of Mosasauridae; and the ingroup relationships of russellosaurines are better resolved.

Although Mosasaurinae is not recovered as it is in Strong et al. (2020) (i.e., *Dallasaurus* is recovered in a polytomy with the halisaurine *Pluridens*, basal to all other mosasaurines), NDGS 10838 is still recovered among mosasaurines (i.e., more closely related to *Mosasaurus* than to *Plioplatecarpus* or *Tylosaurus*) within a basal clade containing *Gnathomortis* and *Clidastes*. Its position within this clade is supported by 15 to 16 maxillary and dentary teeth, and nine of the same autapomorphies

that are recovered in the unweighted tree are recovered as the autapomorphies of NDGS 10838 in the weighted analysis.

DISCUSSION

ANATOMY AND PHYLOGENY OF *Jormungandr walhallaensis*: NDGS 10838 possesses a suite of characters shared with *Clidastes* (e.g., dental counts and morphology) and the Plotosaurini (e.g., subrectangular quadrate, pterygoid teeth that arise from a crest, internarial bar that is T-shaped in cross section, anteriorly ascending dorsal surangular border), as well as unique morphology previously unknown in any mosasaur (e.g., quadrate stapedial pit within a groove that is bounded ventrally; prefrontals separated from postorbitofrontals by a thin ridge on the ventral surface of the frontal). Its discovery thus enhances our understanding of mosasaurine diversity and morphological evolution and has the potential to upend established ingroup relationships of the clade.

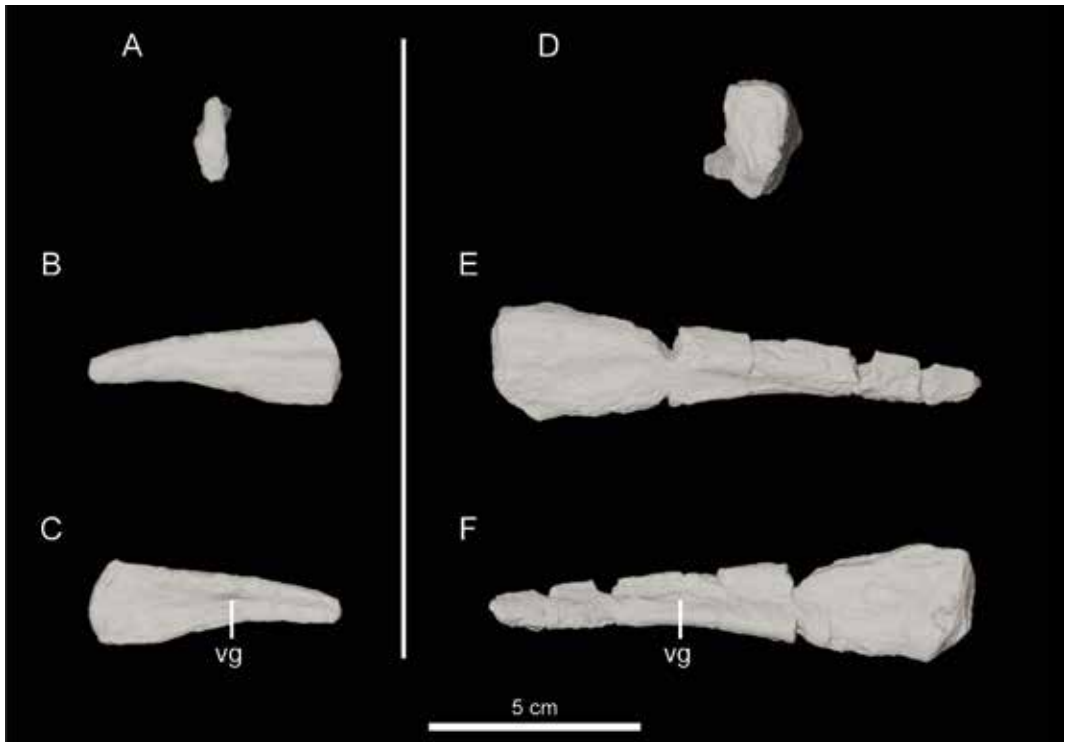


FIGURE 42. Right anterior cervical rib and left posterior cervical rib of NDGS 10838. Right anterior cervical rib in **A**, proximal; **B**, anterior; and **C**, posterior views. Left posterior cervical rib in **D**, proximal; **E**, anterior; and **F**, posterior views. Abbreviation: **vg**, vascular groove.

In all but one variation in which it was included, NDGS 10838 is recovered at the base of Mosasaurinae, either in a basal polytomy, in a polytomy with *Clidastes*, or sister to *Clidastes* (figs. 46–49); when *Shinisaurus crocodilurus* is used as the outgroup, NDGS 10838 is recovered as the node basal to *Clidastes*. This is consistent with its possession of key mosasaurine synapomorphies (e.g., prefrontal supraorbital ridge, notched atlantal arch). However, we predict that future analyses of mosasaur phylogeny, with the addition of new characters that more thoroughly sample mosasaurine variation, will recover *Jormungandr walhallaensis* as more derived within Mosasaurinae, perhaps as a transitional form between *Clidastes* and the plotosaurines (*Mosasauros* + *Plotosaurus* sensu Bell, 1997), given the mosaic of characters it shares with both genera to the exclusion of other mosasaurine taxa (e.g.,

Globidens, *Prognathodon*). We interpret the analysis not recovering this topology to be arising from insufficient character and taxon sampling in the current mosasauroid matrix, which has not been substantially altered since its publication by Bell (1997). In nearly three decades since, although 21 problematic characters have been iteratively removed and several character states have been rephrased (see Simões et al., 2017, and citations therein), only three new characters have been added and several key bones remain completely unrepresented in the matrix despite obvious variation across Mosasauroidae (e.g., femur, lacrimal, ectopterygoid; A.R.Z., personal obs.). Furthermore, the operational taxonomic units remain primarily restricted to North American taxa to the exclusion of over a dozen significant European and Moroccan taxa, a choice that undoubtedly has hindered the accuracy and res-

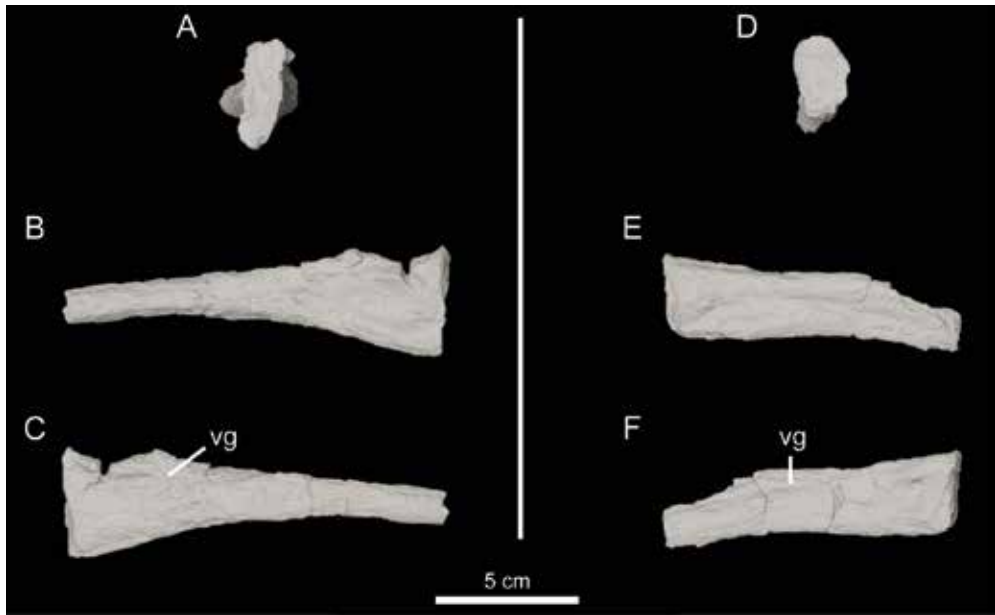


FIGURE 43. Right anterior dorsal rib and left posterior dorsal rib of NDGS 10838. Right dorsal rib one in **A**, proximal; **B**, anterior; and **C**, posterior views. Second left dorsal rib in **D**, proximal; **E**, anterior; and **F**, posterior views. Abbreviation: **vg**, vascular groove.

olution of mosasauroid ingroup relationships recovered thus far (Graybeal, 1998). Therefore, in its unexpected placement among *Clidastes* despite some obvious similarities to the Plotosaurini, *Jormungandr walhallaensis* exemplifies the necessity for a long overdue revision of the foundational dataset used to understand mosasauroid evolution.

BIOSTRATINOMY: Traces interpreted as bite marks are present on the fourth dorsal vertebra (fig. 41). On the left lateral surface directly ventral to the synapophysis, a subcircular puncture (sensu Binford, 1981; Drumheller and Brochu, 2016) is present that extends vertically and slightly medially into the centrum. The deepest portion of the puncture ends in a blunted point roughly 9 mm from the external surface of the cortical bone when measured in the inferred orientation of the puncture. Posteromedial to that puncture on the ventral surface of the centrum a distinct furrow is present that begins near the midline of the centrum and extends posterolaterally toward the left lateral surface of the centrum. The furrow is deep-

est at its anterior end (2.5 mm), is U-shaped in cross section, and shallows as it extends posterolaterally. Given that morphology, we interpret the anterior end as the initial point of impact by the crown. These two bite marks on the ventral surface may be serial marks (sensu Binford, 1981) that were formed during a single biting event, providing insight into the tooth spacing of the trace maker. The distance between the anterior end of the furrow and the center of the puncture is approximately 31 millimeters, similar to the spacing of teeth in the middle portion of the maxilla of NDSG 10838.

A second puncture is present on the left side of dorsal vertebra four, situated on the dorsolateral surface of the neural arch above the synapophysis. It is positioned slightly more posteriorly than the ventral puncture. The puncture is circular to subcircular in cross section. The full depth of the puncture and its exact direction into the bone cannot be determined with certainty. The poor preservation of the externalmost cortical bone on much of the artic-

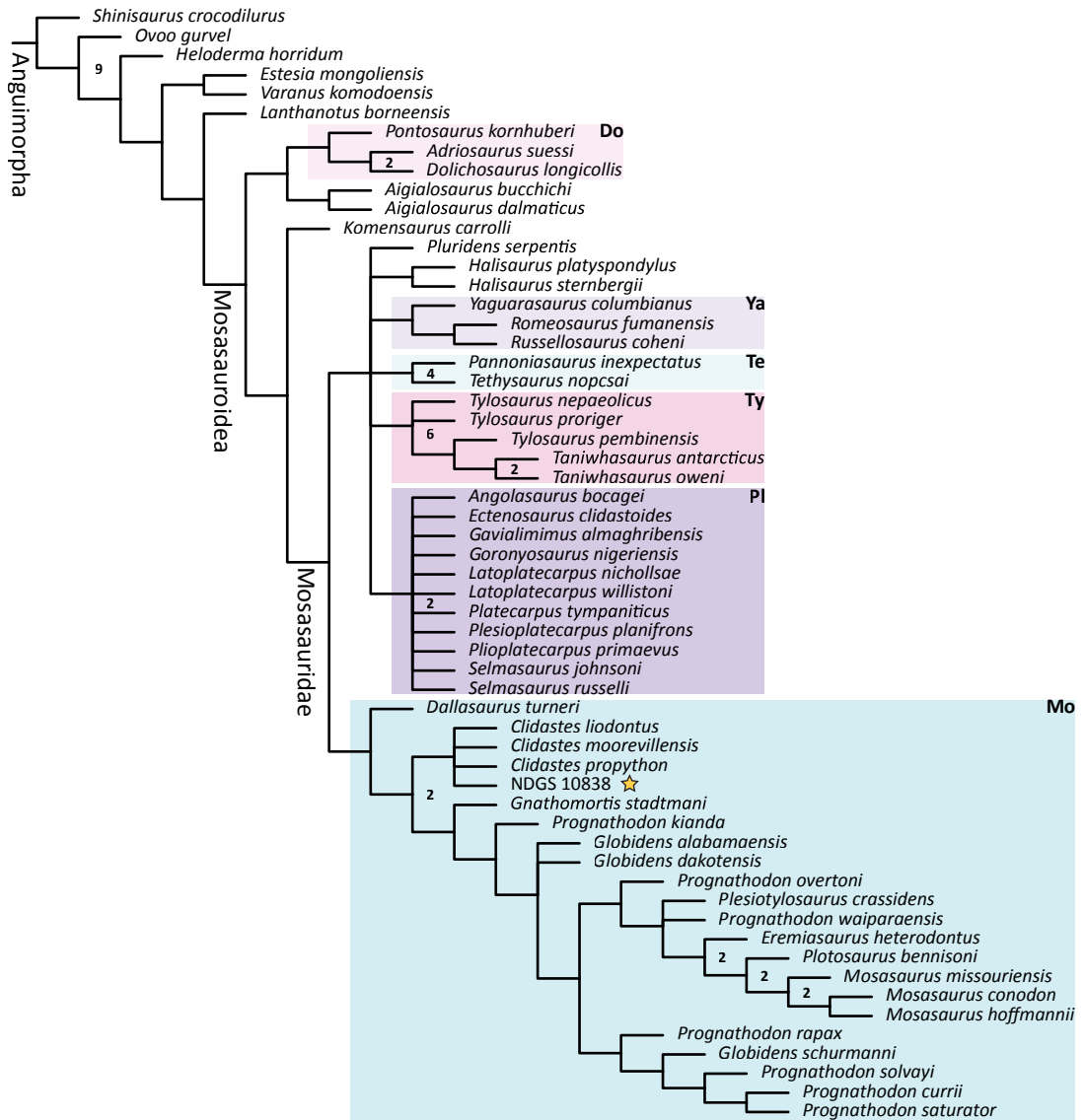


FIGURE 44. Strict consensus of 86 most parsimonious trees (577 steps, CI = 0.286, RI = 0.686, RCI = 0.196) recovered by the unweighted parsimony analysis of our new matrix. Star indicates the position of NDGS 10838, and Bremer support is 1 unless noted. Abbreviations: **Do**, Dolichosauridae; **Mo**, Mosasaurinae; **Pl**, Plioplatecarpinae; **Te**, Tethysaurinae; **Ty**, Tylosaurinae; **Ya**, Yaguarasaurinae.

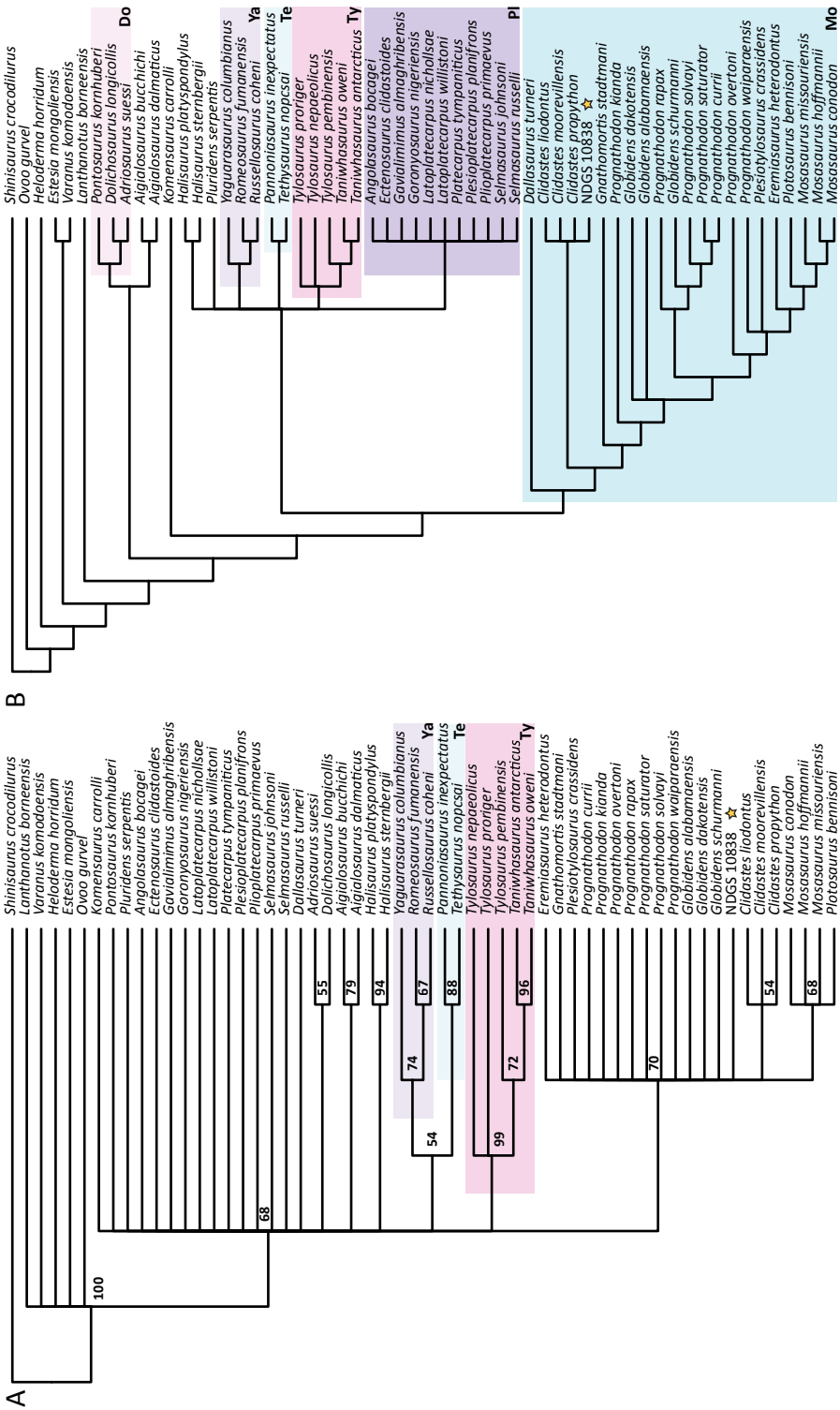


FIGURE 45. **A**, Jackknife and **B**, Adams consensus trees recovered by the unweighted parsimony analysis. Star indicates the position of NDGS 10838. Abbreviations: **Do**, Dolichosauridae; **Mo**, Mosasauridae; **PI**, Plioplatecarpinae; **Te**, Tethysaurinae; **Ty**, Tylosaurinae; **Ya**, Yaguarasaurinae.

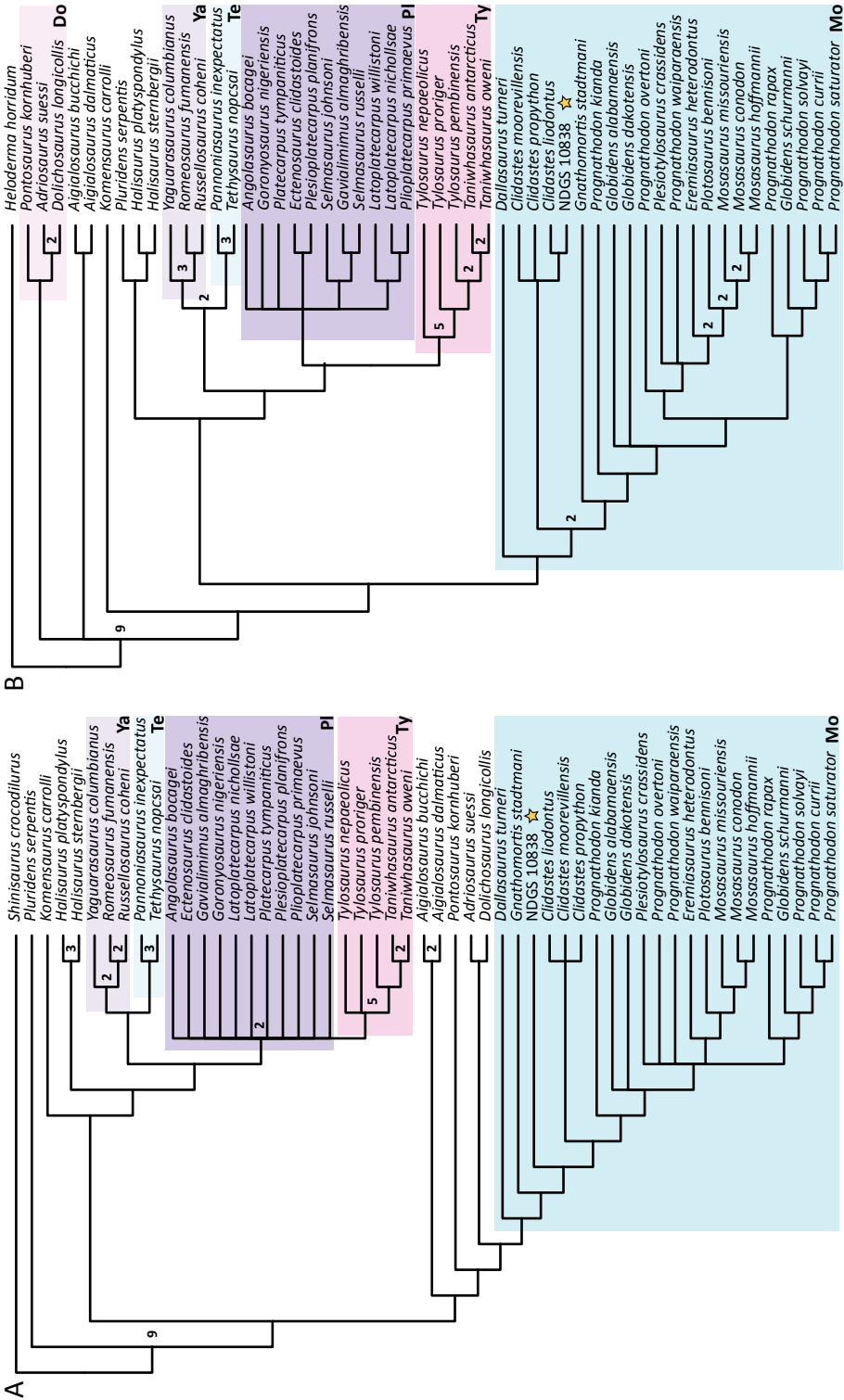


FIGURE 47. Strict consensuses of trees recovered by unweighted parsimony analyses of datasets using **A**, *Shinisaurus crocodilurus* (46 trees, 549 steps, CI = 0.299, RI = 0.673, RCI = 0.201) and **B**, *Heloderma horridum* (eight trees, 550 steps, CI = 0.300, RI = 0.672, RCI = 0.202) as the outgroup. Star indicates the position of NDSGS 10838 and Bremer support is 1 unless noted. Abbreviations: **Do**, Dolichosauridae; **Mo**, Mosasaurinae; **Pi**, Plioplatecarpinae; **Te**, Tethysaurinae; **Ty**, Tylosaurinae; **Ya**, Yaguarasaurinae.

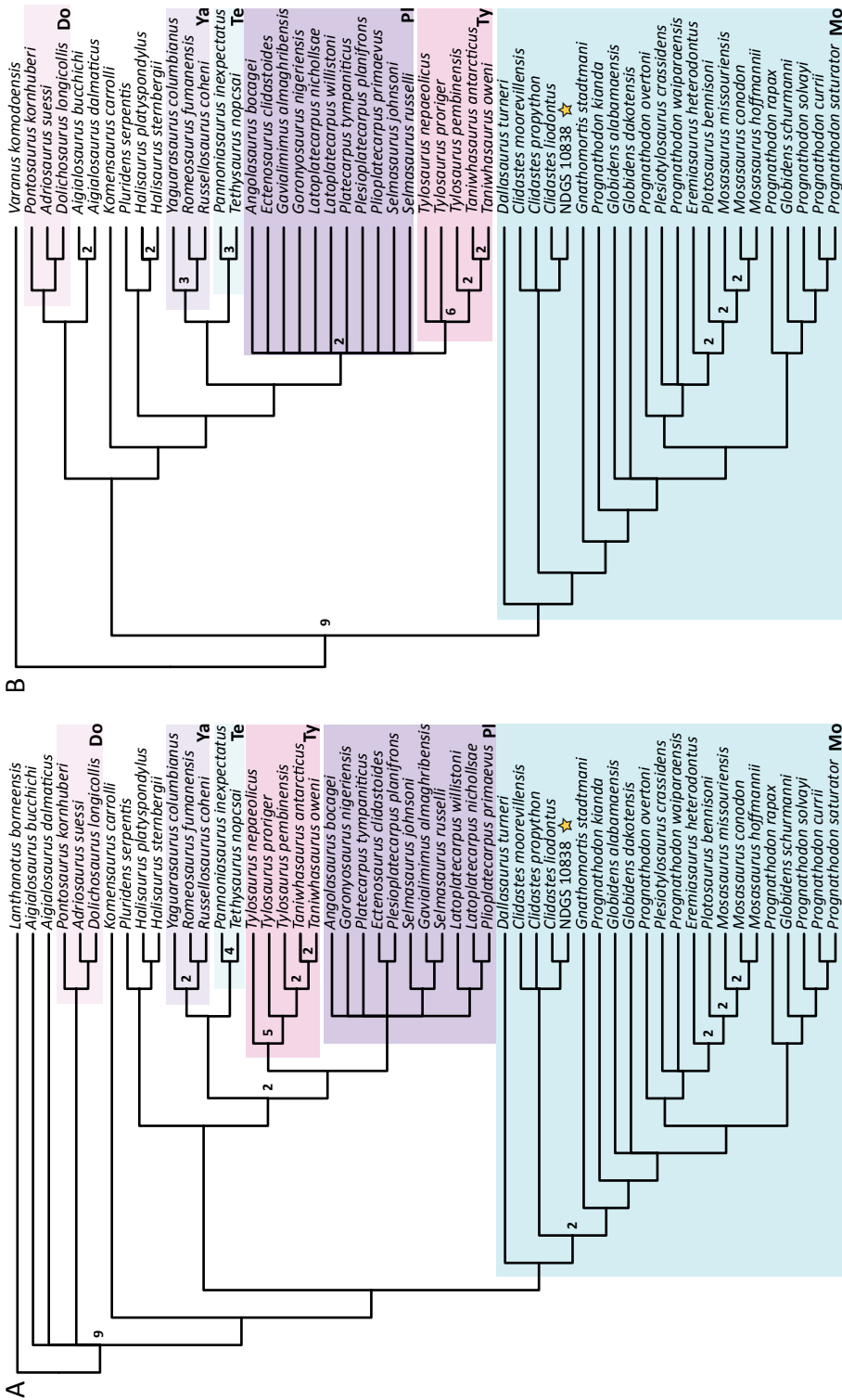


FIGURE 48. Strict consensus of trees recovered by unweighted parsimony analyses of datasets using **A**, *Lanthamotus borneensis* (eight trees, 562 steps, CI = 0.292, RI = 0.662, RCI = 0.193) and **B**, *Varanus komodoensis* (13 trees, 553 steps, CI = 0.273, RI = 0.629, RCI = 0.172) as the outgroup. Star indicates the position of NDGS 10838 and Bremer support is 1 unless noted. Abbreviations: **Do**, Dolichosauridae; **Mo**, Mosasaurinae; **Pl**, Plioplatecarpinae; **Te**, Tethysaurinae; **Ty**, Tylosaurinae; **Ya**, Yaguarosaurinae.

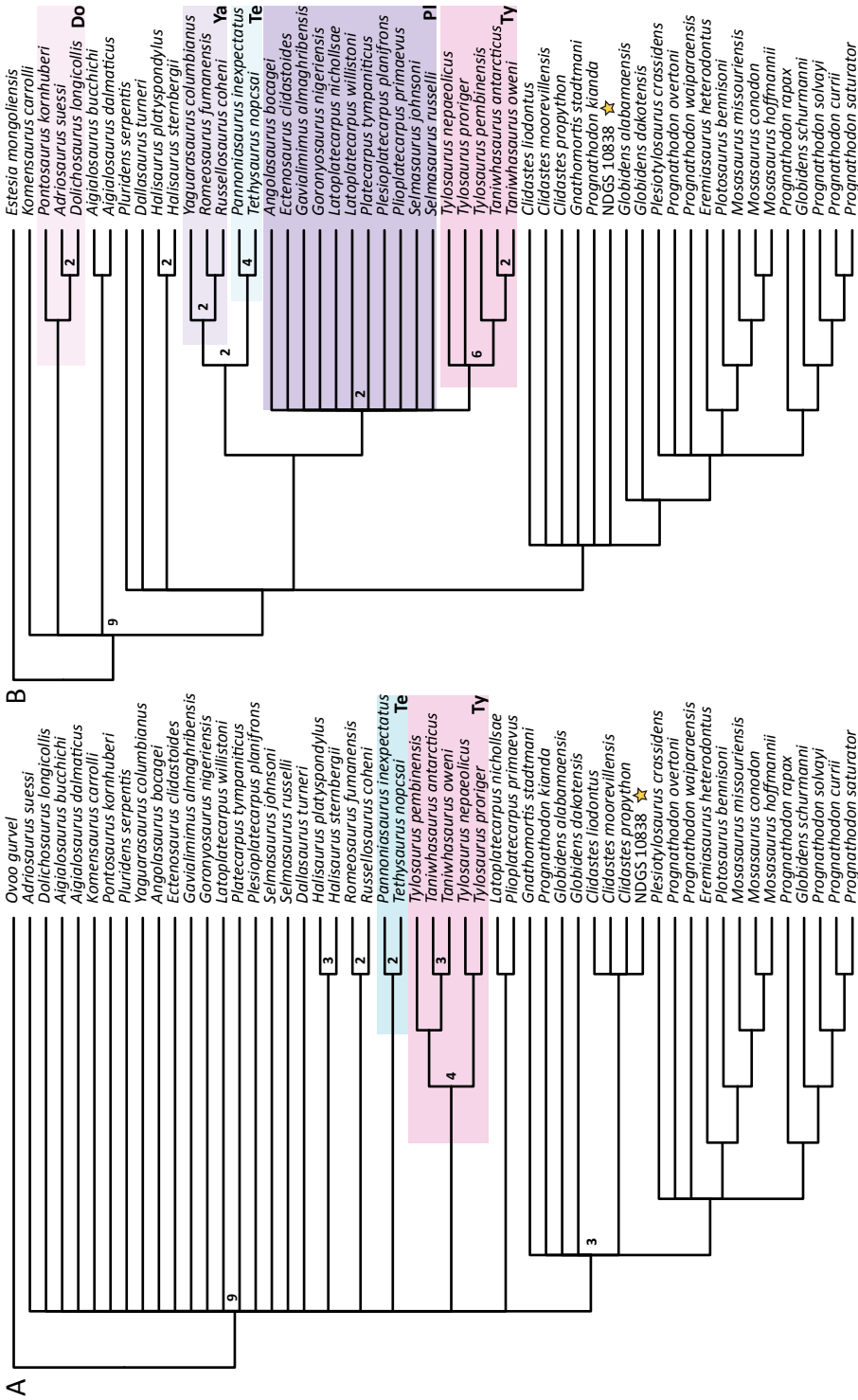


FIGURE 49. Strict consensus of trees recovered by unweighted parsimony analyses of datasets using **A**, *Ovo gurvel* (203 trees, 731 steps, CI = 0.223, RI = 0.503, RCI = 0.112) and **B**, *Estesia mongoliensis* (294 trees, 540 steps, CI = 0.554, RI = 0.887, RCI = 0.491) as the outgroup. Star indicates the position of NDGS 10838, and Bremer support is 1 unless noted. Abbreviations: **Do**, Dolichosauridae; **Mo**, Mososaurinae; **PI**, Plioplatecarpinae; **Te**, Tethysaurinae; **TY**, Tylosaurinae; **Ya**, Yaguarsaurinae.



FIGURE 51. Reconstruction of *Jormungandr walhallaensis* shown engaging in intraspecific combat. Illustration by Henry Sharpe.

ulated series of dorsal vertebrae makes it difficult to determine whether less prominent bite marks like pits or scores (sensu Binford, 1981; Drumheller and Brochu, 2016) were present. The bone surrounding the three identified bite marks shows no signs of healing (fig. 41), indicating they formed near or after the time of death (fig. 51). Some information about the shape of the tooth crowns can be gleaned from these marks. In cross section the crowns were subcircular, perhaps weakly laterally compressed. The shapes of the punctures are inconsistent with those produced by sharks (e.g., Dortangs et al., 2002; Everhart, 2004, 2005; Shimada and Hooks, 2004), but are consistent with the general morphology of mosasaur teeth (Street et al., 2021). Previous studies reported injuries in mosasaurs that were

likely caused by other mosasaurs, with numerous specimens of various taxa preserving both healed and unhealed wounds (see Everhart, 2008; Bastiaans et al., 2020; and citations therein). The shape and depth of the punctures on NDGS 10838 is incompatible with the “dome-shaped” teeth of the mosasaurine *Globidens* that were adapted for consuming mollusks (Martin and Fox, 2007), but ruling out other mosasaur taxa based on tooth morphology is difficult given the poor preservation of the surrounding bone.

Regardless of the exact identity of the trace maker, the presence of the bite marks on the fourth dorsal vertebra near the posterior end of the originally articulated series of seven vertebrae (cervicals six and seven, dorsals one through four) suggests the biting event could be related to

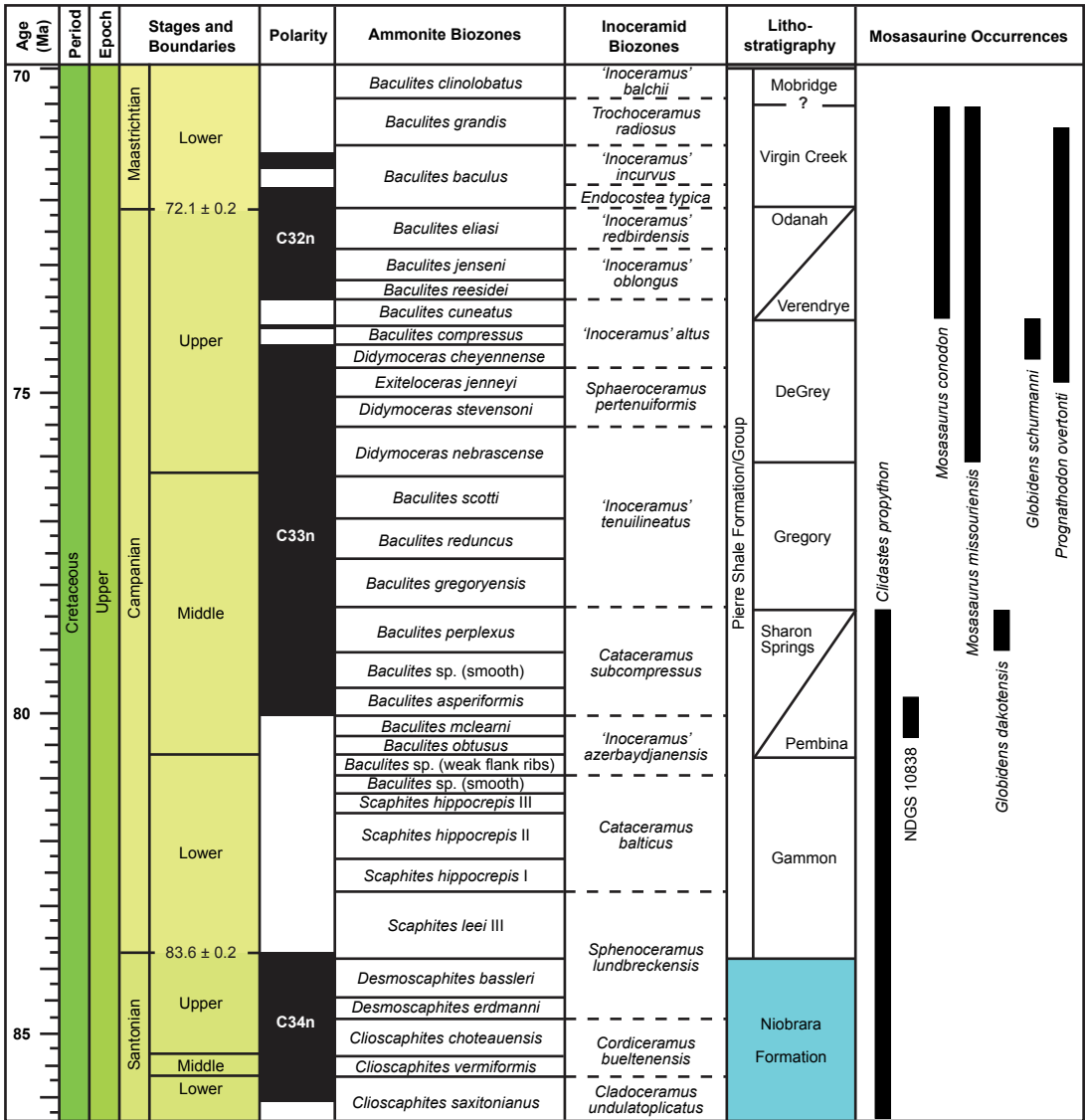


FIGURE 52. Generalized synopsis of mosasaurine temporal distributions in the Pierre Shale Formation and contemporaneous strata showing correlations between magnetostratigraphy, lithostratigraphic units of the Pierre Shale Formation in North and South Dakota, and biostratigraphic zones for both ammonites and inoceramids (Gill and Cobban, 1965; Konishi et al., 2011; Lynd and Slattery, 2017; Driscoll et al., 2019).

the separation of the anterior portion of the skeleton from the remainder of the skeleton. The fact that the anterodorsal portion of dorsal vertebra five remains in articulation with dorsal vertebra four suggests that sufficient soft tissues were present at the time it was broken to keep it secured in place with the other vertebrae rather than becoming disarticulated. Additional support for the presence of some soft tissues on the specimen when the skeleton was separated comes from the fact that this series of articulated vertebrae was recovered roughly in life position relative to the anterior cervical vertebrae and the skull. Disarticulation and slight displacement from life position of the anterior cervical vertebrae and the skull bones likely occurred later as decomposition of the specimen progressed and possibly through the actions of smaller scavengers while on the sea floor. The absence of bite marks on the skull and the cervical vertebrae is interpreted as evidence that the trace maker was focused on feeding upon the posterior portion of the skeleton, which also explains the absence of more posteriorly positioned postcranial material from this specimen at the locality. Alternatively, if the separation of the skeleton occurred well above the sea floor, the anterior portion of the skeleton may have drifted apart from the rest of the skeleton and the two portions settled in different locations.

BIOSTRATIGRAPHY: We placed NDGS 10838 into a temporal context alongside other mosasaurines that are well documented (i.e., identified to the species level) from the Pierre Formation using the ammonite and inoceramid biozones of Gill and Cobban (1965) and Lynds and Slattery (2017) (fig. 52). NDGS 10838 coincides with the latest occurrence of specimens referred to *Clidastes propython* (Sharon Springs Member of the Pierre Shale Formation; ~80 Ma) and predates the earliest known occurrence of specimens referred to Plotosaurini (e.g., *Mosasaurus*) by approximately five million years. We posit that NDGS 10838 is indicative of early Middle Campanian mosasaurine diversity in North America that has, historically,

been masked in part by the extremely problematic taxonomy affiliated with specimens referred to *Clidastes* (for an in-depth discussion, see Lively, 2018). For example, many unpublished specimens referred to *Clidastes propython* exhibit a range of morphological variation outside what is seen in other equally well-sampled mosasaurs (e.g., *Tylosaurus proriger*, A.R.Z., personal obs.; Lively, 2018), including some specimens that are morphologically intermediate between typical Niobrara Formation *Clidastes* specimens and NDGS 10838 (e.g., TMP 1983.019.0002).

SUMMARY

Jormungandr walhallaensis is a new genus and species of mosasaurine mosasaur from the Pembina Member of the Pierre Shale Formation. The presence of several bones that rarely preserve (e.g., ectopterygoid, vomer, potential lacrimal) in mosasaurs provides valuable insight into the morphology and evolution of these bones in Mosasaurinae. It is the earliest known taxon to possess apomorphies of Plotosaurini and shares many apomorphies with *Clidastes*, suggesting it may represent a transitional form between the two. We interpret its placement in our phylogenetic analyses in a polytomy with, or sister to, *Clidastes* reflective of an undersampling of characters in the current matrix, particularly characters codifying lower classification variation (e.g., within Tylosaurinae, Plioplatecarpinae, and Mosasaurinae), and we expect its position to change following the future addition of new characters and taxa. NDGS 10838 represents one of the northernmost occurrences of mosasaurines in the Western Interior Seaway and as such expands the known range of the clade in Campanian North America. Finally, our experiments with outgroup choice show that the inclusion of specific anguimorph outgroups improves resolution of ingroup relationships relative to those analyses in which only dolichosaurs serve as the outgroup, highlighting the importance of keeping analyses of phyloge-

netic matrices consistent with their original taxonomic scope.

ACKNOWLEDGMENTS

We thank the reviewers Takuya Konishi and Anne Schulp for their feedback on the manuscript. We also thank Michael J. Polcyn for reviewing the manuscript prior to submission, sharing data, and helping us identify the trickier fragments of the holotype specimen. We thank Meng Jin, James G. Napoli, Alessandro Palci, Alexander A. Ruebenstahl, Micheal Strager, and Hallie Street for providing invaluable discussion and feedback on our methods and interpretation of the data. The life reconstruction and skull drawings were produced by Henry Sharpe. We also thank Jeff Person (NDGS) for access to the holotype specimen, as well as the curators and collections managers at other institutions (AMNH, FHSM, FMNH, KUVF, MCZ, NJSM, YPM) for access to comparative specimens. We thank Bradly Shelby for sharing resources about the mythology of Jormungandr, and Skye McDavid for help translating French literature. Deborah Shepherd discovered the first part of the holotype exposed at the locality and reported it to employees at the Pembina Gorge State Recreation Area, and we thank the North Dakota Department of Parks and Recreation for providing access to the site and assistance with organizing the Public Fossil Digs that collected the specimen. We also thank the numerous members of the public who assisted with the collection of the holotype from 2015–2018, and Becky Barnes (NDGS), who prepared the specimen. Lastly, we thank Mary Knight and Elizabeth Taylor for facilitating the submission and final formatting of the manuscript to the journal. C.A.B. was supported by the state of North Dakota. A.R.Z. was funded by the National Science Foundation Graduate Research Fellowship Program under grant no. 1938103, the Richard Gilder Graduate School, and the Carter Fund.

REFERENCES

- Álvarez-Herrera, G., F. Agnolin, and F. Novas. 2020. A rostral neurovascular system in the mosasaur *Taniwhasaurus antarcticus*. *Science of Nature* 107: 1–5.
- Augusta, B.G., H. Zaher, M.J. Polcyn, A.R. Fiorillo, and L.L. Jacobs. 2022. A review of non-mosasauroid (dolichosaur and aigialosaur) mosasauroians and their relationships to snakes. In D. J. Gower and H. Zaher (editors), *The origin and early evolutionary history of snakes*, 1st ed.: 157–179. Cambridge: Cambridge University Press.
- Bahl, K.N. 1937. Skull of *Varanus monitor* (Linn.). *Records of the Zoological Survey of India* 39 (2): 133–174.
- Bamburak, J.D., M.P.B. Nicolas, and J. Hatcher. 2013. Radiometric dating of Late Cretaceous bentonite beds in southwestern Manitoba. In *Report of Activities 2013, Manitoba Mineral Resources, Manitoba Geological Survey, Winnipeg*: 129–136.
- Bamburak, J.D., M. Hamilton, and L.M. Heaman. 2016. Geochronology of Late Cretaceous bentonite beds in southwestern Manitoba: 2016 update. In *Report of Activities 2016, Manitoba Growth, Enterprise and Trade, Manitoba Geological Survey, Winnipeg*: 168–175.
- Bardet, N., X.P. Suberbiola, and N.-E. Jalil. 2003. A new mosasauroid (Squamata) from the Late Cretaceous (Turonian) of Morocco. *Comptes Rendus – Palevol* 2 (8): 607–616.
- Bastiaans, D., J.J. Kroll, D. Cornelissen, J.W. Jagt, and A.S. Schulp. 2020. Cranial palaeopathologies in a Late Cretaceous mosasaur from the Netherlands. *Cretaceous Research* 112: 104425.
- Bell, G.L. 1997. A phylogenetic revision of North American and Adriatic Mosasauroida. In E. Nicholls and J. Callaway (editors), *Ancient Marine Reptiles*: 293–332. Bloomington, IN: Academic Press.
- Bellairs, A.A., 1949. Observations on the snout of *Varanus*, and a comparison with that of other lizards and snakes. *Journal of Anatomy* 83 (pt. 2): 116–146.
- Bertin, T.J.C., B. Thivichon-Prince, A.R.H. LeBlanc, M.W. Caldwell, and L. Viriot. 2018. Current perspectives on tooth implantation, attachment, and replacement in Amniota. *Frontiers in Physiology* 9 (NOV): 1–20.
- Bertog, J. 2002. High resolution event stratigraphic and sequence stratigraphic interpretation of the lower Pierre Shale (Campanian) with the description of the new Walhalla and Chamberlain Members. Ph.D. dissertation, Department of Geology, University of Cincinnati.

- Bertog, J. 2010. Stratigraphy of the lower Pierre Shale (Campanian): implications for the tectonic and eustatic controls on facies distributions. *Journal of Geological Research* 2010: 1–15.
- Bertog, J., W. Huff, and J.E. Martin. 2007. Geochemical and mineralogical recognition of the bentonites in the lower Pierre Shale Group and their use in regional correlation. In J.E. Martin and D.C. Parris (editors), *The geology and paleontology of the Late Cretaceous marine deposits of the Dakotas*: 23–50.
- Binford, L.R. 1981. *Bones: ancient men and modern myths*. New York: Academic Press.
- Bullard, T.S., and M.W. Caldwell. 2010. Redescription and rediagnosis of the tylosaurine mosasaur *Hainosaurus peminensis* Nicholls, 1988, as *Tylosaurus peminensis* (Nicholls, 1988). *Journal of Vertebrate Paleontology* 30 (2): 416–426.
- Burbrink, F.T., et al. 2020. Interrogating genomic-scale data for Squamata (lizards, snakes, and amphisbaenians) shows no support for key traditional morphological relationships. *Systematic Biology* 69 (3): 502–520.
- Caldwell, M.W., R. Holmes, G.L. Bell, and J. Wiffen. 2005. An unusual tylosaurine mosasaur from New Zealand: a new skull of *Taniwhasaurus oweni* (Lower Haumurian; Upper Cretaceous). *Journal of Vertebrate Paleontology* 25 (2): 393–401.
- Carroll, R.L., and M. DeBraga. 1992. Aigialosaurs: mid-Cretaceous varanoid lizards. *Journal of Vertebrate Paleontology* 12 (1): 66–86.
- Clayton, L., S.R. Moran, J.P. Bluemle, and C.G. Carlson. 1980. *Geologic map of North Dakota*: U.S. Geological Survey.
- Cobban, W.A., I. Walaszczyk, J.D. Obradovich, and K.C. McKinney. 2006. A USGS zonal table for the Upper Cretaceous middle Cenomanian–Maastrichtian of the Western Interior of the United States based on ammonites, inoceramids, and radiometric ages. U.S. Geological Survey Open-File Report 1250: 1–46.
- Conrad, J.L. 2004. Skull, mandible, and hyoid of *Shinisaurus crocodilurus* Ahl (Squamata, Anguimorpha). *Zoological Journal of the Linnean Society* 141 (3): 399–434.
- Conrad, J.L. 2008. Phylogeny and systematics of Squamata (Reptilia) based on morphology. *Bulletin of the American Museum of Natural History* 310: 1–182.
- Dortangs, R.W., et al. 2002. A large new mosasaur from the Upper Cretaceous of the Netherlands. *Netherlands Journal of Geosciences* 81 (1): 1–8.
- Driscoll, D.A., A.M. Dunhill, T.L. Stubbs, and M.J. Benton. 2019. The mosasaur fossil record through the lens of fossil completeness. *Palaeontology* 62 (1): 51–75.
- Drumheller, S.K., and C.A. Brochu. 2016. Phylogenetic taphonomy: a statistical and phylogenetic approach or exploring taphonomic patterns in the fossil record using crocodylians. *Palaios* 31 (10): 463–478.
- Dutchak, A.R., and M.W. Caldwell. 2006. Redescription of *Aigialosaurus dalmaticus* Kramberger, 1892, a Cenomanian mosasauroid lizard from Hvar Island, Croatia. *Canadian Journal of Earth Sciences* 43 (12): 1821–1834.
- Everhart, M.J. 2004. Late Cretaceous interaction between predators and prey. Evidence of feeding by two species of shark on a mosasaur. *PalArch, Vertebrate Paleontology* 1 (1): 1–7.
- Everhart, M.J. 2005. Bite marks on an elasmosaur (Sauropterygia; Plesiosauria) paddle from the Niobrara Chalk (Upper Cretaceous) as probable evidence of feeding by the lamniform shark, *Cretoxyrhina mantelli*. *PalArch, Vertebrate Paleontology* 2 (2): 14–24.
- Everhart, M. 2008. A bitten skull of *Tylosaurus kansansensis* (Squamata: Mosasauridae) and a review of mosasaur-on-mosasaur pathology in the fossil record. *Transactions of the Kansas Academy of Science* 111 (3–4): 251–262.
- Fernandez, M., and J.E. Martin. 2009. Description and phylogenetic relationships of *Taniwhasaurus antarcticus* (Mosasauridae, Tylosaurinae) from the upper Campanian (Cretaceous) of Antarctica. *Cretaceous Research* 30 (3): 717–726.
- Gauthier, J.A., M. Kearney, J.A. Maisano, O. Rieppel, and A.D.B. Behlke. 2012. Assembling the squamate tree of life: perspectives from the phenotype and the fossil record. *Bulletin of the Peabody Museum of Natural History* 53 (1): 3–308.
- Gervais, P. 1853. Observations relatives aux reptiles fossiles de France. *Comptes Rendus de l'Académie des Sciences Paris* 36: 374–377, 470–474.
- Gill, J.G., and W.A. Cobban. 1965. Stratigraphy of the Pierre Shale, Valley City and Pembina Mountain areas, North Dakota. U.S. Geological Survey Professional Paper 392-A: 1–20.
- Goloboff, P.A. 2014. Extended implied weighting. *Cladistics* 30 (3): 260–272.
- Goloboff, P.A., and S.A. Catalano. 2016. TNT version 1.5, including a full implementation of phylogenetic morphometrics. *Cladistics* 32 (3): 221–238.

- Goloboff, P.A., J.S. Farris, and K.C. Nixon. 2008. TNT, a free program for phylogenetic analysis. *Cladistics* 24 (5): 774–786.
- Goloboff, P.A., A. Torres, and J.S. Arias. 2018. Weighted parsimony outperforms other methods of phylogenetic inference under models appropriate for morphology. *Cladistics* 34 (4): 407–437.
- Graybeal, A. 1998. Is it better to add taxa or characters to a difficult phylogenetic problem? *Systematic Biology* 47 (1): 9–17.
- Hector, J. 1874. On the fossil reptilia of New Zealand. *Transactions of the New Zealand Institute* 6: 333–358.
- Hicks, J.F., J.D. Obradovich, and L. Tauxe. 1999. Magnetostratigraphy, isotope age calibration and intercontinental correlation of the Red Bird section of the Pierre Shale, Niobrara County, Wyoming, USA. *Cretaceous Research* 20 (1): 1–27.
- Holmes, R. 1996. *Plioplatecarpus primaevus* (Mosasauridae) from the Bearpaw Formation (Campanian, Upper Cretaceous) of the North American Western Interior Seaway. *Journal of Vertebrate Paleontology* 16 (4): 673–687.
- Holmes, R.B., and H. Sues. 2000. A partial skeleton of the basal mosasaur *Halisaurus platyspondylus* from the Severn Formation (Upper Cretaceous: Maastrichtian) of Maryland. *Journal of Paleontology* 74 (2): 309–316.
- Houssaye, A., and N. Bardet. 2013. A baby mosasauroid (Reptilia, Squamata) from the Turonian of Morocco – *Tethysaurus* “junior” discovered? *Cretaceous Research* 46: 208–215.
- Ikejiri, T., and S.G. Lucas. 2014. Osteology and taxonomy of *Mosasaurus conodon* Cope 1881 from the Late Cretaceous of North America. *Geologie en Mijnbouw/Netherlands Journal of Geosciences* 94 (1): 39–54.
- Jiménez-Huidobro, P., and M.W. Caldwell. 2019. A new hypothesis of the phylogenetic relationships of the Tylosaurinae (Squamata: Mosasauroida). *Frontiers in Earth Science* 7 (6): 1–15.
- Konishi, T., and M.W. Caldwell. 2007. New specimens of *Platecarpus planifrons* (Cope, 1874) (Squamata: Mosasauridae) and a revised taxonomy of the genus. *Journal of Vertebrate Paleontology* 27 (1): 59–72.
- Konishi, T., and M.W. Caldwell. 2009. New material of the mosasaur *Plioplatecarpus nichollsae* Cuthbertson et al., 2007, clarifies problematic features of the holotype specimen. *Journal of Vertebrate Paleontology* 29 (2): 417–436.
- Konishi, T., and M.W. Caldwell. 2011. Two new plio-platecarpine (Squamata, Mosasauridae) genera from the Upper Cretaceous of North America, and a global phylogenetic analysis of plio-platecarpines. *Journal of Vertebrate Paleontology* 31 (4): 754–783.
- Konishi, T., D. Brinkman, J.A. Massare, and M.W. Caldwell. 2011. New exceptional specimens of *Prognathodon overtoni* (Squamata, Mosasauridae) from the upper Campanian of Alberta, Canada, and the systematics and ecology of the genus. *Journal of Vertebrate Paleontology* 31 (5): 1026–1046.
- Konishi, T., M.G. Newbrey, and M.W. Caldwell. 2014. A small, exquisitely preserved specimen of *Mosasaurus missouriensis* (Squamata, Mosasauridae) from the Upper Campanian of the Bearpaw formation, western Canada, and the first stomach contents for the genus. *Journal of Vertebrate Paleontology* 34 (4): 802–819.
- Konishi, T., M.W. Caldwell, T. Nishimura, K. Sakurai, and K. Tanoue. 2015. A new halisaurine mosasaur (Squamata: Halisaurinae) from Japan: the first record in the western Pacific realm and the first documented insights into binocular vision in mosasaurs. *Journal of Systematic Palaeontology* 14 (10): 809–839.
- LeBlanc, A.R.H., M.W. Caldwell, and J. Lindgren. 2013. Aquatic adaptation, cranial kinesis, and the skull of the mosasaurine mosasaur *Plotosaurus bennisoni*. *Journal of Vertebrate Paleontology* 33 (2): 349–362.
- LeBlanc, A.R.H., I. Paparella, D.O. Lamoureux, M.R. Doschak, and M.W. Caldwell. 2020. Tooth attachment and pleurodont implantation in lizards: Histology, development, and evolution. *Journal of Anatomy* (August): 1–23.
- Lee, M.S.Y. 1997. The phylogeny of varanoid lizards and the affinities of snakes. *Philosophical Transactions of the Royal Society of London B, Biological Sciences* 352 (1349): 53–91.
- Lindgren, J. 2009. Cranial osteology of the giant mosasaur *Plesiotylosaurus* (Squamata, Mosasauridae). *Journal of Paleontology* 83 (3): 448–456.
- Lingham-Soliar, T. 1995. Anatomy and functional morphology of the largest marine reptile known, *Mosasaurus hoffmanni* (Mosasauridae, Reptilia) from the Upper Cretaceous, Upper Maastrichtian of the Netherlands. *Philosophical Transactions of the Royal Society of London B, Biological Sciences* 347 (1320): 155–180.
- Lingham-Soliar, T. 2000. The mosasaur *Mosasaurus lemmonieri* (Lepidosauromorpha, Squamata) from the Upper Cretaceous of Belgium and the Netherlands. *Paleontological Journal* 34: 1–17.

- Lively, J.R. 2018. Taxonomy and historical inertia: *Cleidastes* (Squamata: Mosasauridae) as a case study of problematic paleobiological taxonomy. *Alcheringa: an Australasian Journal of Palaeontology* 42 (4): 516–527.
- Lively, J.R. 2020. Redescription and phylogenetic assessment of *Prognathodon stadtmani*: implications for Globidensini monophyly and character homology in Mosasaurinae. *Journal of Vertebrate Paleontology* 40 (3): 1–17.
- Longrich, N.R., N. Bardet, F. Khaldoune, O.K. Yazami, and N.-E. Jalil. 2021. *Pluridens serpentis*, a new mosasaurid (Mosasauridae: Halisaurinae) from the Maastrichtian of Morocco and implications for mosasaur diversity. *Cretaceous Research* 126: 104882.
- Longrich, N.R., et al. 2022. *Thalassotitan atrox*, a giant predatory mosasaurid (Squamata) from the upper Maastrichtian phosphates of Morocco. *Cretaceous Research* 140: 105315.
- Lynds, R.M., and Slattery, J.S. 2017. Correlation of the Upper Cretaceous strata of Wyoming: Wyoming State Geological Survey Open File Report 2017-3.
- Makádi, L., M.W. Caldwell, and A. Ősi. 2012. The first freshwater mosasauroid (Upper Cretaceous, Hungary) and a new clade of basal mosasauroids. *PLoS ONE* 7 (12): 1–16.
- Martin, J.E. 2007. A new species of the durophagous mosasaur, *Globidens* (Squamata: Mosasauridae) from the Late Cretaceous Pierre Shale Group of central South Dakota, USA. *Special Papers, Geological Society of America* 427: 177–197.
- Martin, J.E., and J.E. Fox. 2007. Stomach contents of *Globidens*, a shell-crushing mosasaur (Squamata), from the Late Cretaceous Pierre Shale Group, Big Bend area of the Missouri River, central South Dakota. In J.E. Martin and D.C. Parris (editors), *The geology and paleontology of the Late Cretaceous marine deposits of the Dakotas*: 167–176. Geological Society of America, Special Paper 427.
- Martin, J.E., J.L. Bertog, and D.C. Parris. 2007. Revised lithostratigraphy of the lower Pierre Shale Group (Campanian) of central South Dakota, including newly designated members. In J.E. Martin and D.C. Parris (editors), *The geology and paleontology of the Late Cretaceous marine deposits of the Dakotas*: 9–22. Geological Society of America, Special Paper 427.
- McDowell, S.B., and C.M. Bogert. 1954. The systematic position of *Lanthanotus* and the affinities of the anguinomorph lizard. *Bulletin of the American Museum of Natural History* 105 (1): 1–142.
- Murphy, E.C., S.H. Nordeng, B.J. Juenker, and J.W. Hoganson. 2009. North Dakota stratigraphic column. North Dakota Geological Survey, Miscellaneous Series 91: 1–1.
- Napoli, J.G., A. Ruebenstahl, B.A.S. Bhullar, A.H. Turner, and M.A. Norell. 2021. A new dromaeosaurid (Dinosauria: Coelurosauria) from Khulsan, central Mongolia. *American Museum Novitates* 3982: 1–47.
- Nicholls, E.L. 1988. Marine vertebrates of the Pembina member of the Pierre Shale (Campanian, upper cretaceous) of Manitoba and their significance to the biogeography of the Western Interior Seaway. Ph.D. dissertation, Department of Biological Sciences, University of Calgary.
- Norell, M.A., and K.Q. Gao. 1997. Braincase and phylogenetic relationships of *Estesia mongoliensis* from the Late Cretaceous of the Gobi Desert and the recognition of a new clade of lizards. *American Museum Novitates* 3211: 1–25.
- Norell, M., M.C. McKenna, and M.J. Novacek. 1992. *Estesia mongoliensis*: a new fossil varanoid from the late Cretaceous Barun Goyot Formation of Mongolia. *American Museum Novitates* 3045: 1–24.
- Norell, M.A., K.Q. Gao, and J.L. Conrad. 2008. A new platynotan lizard (Diapsida: Squamata) from the Late Cretaceous Gobi Desert (Ömnögov), Mongolia. *American Museum Novitates* 3605: 1–22.
- Obradovich, J.D. 1993. A Cretaceous time scale. In W.G.E. Caldwell and E.G. Kaufman (editors), *Evolution of the Western Interior Basin: Geological Association of Canada Special Paper* 39: 379–396.
- Oelrich, T.M. 1956. The anatomy of the head of *Ctenosaura pectinata*. *Copeia* 4: 1–268.
- Oppel, M. 1811. *Die Ordnungen, Familien und Gattungen der Reptilien als Prodrum einer Naturgeschichte derselben*. Comm. Munich: Lindauer, 86 pp.
- Osborn, H.F. 1899. A complete mosasaur skeleton, osseous and cartilaginous. *Science* 10 (260): 919–925.
- Palci, A., M.W. Caldwell, and C.A. Papazzoni. 2013. A new genus and subfamily of mosasaurs from the Upper Cretaceous of northern Italy. *Journal of Vertebrate Paleontology* 33 (3): 599–612.
- Palci, A., T. Konishi, and M.W. Caldwell. 2021. A comprehensive review of the morphological diversity of the quadrate bone in mosasauroids (Squamata: Mosasauroidae), with comments on the homology of the infrastapedial process. *Journal of Vertebrate Paleontology* 40 (6): 1–11.

- Páramo-Fonseca, M.E. 2000. *Yaguarasaurus columbiana* (Reptilia, Mosasauridae), a primitive mosasaur from the Turonian (Upper Cretaceous) of Colombia. *Historical Biology* 14 (1–2): 121–131.
- Polcyn, M.J., and G.L. Bell. 2005. *Russellosaurus coheni* n. gen., n. sp., a 92 million-year-old mosasaur from Texas (USA), and the definition of the parafamily Russellosaurina. *Geologie en Mijnbouw/Netherlands Journal of Geosciences* 84 (3): 321–333.
- Polcyn, M.J., and J. Lamb. 2012. The snout of *Halisaurus platyspondylus* Marsh 1869: Phylogenetic and functional implications. *Bulletin de la Société Géologique de France* 183 (2): 137–143.
- Polcyn, M.J., L.L. Jacobs, R. Araújo, A.S. Schulp, and O. Mateus. 2014. Physical drivers of mosasaur evolution. *Palaeogeography, Palaeoclimatology, Palaeoecology* 400: 17–27.
- Polcyn, M.J., B.G. Augusta, and H. Zaher. 2022. Reassessing the morphological foundations of the pythonomorph hypothesis. In D.J. Gower and H. Zaher (editors), *The origin and early evolutionary history of snakes*, 1st ed.: 125–156. Cambridge: Cambridge University Press.
- Reeder, T.W., et al. 2015. Integrated analyses resolve conflicts over squamate reptile phylogeny and reveal unexpected placements for fossil taxa. *PLoS ONE* 10 (3): 1–22.
- Rieppel, O., and H. Zaher. 2001. Re-building the bridge between mosasaurs and snakes. *Neues Jahrbuch für Geologie und Paläontologie-Abhandlungen* 221 (1): 111–132.
- Romer, A.S., 1956. *Osteology of the reptiles*. Chicago: University of Chicago Press.
- Russell, D. 1967. Systematics and morphology of American mosasaurs. *Bulletin of the Peabody Museum of Natural History* 23: 1–241.
- Shimada, K., and G.E. Hooks. 2004. Shark-bitten protostegid turtles from the Upper Cretaceous Mooreville Chalk, Alabama. *Journal of Paleontology* 78 (1): 205–210.
- Simões, T.R., O. Vernygora, I. Paparella, P. Jimenez-Huidobro, and M.W. Caldwell. 2017. Mosasauroid phylogeny under multiple phylogenetic methods provides new insights on the evolution of aquatic adaptations in the group. *PLoS ONE* 12 (5): 1–20.
- Street, H.P., and M.W. Caldwell. 2017. Rediagnosis and redescription of *Mosasaurus hoffmannii* (Squamata: Mosasauridae) and an assessment of species assigned to the genus *Mosasaurus*. *Geological Magazine* 154 (3): 521–557.
- Street, H., A. LeBlanc, and M. Caldwell. 2021. A histological investigation of dental crown characters used in mosasaur phylogenetic analyses. *Vertebrate Anatomy Morphology Paleontology* 9 (1): 83–94.
- Strong, C.R.C., M.W. Caldwell, T. Konishi, and A. Palci. 2020. A new species of longirostrine plioplacarpine mosasaur (Squamata: Mosasauridae) from the Late Cretaceous of Morocco, with a re-evaluation of the problematic taxon '*Platycarpus ptychodon*'. *Journal of Systematic Palaeontology*: 1–36.
- Wiffen, J. 1990. New mosasaurs (Reptilia; family Mosasauridae) from the upper Cretaceous of North Island, New Zealand. *New Zealand Journal of Geology and Geophysics* 33 (1): 67–86.
- Willman, A.J., T. Konishi, and M.W. Caldwell. 2021. A new species of *Ectenosaurus* (Mosasauridae: Plioplacarpinae) from western Kansas, USA, reveals a novel suite of osteological characters for the genus. *Canadian Journal of Earth Sciences* 58 (9): 741–755.
- Yi, H.Y., and M.A. Norell. 2013. New materials of *Estesia mongoliensis* (Squamata: Anguimorpha) and the evolution of venom grooves in lizards. *American Museum Novitates* 3767: 1–31.
- Zietlow, A.R. 2020. Craniofacial ontogeny in Tylosaurinae. *PeerJ* 8 (e10145): 1–47.

APPENDIX 1

CHARACTER LIST USED IN THE PARSIMONY ANALYSES OF MOSASAUROID PHYLOGENY, MODIFIED FROM THAT OF STRONG ET AL. (2020).

Our character list is modified from that of Strong et al. (2020), which is the most recent version of the original comprehensive mosasaur matrix by Bell (1997). Eleven taxa (five mosasaurids, four extant nonmosasauroid anguimorphs, two extinct nonmosasauroid anguimorphs) were added and one was removed, bringing the total number of operational taxonomic units to 58. The scores for 22 taxa were modified based on firsthand and literature observations by A.R.Z.; the exact specimens and sources, when relevant, upon which these observations are based are noted below. The states and/or names of 11 existing characters were modified to better represent the range of variation present in observed specimens.

In addition to those listed in Institutional Abbreviations, the following abbreviations are used: BYU, Brigham Young University Museum of Paleontology, Provo, UT; GBA, Geologisches Bundesanstalt Osterreich, Vienna, Austria; IAA, Instituto Antártico Argentino, Buenos Aires, Argentina; IGM, Mongolian Institute for Geology, Ulaanbaatar, Mongolia; OCP, Office Chéri-fien des Phosphates, Khouribga, Morocco; SDSM, South Dakota School of Mines and Technology Museum of Geology, Rapid City, SD; UCMP, University of California Museum of Paleontology, Berkeley, CA; UF, University of Florida Museum of Natural History, Gainesville, FL; USNM, United States National Museum, Washington, D.C.

MODIFICATIONS

TAXA ADDED:

Varanus komodoensis, scored from firsthand observation of AMNH R-37909 and AMNH R-37879.

Lanthanotus borneensis, scored from CT scans of (AMNH R-87375, AMNH R-113983, and UF Herp 16268), as well as the description by McDowell and Bogert (1954).

Heloderma horridum, scored from firsthand observation of AMNH R-71664 and a CT scan of UF Herp 153328.

Shinisaurus crocodilurus, scored from firsthand observation of AMNH R-44928, a CT scan of UF Herp 60925, and the descriptions of the skull and postcrania by Conrad (2004, 2008).

Estesia mongoliensis, scored from CT scans and firsthand observation of the holotype IGM 3/14 (limb, cast of skull and jaws) and IGM 3/196, as well as the descriptions of various specimens by Norell et al. (1992), Norell and Gao (1997), and Yi and Norell (2013).

Ovo o gurvel, scored from CT scans and firsthand observation of [IGM 3/767], as well as the description by Norell et al. (2008).

Pluridens serpentis, scored from the description of the syntypes, OCP DEK-GE 548 and MHN.M.KH.262, by Longrich et al. (2021).

Tylosaurus peminensis, scored from the description of various specimens by Bullard and Caldwell (2010) and the matrix of Jiménez-Huidobro and Caldwell (2019).

Latoplatecarpus nichollsae, scored from the description of various specimens by Konishi and Caldwell (2009) and Willman et al. (2021).

Gnathomortis stadtmani, scored from the description, matrix, and literature photographs of the holotype, BYU 13082, by Lively (2020).

Globidens schurmanni, scored from the description of the holotype, SDSM 74764, by Martin (2007) and literature photographs (Palci et al. 2021: supplemental fig. S2).

TAXON REMOVED:

Tylosaurus bernardi was removed because its scores were identical to, but less complete than, the scores for *Tylosaurus proriger*.

TAXA MODIFIED:

Aigialosaurus buccichi was scored based on descriptions of the holotype GBA 1901 by Carroll and DeBraga, 1992) and Dutchak and Caldwell (2006); character 121 was changed from ? to 0.

Halisaurus platyspondylus was scored using first-hand observation of NJSM 12146 and its description by Polcyn and Lamb (2012), as well as the description of USNM 442450 by Holmes and Sues (2000): character 1 was changed from 1 to 0; character 22 was changed from ? to 0; character 24 was changed from ? to 0; and character 36 was changed from ? to 0.

Yaguarasaurus columbianus was scored based on the description of various specimens by Páramo-Fonseca (2000); character 68 was changed from ? to 0.

Pannoniasaurus "osii" was modified to instead represent the type species, *Pannoniasaurus inexpectatus*, as we could not find any documentation in the literature of a *Pannoniasaurus "osii."* Using the description of various specimens by Makádi et al. (2012), character 46 was changed from ? to 0.

Tethysaurus nopcsai was scored using the descriptions of various specimens by Bardet et al. (2003) and Houssaye and Bardet (2013); character 12 was changed from ? to 0; character 35 changed from ? to 0; character 54 changed from ? to 1; character 73 changed from ? to 1; character 74 changed from ? to 0; and character 97 was changed from ? to 0.

Taniwhasaurus antarcticus was scored using the descriptions and photographs of the holotype IAA 20000-JR-FSM-1 by Fernandez and Martin (2009) and Álvarez-Herrera et al. (2020); character 15 was changed from ? to 3; character 21 changed from ? to 0; character 24 changed from ? to 0; character 29 changed from ? to 3; and character 54 changed from ? to 3.

Taniwhasaurus oweni was scored using the descriptions of various specimens by Hector (1874) and Caldwell et al. (2005); character 30 was changed from ? to 0; character 35 changed from ? to 0; character 70 changed from ? to 0;

character 94 changed from ? to 1; character 95 changed from ? to 1; character 96 changed from ? to 0; character 97 changed from ? to 1; character 98 changed from ? to 0; character 99 changed from ? to 1; and character 54 changed from ? to 3.

Tylosaurus nepaeolicus was scored using first-hand observation of holotype AMNH FARB 1565, AMNH FARB 1561, FHSM VP-2209, and the matrix of Jiménez-Huidobro and Caldwell (2019): character 10 changed from 0 to 0,1; character 15 changed from ? to 3; character 39 changed from ? to 0; character 56 changed from 0 to 1; character 68 changed from 1 to 0; character 72 changed from 1 to 0; and character 100 changed from 2 to ?.

Tylosaurus proriger was scored using firsthand observation of holotype MCZ 4374, AMNH FARB 221, AMNH FARB 1555, FMNH UR902, KUVVP 28705, and the matrix of Jiménez-Huidobro and Caldwell (2019): character 15 changed from ? to 3; character 21 changed from ? to 0; character 30 changed from 0 to 0,1; character 34 changed from 0 to 1; character 39 changed from ? to 1; character 41 changed from 2 to 1; character 56 changed from 0 to 1; character 68 changed from 1 to 0,1; character 72 changed from 1 to 0,1; character 86 changed from 1 to 0; character 100 changed from 2 to 1; and character 117 changed from ? to 2.

Ectenosaurus clidastoides was scored using first-hand observation of holotype FHSM VP-401: character 49 was changed from ? to 1; character 52 changed from 3 to 1.

Gavialimimus almaghribensis was scored using the descriptions of the holotype MNHN. KHG.1231 by Strong et al. (2020).

Latoplatecarpus willistoni was scored using the description of various specimens by Konishi and Caldwell (2011).

Platecarpus tympaniticus was scored using first-hand observation of FHSM VP-322, KUVVP 1001, and KUVVP 1007: character 24 was changed from ? to 0; and character 76 was changed from 1 to -, because character 75,

zygosphe and zyantra presence, is scored as 0 (absent), and therefore character 76, zygosphe and zyantra number, is inapplicable.

Plesioplatecarpus planifrons was scored using firsthand observation of FHSM VP-2116 and FHSM VP-2181: character 24 was changed from ? to 0; and character 27 changed from ? to 0.

Plioplatecarpus sp. was modified to represent *Plioplatecarpus primaevus* specifically, based on the description of various specimens by Holmes (1996). The following changes to character states were made: character 1 changed from ? to 0; character 2 changed from ? to 1; character 3 changed from ? to 0; character 10 changed from 1 to 2; character 29 changed from ? to 3; character 31 changed from ? to 0; character 33 changed from 1 to 0; character 51 changed from 2 to 1; character 54 changed from 2/3 to 2; character 55 changed from 1 to 0; character 73 changed from ? to 1; character 74 changed from ? to 0; character 77 changed from ? to 0; character 86 changed from ? to 1; character 87 changed from ? to 1; character 102 changed from ? to 1; character 115 changed from ? to 1; character 116 changed from ? to 0; character 117 changed from ? to 2; character 118 changed from ? to 0; and character 124 changed from 0/1 to 0.

Clidastes liodontus was scored using firsthand observation of AMNH FARB 192 and AMNH FARB 1548: character 13 was changed from ? to 0; character 33 changed from ? to 0; character 34 changed from ? to 1; character 41 was changed from 0 to 1; character 54 changed from 2 to 1; character 56 changed from ? to 0; character 65 changed from ? to 0; character 68 changed from 1 to 0/1; and character 122 changed from 1 to 0.

Mosasaurus conodon was scored using firsthand observation of holotype AMNH FARB 1380: character 52 was changed from 1 to ?; and character 58 changed from ? to 0.

Mosasaurus hoffmannii, was scored for characters new to this work using firsthand obser-

vation of NJSM 11052 and NJSM 11053, as well as the description of various specimens by Street and Caldwell (2017): character 4 was changed from 0 to 2; character 6 was changed from ? to 0; character 12 was changed from ? to 0; character 13 was changed from ? to 0; character 31 changed from ? to 2; character 39 was changed from ? to 0; and character 59 was changed from ? to 1.

Mosasaurus missouriensis, was scored using the description of TMP 2008.036.0001 by Konishi et al. (2014): character 5 was changed from 1 to 0.

Plesiotylosaurus crassidens was scored using the description of UCMP 137249 by Lindgren (2009): character 1 was changed from 2 to 3.

Plotosaurus bennisoni was scored using a CT scan of holotype UCMP 32778: character 12 was changed from ? to 0; character 54 changed from ? to 1.

Globidens dakotensis, was scored using firsthand observation of FMNH PR846: character 1 was changed from 2 to 1.

For all taxa for which character 15 are scored as having state 3, character 16 was scored as inapplicable (-).

Following the change to character 71 discussed below, all taxa that were previously scored as having state 2 were rescored as having state 1.

Following the change to character 86 discussed below, all taxa that were previously scored as having state 2 were rescored as having state 3.

CHARACTERS MODIFIED:

1. **Premaxilla predental rostrum II:** the name of this character was changed to “premaxilla predental rostrum.”

4. **Premaxilla internarial bar base shape:** added state 2, “T-shaped,” to reflect the distinct morphology seen in *Mosasaurus* and *Jormungandr*.

20. **Pineal foramen position I:** the name of this character was changed to “pineal foramen position.”

29. **Maxilla tooth number:** state 3 was changed from “12 to 14” to “14 or fewer,” as *Plioplatecarpus primaevus* has 11 tooth positions (Holmes, 1996).

52. **Dentary tooth number:** state 0 was changed from “20 to 24” to “more than 20,” as specimens of *Pluridens serpentis* have between 26 and 28 dentary teeth. State 5 was changed from “12” to “12 or fewer,” to accommodate the possibility of new taxa having less than 12 tooth positions and because *Lanthanotus* occasionally has 11 dentary teeth.

62. **Surangular-articular suture position:** given that the glenoid articular surface is concave, the word “condyle” was changed to “cotyle.”

71. **Tooth carinae:** following Lively (2020), states 1 (present but weak) and 2 (strong and elevated) were combined into simply “present.” Consequently, all taxa scored with state 2 were rescored as having state 1.

86. **Presacral vertebrae number II:** the name of this character was changed to “presacral vertebrae number.” State 0 was changed from “28 or 29” to “fewer than 29,” to accommodate for the possibility of new taxa having fewer than 29 presacral vertebrae. State 2 was changed from “more than 39” to “32 to 39,” to accommodate for the possibility of new taxa having between 32 and 39 presacral vertebrae, and because 36 and 34 presacral vertebrae were observed in *Lanthanotus* and *Heloderma*, respectively. State 3, “more than 39,” was added to distinguish these taxa from those with between 32 and 39 presacral vertebrae.

117. **Pubic tubercle condition:** added state 2 (absence of pubic tubercle). This state was noted but not scored by Bell (1997) in *Tylosaurus proriger*.

SKULL

1. **Premaxilla premental rostrum:** rostrum absent (0); rostrum very short and obtuse (1); or distinctly protruding (2); or very large and inflated (3). In *Clidastes* a short, acute, protruding rostrum (state 2) produces a V-shaped dorsal profile and, as far as is known, is peculiar to that genus.
2. **Premaxilla shape:** bone broadly arcuate anteriorly (0); or relatively narrowly arcuate or acute anteriorly (1). In virtually all lizards the premaxilla is a very widely arcuate and lightly constructed element, and the base of the internarial process is quite narrow as in *Aigialosaurus bucchichi*. All other mosasaurids have a very narrowed premaxilla with the teeth forming a tight curve and the internarial process being proportionally wider (state 1).
3. **Premaxilla internarial bar width:** narrow, distinctly less than half of the maximum width of the rostrum in dorsal view (0); or wide, being barely narrower than the rostrum (1). Note: for taxa that do not possess a rostrum, this proportion is measured against the width of the premaxilla along its anterior margin; for taxa that do not possess the elongated premaxilla seen in mosasauroids, this width is measured across the premaxilla-maxilla sutures in dorsal view.
4. **Premaxilla internarial bar base shape:** triangular (0); rectangular (1); T-shaped (2). A vertical cross section through the junction of the internarial bar and the dentigerous rostrum produces an inverted triangle in most taxa. But in state 1, this cross section is transversely rectangular because the broad ventral surface of the bar is planar. In state 2, the internarial bar is wide dorsally and thins abruptly into a ventral blade.
5. **Premaxilla internarial bar dorsal keel:** absent (0); or present (1). In state 1 a ridge rises above the level of a normally smoothly continuous transverse arch formed by the bones of the anterior muzzle.
6. **Premaxilla internarial bar venter:** with entrance for the fifth cranial nerve close to

- rostrum (0); or far removed from rostrum (1). The conduit that marks the path of the fifth cranial nerve from the maxilla into the premaxilla is expressed as a ventrolateral foramen within the premaxillo-maxillary sutural surface at the junction of the internarial bar and the dentigerous rostrum. State 1 includes a long shallow groove on the ventral surface of the bar. Anteriorly, this groove becomes a tunnel entering the bone at an extremely shallow angle but disappearing below the surface at least 1 cm behind the rostrum.
7. **Frontal shape in front of the orbits:** sides sinusoidal (0); or bone nearly triangular and sides relatively straight (1). In state 1, the area above the orbits is expanded and an isosceles triangle is formed by the rectilinear sides. In certain taxa, a slight concavity is seen above the orbits, but anterior and posterior to it there is no indication of a sinusoidal or recurved edge.
 8. **Frontal width:** element broad and short (0); intermediate dimensions (1); or long and narrow (2). Mosasauroid frontals can be separated into a group that generally has a maximum length to maximum width ratio greater than 2:1 (state 2), between 1.5:1 and 2:1 (state 1), or equal to or less than 1.5:1 (state 0).
 9. **Frontal narial emargination:** frontal not invaded by posterior end of nares (0); or distinct embayment present (1). In some mosasauroids, the posterior ends of the nares are concomitant with the anterior terminus of the frontal-prefrontal suture and, therefore, there is no marginal invasion of the frontal by the opening. However, in other mosasauroids this suture begins anterior and lateral to the posterior ends of the nares, causing a short emargination into the frontal.
 10. **Frontal midline dorsal keel:** absent (0); or low, fairly inconspicuous (1); or high, thin, and well developed (2).
 11. **Frontal ala shape:** sharply acuminate (0); or more broadly pointed or rounded (1). In state 0, the anterolateral edge of the ala is smoothly concave, thus helping to form the sharply pointed or rounded and laterally oriented posterior corners. In some forms the anterolateral edge of the ala may be concave, but the tip is not sharp and directed laterally.
 12. **Frontal olfactory canal embrasure:** canal not embraced ventrally by descending processes (0); or canal almost or completely enclosed below (1). In state 1, very short descending processes from the sides of the olfactory canal surround and almost, or totally, enclose the olfactory nerve.
 13. **Frontal posteroventral midline:** tabular boss immediately anterior to the frontal-parietal suture absent (0); or present (1). A triangular boss with a flattened ventral surface at the posterior end of the olfactory canal is represented by state 1.
 14. **Frontal-parietal suture overlap orientation:** apposing surfaces with no overlap (0); suture with oblique median frontal and parietal ridges contributing to overlap (1); or with all three ridges almost horizontal (2). In state 0, the median ridge from the frontal and the single parietal ridge are oriented at a distinct angle to the upper skull surface while the outer, or lateral, frontal ridge appears to be nearly horizontal. In *Tylosaurus nepaeolicus* and *T. proriger* (state 2), the obliquity of the intercalating ridges is reclined almost to the horizontal, greatly extending the amount of lateral overlap.
 15. **Frontal invasion of parietal I:** lateral sutural flange of frontal posteriorly extended (0); or median frontal sutural flange posteriorly extended (1); or both extended (2); or suture straight (3). In all mosasaurines the oblique median frontal sutural ridge extends onto the dorsal sur-

- face of the parietal table and embraces a portion of the anterior table within a tightly crescentic midline embayment. In *Plioplatecarpus* and *Platecarpus*, the lateral oblique sutural ridge from the frontal is greatly protracted posteriorly to cause a large, anteriorly convex embayment in the dorsal frontal-parietal suture. In this case the entire posterolateral corner of the frontal is extended backward to embrace the anterolateral portion of the parietal table on both sides. Consequently, the pineal foramen is very widely embraced laterally, and the oblique anterior sutural ridge of the parietal occupies a position inside the embayment within the frontal.
16. **Frontal medial invasion of parietal II:** if present, posteriorly extended median sutural flange short (0); or long (1). The median oblique sutural flange is either short, not reaching back to the pineal foramen (state 0), or tightly embraces the foramen while extending backward to a position even with or beyond its posterior edge (state 1).
 17. **Parietal length:** dorsal surface relatively short with epaxial musculature insertion posterior, between suspensorial rami only (0); or dorsal surface elongate, with epaxial musculature insertion dorsal as well as posterior (1).
 18. **Parietal table shape:** generally rectangular to trapezoidal, with sides converging, but not meeting (0); or triangular, with sides contacting in front of suspensorial rami (1); or parietal table elongate, triangular to subrectangular, and highly medially constricted, with a distinct mid- or parasagittal crest anterior to the divergence of the suspensorial rami (2).
 19. **Pineal foramen size:** relatively small (0); or large (1). If the foramen is smaller than or equal to the area of the stapedial pit, it is considered small. If the foramen is significantly larger or if the distance across the foramen is more than half the distance between it and the nearest edge of the parietal table, the derived state is achieved.
 20. **Pineal foramen position:** foramen generally nearer to center of parietal table, well away from frontal-parietal suture (0); or close to or barely touching suture (1); or huge foramen straddling suture and deeply invading frontal (2). Generally in state 1, the distance from the foramen to the suture is about equal to or less than one foramen's length.
 21. **Pineal foramen ventral opening:** opening is level with main ventral surface (0); or opening surrounded by a rounded, elongate ridge (1).
 22. **Parietal posterior shelf:** presence of a distinct horizontal shelf projecting posteriorly from between the suspensorial rami (0); or shelf absent (1). In some mosasauroids, a somewhat crescent-shaped shelf (in dorsal view) lies at the posterior end of the bone medial to, and below, the origination of the suspensorial rami.
 23. **Parietal suspensorial ramus compression:** greatest width vertical or oblique (0); or greatest width horizontal (1). In *Tylosaurus*, the anterior edge of the ramus begins very low on the lateral wall of the descending process, leading to formation of a proximoventral sulcus, but the straps are horizontal distally.
 24. **Parietal union with supratemporal:** suspensorial ramus from parietal overlaps supratemporal without interdigitation (0); or forked distal ramus sandwiches proximal end of supratemporal (1).
 25. **Prefrontal supraorbital process:** process absent, or present as a very small rounded knob (0); or a distinct, medium to large, triangular, or rounded overhanging wing (1).
 26. **Prefrontal-postorbitofrontal contact:** absent (0); prefrontal overlapped ven-

- trally by postorbitofrontal (1); or prefrontal overlapped laterally by postorbitofrontal (2). Postorbitofrontal ventral overlap of the prefrontal is extreme in *Platecarpus tympaniticus* and *Plioplatecarpus*, such that there is even a thin flange of the frontal interjected between the prefrontal above and the postorbitofrontal below. In *T. proriger*, the postorbitofrontal sends a long narrow process forward to fit into a lateral groove on the prefrontal. In *Plesiotylosaurus*, the overlap is relatively short and more oblique, and there is no groove on the prefrontal.
27. **Postorbitofrontal shape:** narrow (0); or wide (1). In *Clidastes* and the Globidenisini, the lateral extent of the element is almost equal to half of the width of the frontal and the outline of the bone is basically squared.
 28. **Postorbitofrontal transverse dorsal ridge:** absent (0); or present (1). In state 1, an inconspicuous, low, and narrowly rounded ridge traces from the anterolateral corner of the parietal suture across the top of the element to disappear behind the origin of the jugal process.
 29. **Maxilla tooth number:** 20–24 (0); or 17–19 (1); or 15–16 (2); 14 or fewer (3).
 30. **Maxillo-premaxillary suture posterior terminus:** suture ends above a point that is anterior to or level with the midline of the fourth maxillary tooth (0); or between the fourth and ninth teeth (1); or level with or posterior to the ninth tooth (2). These somewhat arbitrary divisions of the character states are meant to describe in more concrete terms those sutures that terminate far anteriorly, those that terminate less anteriorly, and those that terminate near the midlength of the maxilla, respectively.
 31. **Maxilla posterodorsal extent:** process absent (0); recurved wing of maxilla prevents emargination of prefrontal on dorsolateral edge of external naris (1); or does not (2).
 32. **Jugal posteroventral angle:** angle very obtuse or curvilinear (0); or slightly obtuse, near 120° (1); or 90° (2).
 33. **Jugal posteroventral process:** absent (0); or present (1).
 34. **Ectopterygoid contact with maxilla:** present (0); or absent (1).
 35. **Pterygoid tooththrow elevation:** teeth arise from robust, transversely flattened main shaft of pterygoid (0); or teeth arise from thin, pronounced vertical ridge (1). In state 0, the teeth emanate from the relatively planar surface of the thick, slightly dorsoventrally compressed main shaft of the pterygoid. In state 1, a tall, thin dentigerous ridge emanates ventrally from a horizontal flange that forms the base of the quadratic ramus and the ectopterygoid process, thus causing the main shaft to be trough shaped.
 36. **Pterygoid tooth size:** anterior teeth significantly smaller than marginal teeth (0); or anterior teeth large, approaching size of marginal teeth (1).
 37. **Quadrate suprastapedial process length:** process short, ends at a level well above midheight (0); or of moderate length, ending very near midheight (1); or long, distinctly below midheight (2); suprastapedial process absent (3).
 38. **Quadrate suprastapedial process constriction:** distinct dorsal constriction (0); or virtually no dorsal constriction (1). Lack of constriction results in an essentially parallel-sided process in posterodorsal view but can also include the tapering form characteristic of some *Tylosaurus*. **Remarks (Strong et. al., 2020):** This character refers to whether the sides of the suprastapedial process are parallel or not in posterodorsal view. State 0 occurs when there is a localized narrowing or “pinching” of the suprastapedial process near its attachment with

- the quadrate shaft, causing the sides of the process to be nonparallel. This is generally typical of mosasaurines (see *Cli-dastes* as an exemplar). In some other taxa (e.g., *Selmasaurus*, *Gavialimimus*), the suprapedial process is “dorsally constricted,” i.e., broadly excavated medially; however, this is different from the morphology to which the present character is referring. Rather than being “pinched in” at the junction of the suprapedial process and quadrate shaft, the sides of the suprapedial process remain continuous/parallel throughout its length in these taxa (see holotypes of *Gavialimimus* or *Selmasaurus* as exemplars). Based on the above criterion that a parallel-sided process reflects lack of constriction, these taxa would fall under state 1 (dorsal constriction—the narrowed base of the suprapedial process—is not present).
39. **Quadrate suprapedial ridge:** if present, ridge on ventromedial edge of suprapedial process indistinct, straight and/or narrow (0); or ridge wide, broadly rounded, and curving downward, especially above stapedial pit (1).
 40. **Quadrate suprapedial process fusion:** no fusion present (0); or process fused to, or in extensive contact with, elaborated process from below (1). A posterior rugose area may be inflated and broadened mediolaterally to partially enclose the ventral end of a broad and elongate suprapedial process as in *Halisaurus*. In *Globidens*, *Prognathodon*, and *Plesiotylosaurus*, the process is fused ventrally to a narrow pedunculate medial extension of the tympanic rim. A similar condition is present in *Ectenosaurus*, except that the tympanic rim is not medially extended and has a short projection that overlaps a portion of the suprapedial process posteriorly.
 41. **Quadrate stapedial pit shape:** pit broadly oval to almost circular (0); or relatively narrowly oval (1); or extremely elongate with a constricted middle (2). In state 0, the length to width ratio is less than 1.8:1; in state 1 it ranges from 1.8:1 to 2.4:1; and in state 2, it is greater than 2.4:1.
 42. **Quadrate posteroventral ascending tympanic rim condition:** ascending ridge small or absent (0); or a high, elongate triangular crest (1); or a crest extremely produced laterally (2). In state 1, this extended rim causes a fairly deep sulcus in the ventral portion of the intratympanic cavity. In *Plioplatecarpus*, the entire lower tympanic rim and ala are expanded into a large conch (state 2), which tremendously increases the depth of the intratympanic cavity.
 43. **Quadrate ala thickness:** ala thin (0); or thick (1). In state 0, the bone in the central area of the ala is only about 1 mm thick in medium-sized specimens and that area is usually badly crushed or completely destroyed. Alternatively, the ala extends from the main shaft with only minor thinning, providing a great deal of strength to the entire bone.
 44. **Quadrate conch:** ala and main shaft encompassing a deeply bowled area (0); or alar concavity shallow (1). A relatively deeper sulcus in the anterior part of the intratympanic cavity and more definition to the ala and the main shaft are features of state 0.
 45. **Basisphenoid pterygoid process shape:** process relatively narrow with articular surface facing mostly anterolaterally (0); or somewhat thinner, more fan shaped with a posterior extension of the articular surface causing a more lateral orientation (1).
 46. **Quadrate ala groove:** absent (0); or long, distinct, and deep groove present in anterolateral edge of ala (1); or groove along dorsal margin of quadrate ala (2).
 47. **Quadrate median ridge:** single thin, high ridge, dorsal to ventral (0); ridge low

- and rounded with divergent ventral ridges (1); or single thin ridge developed into a conspicuous medial flange (2). State 2 was first codified by Palci et al. (2013), but a description of it is missing in character lists since because the authors forgot to include it (A. Palci, personal commun.).
48. **Quadrate anterior ventral condyle modification:** no upward deflection of anterior edge of condyle (0); or distinct deflection present (1). A relatively narrow bump in the otherwise horizontal trace of the anterior articular edge is also super-tended by a sulcus on the anteroventral face of the bone.
 49. **Quadrate ventral condyle:** condyle saddle shaped, concave in anteroposterior view (0); or gently domed, convex in any view (1).
 50. **Basioccipital tubera size:** short (0); or long (1). Long tubera are typically parallel sided in posterior profile and protrude ventrolaterally at exactly 45° from horizontal. Short tubera have relatively large bases that taper distally and emanate more horizontally.
 51. **Basioccipital canal:** absent (0); or present as a pair separated by a median septum (1); or present as a single bilobate canal (2).
 52. **Dentary tooth number:** more than 20 (0); 17–19 (1); 15–16 (2); 14 (3); 13 (4); 12 or less (5). It is easy to assume this character is correlated with the number of maxillary teeth, except that is not the case in *Ectenosaurus clidastoides*, which has 16 or 17 maxillary teeth and only 13 dentary teeth.
 53. **Dentary anterior projection:** absent (0); short (1); or long (2). In state 2, the projection of bone anterior to the first tooth is at least the length of a complete tooth space.
 54. **Dentary medial parapet:** parapet positioned at base of tooth roots (0); or elevated and straplike, enclosing about half of height of tooth attachment in shallow channel (1); or strap equal in height to lateral wall of bone (2); or medial parapet taller than lateral wall of bone (3). States 1, 2, and 3 are possible sequential stages of modification from a classically pleurodont dentition to the typical mosasaur subthecodont dentition.
 55. **Splenic-angular articulation shape:** splenic articulation in posterior view almost circular (0); or laterally compressed (1).
 56. **Splenic-angular articular surface:** essentially smooth concavoconvex surfaces (0); or distinct horizontal tongues and grooves present (1).
 57. **Coronoid shape:** coronoid with slight dorsal curvature, posterior wing not widely fan shaped (0); or very concave above, posterior wing greatly expanded (1).
 58. **Coronoid posteromedial process:** small but present (0); or absent (1).
 59. **Coronoid medial wing:** does not reach angular (0); or contacts angular (1).
 60. **Coronoid posterior wing:** without medial crescentic pit (0); or with distinct excavation (1). In state 1, there is a posteriorly open, C-shaped excavation in the medial side of the posterior wing of this element.
 61. **Surangular coronoid buttress:** low, thick, about parallel to lower edge of mandible (0); or high, thin, rapidly rising anteriorly (1). A rounded dorsal edge of the surangular remains almost parallel to the ventral edge as it approaches the posterior end of the coronoid, meeting the latter element near its posteroventral edge in state 0. In state 1, the dorsal edge rises and thins anteriorly until meeting the posterior edge of the coronoid near its apex, producing a triangular posterior mandible in lateral aspect.
 62. **Surangular-articular suture position:** behind the glenoid cotyle in lateral view

- (0); or at middle of cotyle on lateral edge (1); anterior to cotyle (2). In state 1, there is usually an interdigitation in the dorsal part of the suture.
63. **Surangular-articular lateral suture trace:** suture descends and angles or curves anteriorly (0); or is virtually straight throughout its length (1). In state 1, the suture trails from the glenoid posteriorly about halfway along the dorsolateral margin of the retroarticular process, then abruptly turns anteriorly off the edge and strikes in a straight line for the posterior end of the angular.
64. **Articular retroarticular process inflection:** moderate inflection, less than 60° (0); or extreme inflection, almost 90° (1).
65. **Articular retroarticular process innervation foramina:** no large foramina on lateral face of retroarticular process (0); or one to three large foramina present (1).
66. **Tooth surface I:** teeth finely striate lingually (0); or not lingually striate (1). In “Russellosaurinae” lingual tooth striations are very fine and groups of tightly spaced striae are usually set apart by facets, leading to a fasciculate appearance.
67. **Tooth surface II:** teeth not coarsely textured (0); or very coarsely ornamented with bumps and ridges (1). In both species of *Globidens* and in *Prognathodon overtoni*, the coarse surface texture is extreme, consisting of thick pustules, and vermiform or anastomosing ridges. Teeth in *P. rapax* are smooth over the majority of their surface, but usually a few widely scattered, large, very long, sharp-crested vermiform ridges are present.
68. **Tooth facets:** absent (0); or present (1). *Halisaurus* teeth are smoothly rounded except for the inconspicuous carinae. *Clidastes* is described in numerous places as having smooth unfaceted teeth, but many immature individuals and some larger specimens have teeth with three distinct facets on the lingual faces. Some large *Tylosaurus* have indistinct facets. *Mosasauros* has taken this characteristic to the extreme.
69. **Tooth fluting:** absent (0); or present (1). In *Ectenosaurus*, and some *Platecarpus planifrons*, several broadly rounded vertical ridges alternate with shallow, round-bottomed grooves completely around the teeth.
70. **Tooth inflation:** crowns of posterior marginal teeth conical, tapering throughout (0); or crowns of posterior marginal teeth swollen near the tip or above the base (1). The rear teeth of *Globidens* and *Prognathodon overtoni* are distinctly fatter than other mosasauroid teeth, but those of *P. rapax* are also swollen immediately distal to the base.
71. **Tooth carinae I:** absent (0); or present (1). Character states 1 and 2, “present but weak” and “present and strong and elevated,” were combined into simply “present” by Lively (2020). *Halisaurus* exhibits the minimal expression of this character (state 1) in that its marginal teeth are almost perfectly round in cross section; the carinae are extremely thin and barely stand above the surface of the teeth.
72. **Tooth carinae serration:** absent (0); or present (1).

AXIAL SKELETON

73. **Atlas neural arch:** notch in anterior border (0); or no notch in anterior border (1).
74. **Atlas synapophysis:** extremely reduced (0); or large and elongate (1). In state 1, a robust synapophysis extends well posteroventral to the medial articular surface for the atlas centrum, and it may be pedunculate (*Clidastes*) or with a ventral “skirt” that gives it a triangular shape (*Mosasauros*). A very small triangular synapophysis barely, if at all,

- extends posterior to the medial articular edge in state 0.
75. **Zygosphenes and zygantra:** absent (0); or present (1). This character assesses only the presence of zygosphenes and zygantra, not their relative development. Nonfunctional and functional are considered as present.
 76. **Zygosphene and zygantra number:** present on many vertebrae (0); or present on only a few (1).
 77. **Hypapophyses:** last hypapophysis occurs on or anterior to seventh vertebra (0); or on eighth vertebra or posteriorly (1).
 78. **Synapophysis height:** facets for rib articulations tall and narrow on posterior cervicals and anterior trunk vertebrae (0); or facets ovoid, shorter than the centrum height on those vertebrae (1).
 79. **Synapophysis length:** synapophyses of middle trunk vertebrae not laterally elongate (0); or distinctly laterally elongate (1). The lateral extension of the synapophyses from the middle of the trunk is as much as 70%–80% of the length of the same vertebra is represented by state 1.
 80. **Synapophysis ventral extension:** synapophyses extend barely or not at all below ventral margin of cervical centra (0); or some extend far below ventral margin of centrum (1). In state 1, two or more anterior cervical vertebrae have rib articulations that dip well below the centrum, causing a very deeply concave ventral margin in anterior profile.
 81. **Vertebral condyle inclination:** condyles of trunk vertebrae inclined (0); or condyles vertical (1).
 82. **Vertebral condyle shape I:** condyles of anteriormost trunk vertebrae extremely dorsoventrally depressed (0); or essentially equidimensional (1). In state 0, posterior height: width ratios of anterior trunk vertebrae are close to 2:1. In state 1, they are between to 4:3 and 1:1.
 83. **Vertebral condyle shape II:** condyles of posterior trunk vertebrae not higher than wide (0); or slightly compressed (1). In state 1, the posterior condylar aspect reveals outlines that appear to be higher than wide and even perhaps slightly subrectangular, due to the slight emargination for the dorsal nerve cord.
 84. **Vertebral synapophysis dorsal ridge:** sharp ridge absent on posterior trunk synapophyses (0); or with a sharp-edged and anteriorly precipitous ridge connecting distal synapophysis with prezygapophysis (1). In state 0, the ridge in question, if present, may be incomplete or it may be rounded across the crest with the anterior and posterior sides about equally sloping.
 85. **Vertebral length proportions:** cervical vertebrae distinctly shorter than longest vertebrae (0); or almost equal or are the longest (1).
 86. **Presacral vertebrae number:** Fewer than 29 (0); 30 or 31 (1); 32 to 39 (2); more than 39 (3). For mosasauroids, presacral vertebrae are considered to be all those anterior to the first bearing an elongate transverse process.
 87. **Sacral vertebrae number:** two (0); or less than two (1). Numerous well-preserved specimens of derived mosasauroids have failed to show any direct contact of the pelvic girdle with vertebrae in the sacral area. Certainly, no transverse processes bear any type of concave facet for the ilium, and so it is generally assumed that a ligamentous contact was established with only one transverse process. Depending on one's perspective, it could be said that derived mosasauroids have either no or one sacral vertebra.
 88. **Caudal dorsal expansion:** neural spines of tail all uniformly shortened posteriorly (0); or several spines dorsally elongated behind middle of tail (1).

89. **Hemal arch length:** hemal arches about equal in length to neural arch of same vertebra (0); or length about 1.5× greater than neural arch length (1). This ratio may be as great as 1.2:1 in state 0. Comparison is most accurate in the middle of the tail and is consistent even on those vertebrae in which the neural spines are also elongated.
90. **Hemal arch articulation:** arches articulating (0); or arches fused to centra (1).
91. **Tail curvature:** no structural downturn of tail (0); or tail with curved posterior portion (1).
92. **Body proportions:** head and trunk shorter than or about equal to tail length (0); or head and trunk longer than tail (1).

APPENDICULAR SKELETON

93. **Scapula/coracoid size:** both bones about equal (0); or scapula about half the size of coracoid (1).
94. **Scapula width:** no anteroposterior widening (0); or distinct fan-shaped widening (1); or extreme widening (2). In state 0, the anterior and posterior edges of the scapula encompass less than one quarter of the arc of a circle, but in state 1, the arc is increased to approximately one third. In state 2, the distal margin encompasses almost a half circle and the anterior and posterior borders are of almost equal length.
95. **Scapula dorsal convexity:** if scapula widened, dorsal margin very convex (0); or broadly convex (1). In state 0, the anteroposterior dimension is almost the same as the proximodistal dimension. In state 1, the anteroposterior dimension is much larger.
96. **Scapula posterior emargination:** posterior border of bone gently concave (0); or deeply concave (1). In state 1, there is a deeply arcuate emargination on the posterior scapular border, just dorsal to the glenoid. It is immediately bounded dorsally by a corner, which begins a straight-edged segment that continues to the dorsal margin.
97. **Scapula-coracoid suture:** unfused scapula-coracoid contact has interdigitate suture anteriorly (0); or apposing surfaces without interdigitation (1).
98. **Coracoid neck elongation:** neck rapidly tapering from medial corners to a relatively broad base (0); or neck gradually tapering to a relatively narrow base (1); coracoid neck absent (2). In state 1, this character describes an outline of the bone, which is nearly symmetrical and gracefully fan shaped, with gently concave, nearly equidistant sides.
99. **Coracoid anterior emargination:** present (0); or absent (1).
100. **Humerus length:** humerus distinctly elongate, about three or more times longer than distal width (0); or greatly shortened, about 1.5 to 2× longer than distal width (1); or length and distal width virtually equal (2); or distal width slightly greater than length (3).
101. **Humerus postglenoid process:** absent or very small (0); or distinctly enlarged (1).
102. **Humerus glenoid condyle:** if present, condyle gently domed and elongate, ovoid in proximal view (0); or condyle saddle shaped, subtriangular in proximal view and depressed (1); or condyle highly domed or protuberant and short ovoid to almost round in proximal view (2). In some taxa, the condylar surfaces of the limbs were finished in thick cartilage and there was no bony surface of the condyle to be preserved. This condition is scored as not represented. In some taxa, the glenoid condyle extends more proximally than does the postglenoid process (state 2), and it is not ovoid as state 0.
103. **Humerus deltopectoral crest:** crest undivided (0); or split into two separate inser-

- tional areas (1). In state 1, the deltoid crest occupies an anterolateral or anterior position confluent with the glenoid condyle, while the pectoral crest occupies a medial or anteromedial area that may or may not be confluent with the glenoid condyle. The deltoid crest is often quite short, broad, and indistinct, and easily erased by degradational taphonomic processes.
104. **Humerus pectoral crest:** located anteriorly (0); or medially (1). In state 1, the pectoral crest is located near the middle of the flexor (or medial) side on the proximal end of the bone.
105. **Humerus ectepicondylar groove:** groove or foramen present on distolateral edge (0); or absent (1).
106. **Humerus ectepicondyle:** absent (0); or present as a prominence (1). A radial tuberosity is reduced in size in *Prognathodon*, but very elongated in *Plesiotylosaurus*.
107. **Humerus entepicondyle:** absent (0); or present as a prominence (1). The ulnar tuberosity protrudes posteriorly and medially from the posterodistal corner of the bone immediately proximal to the ulnar facet, causing a substantial dilation of the posterodistal corner of the humerus.
108. **Radius shape:** radius not expanded anterodistally (0); or slightly expanded (1); or broadly expanded (2).
109. **Ulna contact with centrale:** broad ulnare prevents contact (0); or ulna contacts centrale (1). In state 1, the ulnare is omitted from the border of the antebrachial foramen. There is usually a well-developed faceted articulation between the ulna and the centrale (or *intermedium*, as used by Russell, 1967).
110. **Radiale size:** large and broad (0); or small to absent (1).
111. **Carpal reduction:** carpals number six or more (0); or five or less (1).
112. **Pisiform:** present (0); or absent (1).
113. **Metacarpal I expansion:** spindle shaped, elongate (0); or broadly expanded (1). The broad expansion is also associated with an anteroproximal overhanging crest in every case observed.
114. **Phalanx shape:** phalanges elongate, spindle shaped (0); or blocky, hourglass shaped (1). *Mosasaurus* and *Plotosaurus* have phalanges that are slightly compressed and anteroposteriorly expanded on both ends.
115. **Ilium crest:** crest bladelike, articulates with sacral ribs (0); or elongate, cylindrical, does not articulate with sacral ribs (1).
116. **Ilium acetabular area:** arcuate ridge supertending acetabulum (0); or acetabulum set into broad, short V-shaped notch (1). The primitive ilium has the acetabulum impressed on the lateral wall of the bone, with a long narrow crest anterodorsally as the only surrounding topographic feature. In state 1, the acetabular area is set into a short, broadly V-shaped depression that tapers dorsally. The lateral walls of the ilium are therefore distinctly higher than the rim of the acetabulum.
117. **Pubic tubercle condition:** tubercle an elongate protuberance located closer to the midlength of the shaft (0); or a thin semicircular crestlike blade located close to the acetabulum (1); or absent (2). Bell (1997) noted the absence of this structure in *Tylosaurus proriger*.
118. **Ischiadic tubercle size:** elongate (0); or short (1). In state 0, the tubercle is as long as the shaft of the ischium is wide, but it is only a short narrow spur in state 1.
119. **Astragalus:** notched emargination for the crural foramen, without pedunculate fibular articulation (0); or without notch, pedunculate fibular articulation present (1). For state 0, the tibia and fibula are of equal length about the crural foramen and the astragalus contacts both to about the same degree. The form of the latter

element is symmetrical and subcircular with a sharp proximal notch. In state 1, the outline of the element is basically reniform and the tibial articulation is on the same line as the crural emargination. The fibula is also shortened and its contact with the astragalus is narrow.

120. **Appendicular epiphyses:** formed from ossified cartilage (0); or from thick unossified cartilage (1); or epiphyses missing or extremely thin (2). Ends of the limb bones show distinct vascularization and rugose surfaces indicating an apparently thick nonvascularized, unossified cartilage cap. Extremely smooth articular surfaces suggest the epiphyses were excessively thin or perhaps even lost.
121. **Hyperphalangy:** absent (0); or present (1). Hyperphalangy is defined as presence of one or more extra phalanges as compared to the primitive amniote formula of 2-3-4-5-3.

NEW CHARACTERS

These characters are those that have been added since publication of the original Bell (1997) matrix.

122. **Posterior thoracic vertebra:** not markedly longer than anterior thoracic vertebrae (0); or are markedly longer (1).
123. **Ectopterygoid process of pterygoid:** distal portion of process not offset anterolaterally and/or lacking longitudinal grooves and ridges (0); distal portion of process is offset anterolaterally and bears longitudinal grooves and ridges (1).
124. **Quadrangle midshaft lateral deflection:** absent (0); present (1). In state 1, the quadrangle shaft is bent laterally such that the suprastapedial process is deflected dorsolaterally relative to the main shaft of the quadrangle.

APPENDIX 2 *continued*

Halisaurus sternbergii

0100?0021000003-0010100000?020?0020?1?000?0?01?0?01101?0?0100010?0010?10?001
00?0111010111111001001000010111001111?010?0

Pluridens serpentis

?01?0?00110????1011?1?0011?12021???2??1??10?0????010??1???1?000?{0 1}{0 1}010??
??

Yaguarasaurus columbianus

010?0?02000??1201200?110000?302111??210020011000001311?????????0000010??1?????????????????
?????????????????????????????????0?0

Romeosaurus fumanensis

????????????????????????1??20?21?1021002011?2011??211??00000100?1000010????01101??0????????-
11?00?00?00????????????????10

Russellosaurus coheni

11??0002000112012000110000120221100210020011200001201100000010010000010?????????????????
??10

Pannoniasaurus inexpectatus

000?0????????????????????0????????01002000?0200?0020010?00?000001010??10?1110000?0?0?0????
01??0??000?0????00?0????0

Tethysaurus nopcsai

000?0?021100?1201200?110000?10?21?00010020001?2000110110010001000000{0 1}00-101
0?111000?????0??1110000????000?????000?????00

Taniwasaurus antarcticus

31111?00?210?23-10010110020030?21???11?02000?0010??231000?00?0?0111011?0?????
1?1????00????????????????????????????????0?1

Taniwasaurus oweni

31111?00?21?2????01????020030?21?0011?02000?0010??323?00?0????011101?100????01010????00??
1100101?????????????????????0?0

Tylosaurus nepaeolicus

31111?001{0 1}10123-1001?11002003012110011002111100100?42211000000000000010100
?00010101??00????????00010001011100?????000

Tylosaurus peminensis

31?1??001?10123-1001?11002003012??0011101210?00100?{4 5}2210000000010101011100?
?000111011?0?0101101101100010001?????0110?1100

Tylosaurus proriger

311111001110?23-1001011002003{0 1}121100111010001001000422110000000000{0 1}001
{0 1}100000010101010001011011011000100010111001020011000

Angolasaurus bocagei

11??0?01?11??1??1100?1??000?30???1??2100010010001015021?010001001?00101???1?????????????????
?????????????????????????????0?0

Ectenosaurus clidastoides

2100010200111201110001?00011121100010012101110?102112000100000010001010001001001?????
?????010110021???0012010100?????11100

Gavialimimus almaghribensis

010?0?10001?1?0-121111??0110310??00?1??1?0????????503????????11??1001010??0??1?0??
????????????????2?????11?????????????0?

APPENDIX 2 *continued*

Mosasaurus hoffmannii

21021000011001111002111?11003122101000000101?11011031210101110110101001101110110110?1
?11111?02100113111011121000111000121100

Mosasaurus missouriensis

21000?10011??111001?11?1?00302???1000?00100?1?011?312?0101110110101001?011?00001101131?
?11?01??00????????2100?11?????2?1?0

Plesiotylosaurus crassidens

3101??10?11??1111001111?1200312??01100?10110?0?101?212111011100??1010011????00011?10?????
??0110011312101112100010?????2???0

Plotosaurus bennisoni

11001?101010?1111011?1111?001112001000?00100011011?1211?1???10110000011?010?10?011??13??
1?1?0210011311101112100011??1??211?0

Prognathodon currii

100????0111????10???11?1?0030220??1??????0????1??50????????000??100?10????????????????????
????????????????????????????

Prognathodon kianda

11001??00?1??1?10?1?11??0??30?2111?10?10110000101?2121?1000100001000110????????????????
????????????????????????????00

Prognathodon overtoni

11000?10011001111001?1111?103022001110110110?001010312101011100101100111????0?110?13?
1111011100121210111??0???010000211?0

Prognathodon rapax

11000?10001001111001111?1?1?31120?1110?101100001110?021010??000011001110110?00011110???
?1??01?0011212101112100010?????2?1??

Prognathodon saturator

??00??10?110011110111????1000??20?111?010110000101?3?2101??01001011001110?10?01011110???
1?0????????????2???????????????

Prognathodon solvayi

000000100010011010111111100030210?1110010100?001111402?010101?00000?01110?10001011?10?
??????01?01??????????????????????????0

Prognathodon waiparaensis

110000????????????????????21?111??10110?0010?3?101????????00?011????????????????????
?????????????????????0?

Globidens alabamaensis

??????10?111011????????1010?1????1010?111?0?010????1010?1100001100110011??0?011??0????????
??0??21010111????????????2?1??

Globidens dakotensis

110?0?10111??1101001?11?1?1031120?1010?10110?0?1010????????????1100110011?00?011?10??????
????????????????????????????10?

Globidens schurmanni

011????0?0????101?????21?31?????1?11?10??11??1?111?1??????10010-01??010111
?????1??020?10121?????1?100?10????????0

NDGS 10838

3102100101100110????????101121?10?1010001110?1011??22211100010000????01?01110010????????
????????????????????????????00

